

L-751

MR June 1944

NATIONAL ADVISORY COMMITTEE FOR AERONAUTICS

WARTIME REPORT

ORIGINALLY ISSUED

June 1944 as
Memorandum Report

WIND-TUNNEL INVESTIGATION OF CARBURETOR-AIR SCOOPS

FOR THE XTB2D-1 AIRPLANE WITH EMPHASIS ON

MEANS FOR BYPASSING THE BOUNDARY LAYER

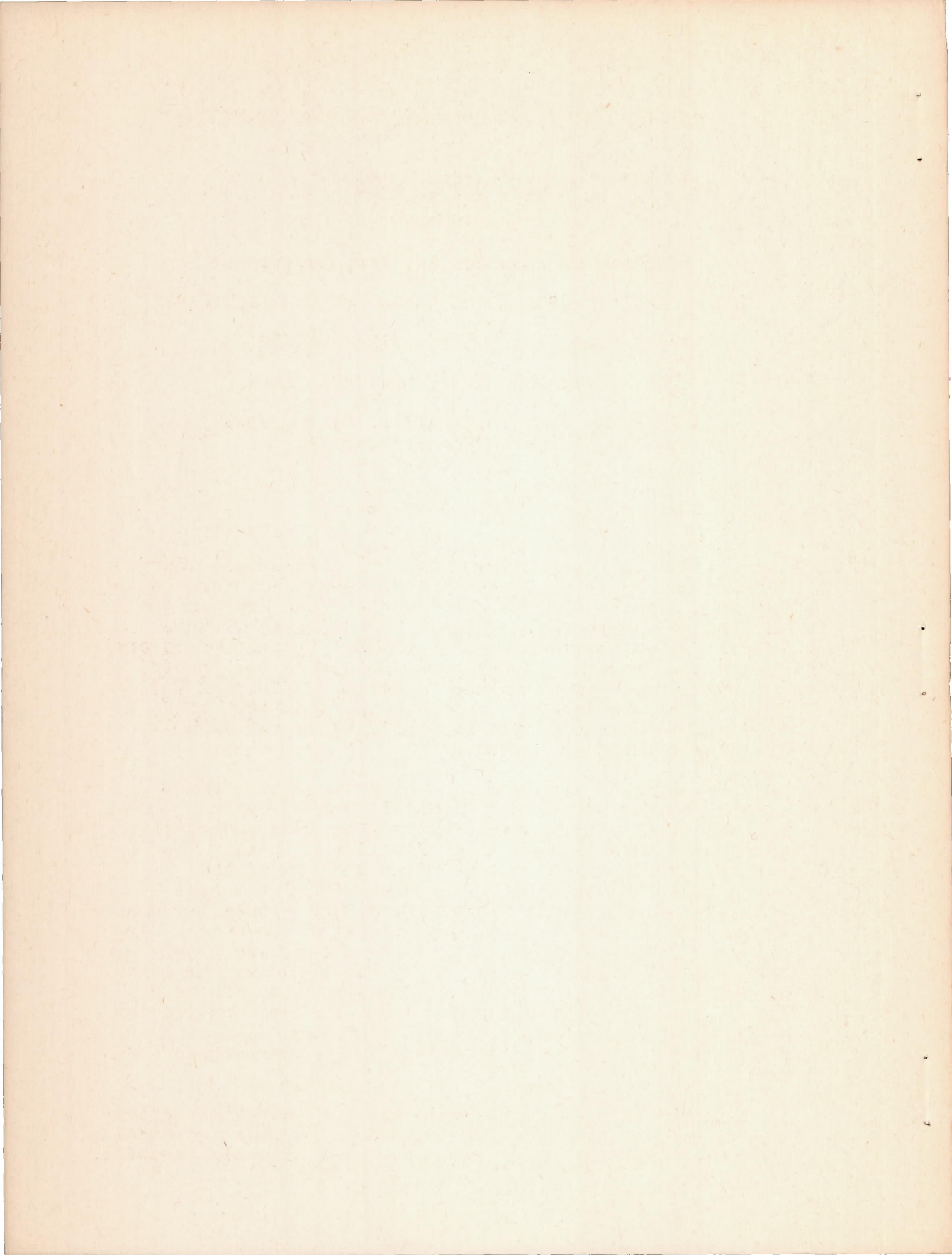
By Mark R. Nichols, Arvid L. Keith, Jr.,
and Robert W. Boswinkle, Jr.

Langley Memorial Aeronautical Laboratory
Langley Field, Va.



WASHINGTON

NACA WARTIME REPORTS are reprints of papers originally issued to provide rapid distribution of advance research results to an authorized group requiring them for the war effort. They were previously held under a security status but are now unclassified. Some of these reports were not technically edited. All have been reproduced without change in order to expedite general distribution.



NATIONAL ADVISORY COMMITTEE FOR AERONAUTICS

MEMORANDUM REPORT

for the
Bureau of Aeronautics, Navy Department

WIND-TUNNEL INVESTIGATION OF CARBURETOR-AIR SCOOPS
FOR THE XTB2D-1 AIRPLANE WITH EMPHASIS ON
MEANS FOR BYPASSING THE BOUNDARY LAYER

By Mark R. Nichols, Arvid L. Keith, Jr.,
and Robert W. Boswinkle, Jr.

INTRODUCTION

At the request of the Bureau of Aeronautics, Navy Department, an investigation of carburetor-air scoops designed for the XTB2D-1 airplane has been made in the NACA propeller-research tunnel. The purpose of this investigation was to determine the performance of several scoops and to make modifications necessary to improve the pressure recovery without adversely affecting the drag of the airplane. The test model consisted of a 3/10-scale mock-up of the forward part of the XTB2D-1 fuselage mounted on a stub wing.

The XTB2D-1 airplane is a carrier-based torpedo bomber powered by a Pratt & Whitney R-4360 engine equipped with a two-speed single-stage supercharger; an eight-blade dual-rotating propeller is used. The carburetor-air scoop is mounted on the top of the engine cowl approximately 73 inches aft of the cowl inlet where visibility requirements necessitate the use of very low inlets of high aspect ratio. Because previous investigations of similar scoops have shown that large pressure losses can be avoided only through adequate control of the boundary layer ahead of the inlet, detailed studies of the boundary layer on the cowl were included in these tests as a prerequisite to the development of suitable boundary-layer-bypass configurations.

The investigation included tests of nine carburetor-air scoops with numerous boundary-layer-bypass and ducting modifications, the original engine cowl, and two canopies.

Pressures were measured in the carburetor duct, in the carburetor-duct bypass, in the engine cowl, in the cowling boundary layer, and at the surface of the cowling, carburetor scoop, and canopy. Incidental tests were also made with a windmilling propeller to determine the effects of propeller disturbance. Tuft observations and force measurements were also made at various stages of the testing.

DEFINITION OF SYMBOLS

- A cross-sectional area of duct or cowl, square feet
 - C_D drag coefficient, $D/q_0 S$
 - D drag force, pounds
 - g_{accel} acceleration of gravity, 32.2 feet per second per second
 - H total pressure, pounds per square foot
 - p static pressure, pounds per square foot
 - q dynamic pressure, pounds per square foot
 - Q volume rate of flow, cubic feet per second
 - S wing area, square feet
 - V velocity, feet per second
 - α geometric angle of attack (angle between thrust axis and center line of tunnel), degrees
(See fig. 10.)
 - δ cowl-flap angle from flush position, degrees
- Subscripts denote conditions:
- a at cabin-ventilating-duct inlet
 - b in carburetor scoop bypass
 - c at cowl inlet
 - d at upper deck of carburetor

e at cowl-exit.

i at carburetor-duct inlet

o in free stream

s at surface of model

A bar above a symbol denotes an arithmetic average.

MODEL

The test model consisted of a 3/10-scale mock-up of the forward portion of the XTB2D-1 fuselage mounted on a stub wing; the rear part of the fuselage was replaced by a short fairing. The general arrangement and principal dimensions of the model are given in figure 1; a cutaway drawing showing the interior arrangement is presented as figure 2. A photograph of the model mounted in the propeller-research tunnel is presented as figure 3.

The engine cowling and basic scoop configurations are shown in figures 4 and 5. Detailed dimensions of these components and of the original and modified canopies are given in figures 6 through 8. The basic scoop configurations A, E, F, and G were designed and furnished by the manufacturer; configurations H and I were designed and constructed at the Laboratory; scoops B, C, and D were modifications to the A configuration.

A summary of physical data on the several basic scoops is given below:

Configuration	Scoop					Bypass	
	Distance from cowl nose (in.)	Height of inlet (in.)	Width of inlet (in.)	Inlet area (sq ft)	Carburetor deck area (sq ft)	Inlet area (sq ft)	Total exit area (sq ft)
A	22.00	1.19	7.13	0.0475	0.0934	0.0118	0.0049
B	21.00	.78	6.00	.0321	.0934	.0066	.0049
C	22.00	1.06	9.69	.0578	.0934	.0099	.0093
D	22.00	1.06	9.69	.0472	.0934	.0099	.0197
E	21.94	1.19	7.13	.0505	.0934	.0106	.0110
F	21.06	1.16	7.19	.0490	.0934	.0150	.0140
G	21.09	1.25	5.81	^b .0461	.0522	.0125	.0184
H	21.75	1.27	5.75	.0508	.0934	.0088	.0301
I	0	1.25	^a 5.37	.0500	.0934	0	0

^aPer side.

^bDoes not include area of auxiliary inlet for cabin ventilation (0.0084 square foot).

Configurations A, B, C, D, E, and H had raised bypass inlet scoops of the same type as the carburetor scoop; configurations F and G had "suction slit" type bypass inlets. The bypass exits of A, B, and C were located beneath the cowl flaps, and those of scoop E were located downstream of the cowl flaps. Scoop D had a bypass exit beneath the flaps and an additional passage through a vertical vane in the center of the duct. Scoops F, G, and H had bypass exits located on the sides of the scoops. Scoop F had a suction slit downstream of the bend connected to exits behind the cowl flaps.

METHODS AND TESTS

The air flow through the cowling was fixed by setting one of two cowl-flap positions. The flow resistance of the engine was represented by a calibrated orifice plate which had an effective area of 0.206 square foot. The air flow through the carburetor duct was controlled by a variable-speed centrifugal fan which

drew air into the scoop and exhausted through a calibrated venturi in the wing tip. Additional control of the charge-air flow was provided by a valve at the venturi exit.

The instrumentation of the orifice plate (fig. 9) consisted of four orifices in the web of the plate at the mean radius of its upstream face, four orifices in the downstream face spaced between the front orifices, and a thermocouple in the upstream face of the plate. Static orifices were installed on the inner surface of the cowl skirt just ahead of the trailing edge of the flaps, and on the left side of the inner cowl in the plane of the trailing edge of the flap and $1\frac{1}{8}$ inch to either side of this plane.

Total pressures in the boundary layer in front of the original scoop were measured by a rake of twenty 0.030-inch-diameter stainless-steel tubes with ends flattened to form openings 0.005 by about 0.05 inches. Total pressures at the scoop inlet and at the carburetor deck were measured by grids of 1/16- and 1/8-inch tubes, respectively. Static pressures were measured at the carburetor decks of scoops E, F, G, H, and I by means of eight 1/8-inch static tubes. Pressures were measured in the bypass exits by 1/16-inch total and static tubes and by surface orifices. Instrumentation of the carburetor-duct venturi consisted of static-pressure manifolds at the bell and throat and a thermocouple at the center of the duct 2 feet upstream from the throat.

Surface pressures over the cowling were measured by a "pressure belt" in accordance with the technique of reference 1. Surface pressures over the carburetor scoop and the canopy were measured by flush orifices.

Each of these scoops was tested at several angles of attack at a tunnel speed of approximately 100 miles per hour with propeller removed. At angles of attack greater than 7.5° , the tunnel speed was reduced to 80 miles per hour to avoid excessive wing flutter. It is noted that the values of α presented in this report are geometric angles between the thrust axis of the model and the center line of the tunnel. The calculated relationship between this angle and the effective angle of attack is shown in figure 10. At a geometric angle of attack of 0° , the two angles are very nearly

the same; the difference increases to 0.6° at a geometric angle of 10° .

For several tests, a three-blade, 4-foot-diameter propeller with blades set at 35° at the three-quarter radius was mounted on a floating spindle in the spinner to permit a study of the effects of propeller disturbances on the flow. (See fig. 4(a).) At a test speed of 100 miles per hour, this propeller windmilled at speeds which varied from 930 rpm at $\alpha = 0^\circ$ to 550 rpm at $\alpha = 7.5^\circ$.

RESULTS AND DISCUSSION

The results of these tests are presented in four sections which deal separately with (1) the flow through and around the engine cowling, (2) the flow in the several carburetor ducts, (3) the surface pressures on the model, and (4) the drag of several configurations.

Flow Through and Around Engine Cowl

A study of the flow through and around the engine cowling was made as a preliminary to the carburetor-air scoop investigation to establish the conditions under which these scoops were operating. Measurements of the inlet-velocity ratio, pressure recovery at the cowl orifice plate, static pressures in the cowl exit, and cowling boundary layer were made over a wide range of angles of attack and tunnel airspeeds.

Internal flow. - The inlet-velocity ratio for the cowling $Q_c/A_c V_o$ with propeller removed is shown in figure 11 to have been about 0.55 with flush cowl flaps and about 0.81 with cowl flaps opened 16° . Installation of the windmilling propeller reduced the inlet-velocity ratio by approximately 0.09 and 0.06 for the 0° and 16° flap positions, respectively. These values were essentially constant throughout the angle-of-attack range investigated.

Typical pressure distributions over the front and rear faces of the orifice plate at inlet-velocity ratios of 0.55 and 0.81 are presented for several angles of

attack in figure 12. These data indicate very little change in pressure recovery on the horizontal center line over the complete angle-of-attack range. The recovery at the top and bottom of the plate, however, was very sensitive to changes in α . This latter variation is shown more clearly in figure 13. The cause of the large decrease in recovery at the top of the plate at high angles of attack is shown in the tuft diagrams of figure 14. At an inlet-velocity ratio of 0.55 and $\alpha = 2.5^\circ$, the tufts showed a region of stagnant or reversed flow at the spinner surface at the top of the inlet; at $\alpha = 10^\circ$ the tufts showed a rapid upsweep in the flow in front of the top lip, thus indicating a small flow into the top of the inlet and possible spillage of the internal flow over the lip.

In configurations A through D the available pressure drop across the boundary-layer bypass ducts, and hence the quantity flow through these passages, was a function of the static pressure in the cowl exit. With propeller removed these pressures averaged about $0.2q_0$ above the free-stream static pressure for the flush-cowl-flap condition. (See fig. 15.) With a cowl-flap angle of 16° , they varied from about $-0.2q_0$ to $-0.35q_0$. Installation of the windmilling propeller raised the average static pressure with flaps deflected by approximately $0.03q_0$ but had negligible effect when the flaps were in the flush position.

Cowling boundary layer.— Total-pressure distributions in the cowling boundary layer are shown in figure 16. The thickness of the boundary layer increased rapidly with increases in α and with decreases in the distance of the measuring point from the scoop inlet. Decreases in the inlet-velocity ratio of the scoop caused appreciable increases in thickness at the station 1 inch in front of the inlet. Flow separation is noted at this station for configuration A-1 (no bypass) with the cowl flaps opened 16° but apparently did not occur with the flaps at 0° . The separation with open flaps may have been caused by the influence of the positive pressure field of the flaps on the already steep adverse pressure gradient in front of the scoop.

Flow in Carburetor Ducts

Data on the flow in the several carburetor ducts and carburetor-duct bypasses are given in figures 17 through 32. Pressure recoveries and pressure distributions at the inlets and deck flanges are presented as functions of the free-stream velocity, the inlet-velocity ratio $Q_i/A_i V_o$, the angle of attack α , and the cowl-flap angle δ . Complete test data are presented for a representative configuration.

The pressure recovery at the inlet and deck of a typical configuration (A-5) is shown in figure 17 as a function of the free-stream velocity. The scale effect is shown to have been appreciable below 70 feet per second but negligible over the test range of from 117 to 146 feet per second.

Variations of the average pressure recovery with $Q_i/A_i V_o$ at constant values of α are shown in figure 18 at the inlet and in figure 19 at the carburetor deck of a typical configuration. The pressure recovery at the inlet increased with:

- (1) Increases in $Q_i/A_i V_o$ (because of reduced boundary-layer thickness, fig. 16)
- (2) Decreases in α (because of decreases in the thickness of the cowling boundary layer and changes in the direction of the entering flow)
- (3) Increases in the cowl-flap angle (because of more complete boundary-layer removal due to the reduction in static pressure at the bypass exits).

The pressure recovery at the deck increased initially with increases in $Q_i/A_i V_o$ because of the increased recovery at the inlet and then decreased because the internal losses increased with the internal flow. Decreases in α and increases in δ produced pressure increases at the deck similar to those obtained at the inlet. To facilitate analysis, these data are cross-faired and replotted in figure 20 along with data for the other configurations tested over wide ranges of α and $Q_i/A_i V_o$.

Series A carburetor ducts.- In the original duct (figs. 5(a) and 7(a)) the ramming pressure at the carburetor deck flange averaged but $0.60q_0$ over the high-speed range. (See fig. 20.) Inspection of the local pressures at the inlet and deck (fig. 21) shows that large losses in ram occurred ahead of the scoop as well as in the duct. These data indicate that the losses ahead of the scoop occurred because of inadequate boundary-layer removal. Opening the cowl flaps increased the pressures at the inlet and deck by $0.03q_0$ to $0.08q_0$ as a result of increased flow through the boundary-layer bypass.

The ineffectiveness of the original boundary-layer bypass with flaps closed is shown by a comparison of the pressure recoveries obtained with configurations A and A-1. (See fig. 20.) Fairing out the bypass, configuration A-1 (fig. 5(b)), had negligible effect on the pressure at the inlet and deck.

A number of extensions varying in length, camber, leading-edge radius, and height above cowl surface was made to the bypass lip in an attempt to obtain adequate boundary-layer removal. The more effective extensions had moderate camber with well-rounded leading edges. Use of the airfoil-shaped lip extension of configuration A-7 increased the average inlet pressure at $\alpha = 2.5^\circ$, $Q_i/A_i V_0 = 0.59$, and $\delta = 0^\circ$, to $0.84q_0$, $0.04q_0$ higher than the inlet pressure obtained by configuration A. (See fig. 21.) Several of the extensions were also tested in conjunction with modified duct lines, configurations A-4 through A-6, but no substantial improvement in available ram was obtained.

Although the various extensions to the divider between the boundary-layer and carburetor-air ducts improved the flow to the carburetor, large losses continued to occur because of inadequate flow through the bypass. To provide increased flow with more uniform removal of the boundary layer, direct passages were cut from the bypass inlet to the low pressure area just downstream of the bend in the carburetor duct. For these configurations (A-14, A-15, and A-16), at $\alpha = 2.5^\circ$, $Q_i/A_i V_0 = 0.59$, and $\delta = 0^\circ$, the average pressure at the inlet was increased to $0.89q_0$, $0.90q_0$, and $0.87q_0$, respectively. (See fig. 21.) This result

stresses the importance of obtaining a high rate of flow through the bypass and uniform boundary-layer removal across the inlet. It is noted that the pressure recoveries at the decks of A-14, A-15, and A-16 were low because of the large quantity of low-energy air bled into the main duct.

Series B carburetor ducts.- The inlet area of the original scoop was decreased to 0.0321 square foot, configuration B (figs. 5(c) and 7(b)), by adding a wooden extension to the original scoop. It was reasoned that increasing the inlet-velocity ratio would reduce the adverse static-pressure gradient in front of the duct inlet and thus reduce the tendency toward boundary-layer separation in front of the scoop. The inlet pressures obtained were higher than the corresponding pressures for configuration A but were not as high as those obtained by configurations A-14, A-15, or A-16; large pressure losses in the duct reduced the recovery at the deck to approximately one-fourth of the free-stream dynamic pressure. (See fig. 22.)

Series C carburetor ducts.- The inlet area of configuration C (figs. 5(d) and 7(c)) was increased to 0.0578 square foot by widening the original inlet; the bypass exits were enlarged to 0.0047 square foot per side and the interior lines of the bend were refaired. The pressure recovery at the deck in the high-speed region was $0.60q_0$, the same as was obtained by configuration A (fig. 20). Several significant changes in the flow are evident from the data presented in figures 20, 21, and 23:

(1) The pressure recovery at the deck of configuration C was higher over a larger range of $Q_i/A_i V_0$ than with configuration A.

(2) Opening the cowl flaps caused larger increases in the pressure recovery at the deck with configuration C than with A.

(3) The pressures at the inlet were much lower than the corresponding pressures for configuration A, and the losses between the inlet and deck were smaller than for the A configurations.

Restoring the original duct lines downstream of the widened inlet reduced the ramming pressure at the deck

by $0.10q_0$. (Cf. data for configurations C and C-1 from fig. 23.)

Series D carburetor ducts.- An additional boundary-layer bypass was provided in the D configurations through a vertical vane in the center of the duct. (See figs. 5(e) and 7(d).) Configurations D, D-1, and D-2 had propeller-removed pressure recoveries at the inlet of $0.86q_0$ at $\alpha = 2.5^\circ$, $Q_i/A_i V_0 = 0.55$ to 0.60 , and $\delta = 0^\circ$. (See fig. 24.) These recoveries approach those obtained for configurations A-14, A-15, and A-16 and again emphasize the desirability of a large bypass flow. The pressure recoveries at the decks of the three configurations were very low because of high internal duct losses.

Installation of the windmilling propeller reduced the pressure recovery at $\alpha = 2.5^\circ$, $Q_i/A_i V_0 = 0.60$, and $\delta = 0^\circ$ by $0.13q_0$ at the inlet and $0.10q_0$ at the deck. (See fig. 24.) Pressure measurements on the cowling indicated that most of this difference was caused by the negative thrust of the windmilling propeller.

Series E carburetor ducts.- In configuration E (figs. 5(f) and 7(e)) the bypass exits were enlarged to 0.0055 square foot per side and moved to a position behind the cowl flaps, and the interior duct lines were refaired. The pressure recovery within the high-speed region averaged $0.65q_0$ (fig. 20), a value $0.02q_0$ higher than obtained by any previous configuration. Fairing out the bypass inlet, configuration E-1 (fig. 20), decreased the average high-speed pressure recovery by approximately $0.07q_0$. Pressure distributions for the duct (fig. 25) show that the total pressure at the rear of the deck was much higher than at the front and that the static pressure was nearly uniform at this station. The small differences between the total and static pressures at the front indicate that there was very little flow through this area. It is observed that configurations E and E-1 were extremely sensitive to changes in inlet-velocity ratio but varied only slightly with changes in α .

Series F carburetor ducts.- In configuration F (figs. 5(g) and 7(f)) the scoop was extended 1 inch

forward, the interior duct lines and the lines of the bypass inlet were refaired, the bypass exits were moved to the sides of the scoop, and a suction slit was installed at the downstream end of the bend. The bypass and suction-slit ducts had exit areas of 0.0070 square foot and 0.0045 square foot per side, respectively. The average pressure recovery within the high-speed region was $0.68q_0$ (fig. 20). Pressure distributions for the duct (fig. 26) also indicate a substantial flow through the forward portion of the deck. Fairing out the suction slit downstream of the bend, configuration F-1, decreased the average high-speed pressure recovery by $0.05q_0$; fairing out the main bypass, configuration F-2, reduced this pressure by an additional $0.03q_0$. (See fig. 20.)

In configurations F-3 and F-4, the interior duct lines were faired to the top of the carburetor venturi instead of the original deck flange, thus reducing expansion ahead of the carburetor. (See fig. 30.) This modification increased the average high-speed pressure recovery for configuration F-3 to $0.76q_0$ (fig. 20) and increased the flow at the forward portion of the deck (fig. 26). Opening the main bypass in configuration F-4 further increased the average high-speed recovery to $0.84q_0$ (fig. 20) and also caused additional increases in flow at the forward portion of the deck. The large increase in recovery over that obtained for configuration F-1 ($0.21q_0$) and the greater uniformity of the flow emphasize the desirability of adopting the contracted interior lines.

Series G carburetor ducts.- Configuration G (figs. 5(h) and 7(g)) was similar to configuration F-4 except for the installation of an auxiliary duct for cabin ventilation with an inlet area of 0.00835 square foot. With the inlet-velocity ratio of the auxiliary duct adjusted to 0.55, the average pressure recovery at the deck within the high-speed region was $0.84q_0$; adjusting the auxiliary-duct inlet-velocity ratio to 0.35 did not cause appreciable changes in the recovery. (See fig. 20.) Fairing out the bypass in configuration G-1 reduced the average high-speed pressure recovery to $0.69q_0$ (fig. 20) and caused substantial reductions in

pressure in the lower part of the inlet and at the forward part of the deck. (See fig. 27.)

Series H carburetor ducts.- Configuration H (figs. 5(i) and 7(h)), designed at this Laboratory, was 0.45 inch higher than the original Douglas design and incorporated a scoop-type bypass inlet with enlarged bypass exits located on the sides of the scoop. To avoid reduction in visibility and interference with the gun sight, a raised canopy (fig. 8) was also designed for use with this scoop. A vane was installed in each side of the bypass to insure uniform boundary-layer removal across the inlet. In the original H configuration the pressure recovery at the deck within the high-speed flight region was $0.69q_0$, a value slightly greater than obtained by any previous configuration in which the duct expanded to the full dimensions of the carburetor flange. (See fig. 20.) Pressure distributions for this duct (fig. 28) indicate almost complete removal of the boundary layer in front of the inlet and low pressures at the forward portion of the deck.

Refairing the interior lines to the top of the carburetor venturi, configuration H-1, increased the average high-speed pressure recovery to $0.81q_0$ (fig. 20) and effected a more uniform distribution at the deck (fig. 28). Refairing the top lines of the duct in configuration H-2 to increase diffusion upstream of the bend increased the high-speed ramming pressure by an additional $0.03q_0$. (See fig. 20.)

In configurations H-3 and H-4, the entire scoop was moved forward $1\frac{1}{4}$ inches to permit a reduction in the angle of bend and an increase in the radius ratio of the elbow. The average recovery at the deck of configuration H-3 for the high-speed flight region was $0.88q_0$. Refairing the top lines of the duct in configuration H-4 to reduce excessive expansion at the start of the bend increased the high-speed pressure recovery to $0.91q_0$, the highest value obtained in the present investigation. The pressure distribution at the deck was also made more uniform by the modification.

Series I carburetor ducts. - Configuration I (figs. 5(j), 5(k), and 7(i)) was a twin-entrance nose duct tested to provide a comparison between this type of installation and the scoops previously tested. The average recovery at the deck over the high-speed flight region was $0.67q_0$. (See fig. 20.) The positive slope of the pressure contours in figure 20 indicates improved inlet alignment at higher angles of attack. Pressure distributions for configuration I (fig. 29) show:

- (1) High pressure recoveries at the inlet except at the inboard corner
- (2) Large pressure losses between the inlet and the bend
- (3) Very small pressure losses in the elbow above the carburetor as a result of the large radius ratio of the elbow and the large area contraction in the bend
- (4) Total pressure and flow distributions at the deck more uniform than those obtained in any previous configuration in which the duct expanded to the full dimensions of the carburetor deck

In configuration I-1 (fig. 5(l)), the sharply curved entrance portions of configuration I were removed and new entrances were formed $1\frac{1}{2}$ inches aft of the original inlets. This modification increased the high-speed pressure recovery at the deck to $0.81q_0$ and decreased the sensitivity to angle-of-attack changes. (See fig. 20.) Pressure distributions for this duct (fig. 29) show a much higher recovery at the start of the bend than that obtained with configuration I.

Summary of bypass flow data. - The variation of the bypass flows with angle of attack for several inlet-velocity ratios is shown for scoops A, E, F, G, and H in figure 31. These data show a small decrease in flow through the bypass with increasing angle of attack; the extent of the change was greatest at low values of $Q_b/A_i V_0$. It is noted in figure 31 that the ratio of bypass flow to charge-air flow decreased rapidly with increases in inlet-velocity ratio; however, the quantity

flow through the bypass was essentially independent of carburetor-air flow. The small flows through the bypass of configuration A were caused by the location of the small bypass exits beneath the cowl flaps. Larger flows were obtained by the bypass of configuration E because of the increased bypass exit area and because the exits were moved to a position behind the flaps. Progressively augmented bypass flows were obtained in configurations F, G, and H by enlarging the bypass exit area and locating the exits on the sides of the scoop in regions of low static pressure.

The inlet pressure recovery for a number of scoops at $\alpha = 2.5^\circ$ is plotted against the ratio of bypass flow to inlet flow in figure 32. The inlet pressure increased almost linearly with bypass flow. An inlet pressure recovery of $0.97q_0$ was obtained by configuration H at $\alpha = 2.5^\circ$ by the removal of 113, 53, and 34 percent of the inlet flow at inlet-velocity ratios of 0.19, 0.45, and 0.70, respectively; these air flows correspond to an approximately constant inlet-velocity ratio of 1.3 into the boundary-layer duct. Corresponding inlet pressure recoveries for similar scoops with no bypass flow were approximately $0.73q_0$, $0.78q_0$, and $0.82q_0$.

Surface Pressures over Model

Surface pressures were measured over the cowling, the carburetor scoop, and the canopy to determine the critical Mach numbers of the components; extrapolation of these pressures to high Mach numbers followed the von Kármán relationship given in reference 2.

Cowling. - Surface pressures along the top of the cowling presented in figure 33 show that:

(1) Changing the inlet-velocity ratio from 0.55 to 0.81 at angles of attack between -2.5° and 5° resulted in relatively small increases in the peak negative pressure.

(2) Increasing the angle of attack from -2.5° to 5° more than doubled the peak negative pressure over the top of the cowl.

(3) The stagnation point invariably occurred on the outside of the cowl lip. The peak negative pressure ($-0.41q_0$, measured at $\alpha = 5^\circ$ and $\frac{Q_c}{A_c V_o} = 0.55$) corresponds to a critical speed of about 525 miles per hour at an altitude of 16,000 feet in standard air. It is noted that the high-speed-flight angle of attack would actually be much lower than 5° .

The location of the stagnation point on the outside of the cowl lip presents evidence of flow distortion at the top of the inlet supplementing the tuft study (fig. 13). The probable streamlines at the inlet as constructed from these data are shown in figure 34. Inasmuch as the distortion of the inlet flow was shown to have caused large losses of pressure at the top of the orifice plate at $\frac{Q_c}{A_c V_o} = 0.55$ (figs. 12 and 13), it is recommended that the flow at the top of the inlet be further investigated.

Carburetor scoop and canopy. - Surface pressures along the top of the original carburetor scoop and the original canopy are presented in figure 35. The negative pressures over both the scoop and the canopy increased with angle of attack. The negative pressures over the scoop also increased rapidly with decreases in the inlet-velocity ratio of the carburetor inlet; pressures on the canopy were not appreciably affected by this variable.

The peak negative pressure over the original carburetor scoop was not definitely established, but it appears probable that it would not exceed $-1.0q_0$ for any of the high-speed conditions.

The peak negative pressures over the original canopy varied from $-1.21q_0$ at $\alpha = -2.5^\circ$ to $-1.48q_0$ at $\alpha = 5^\circ$. These pressures correspond to critical speeds, in standard air at 16,000 feet, of 398 and 371 miles per hour, respectively. The canopy appears, therefore, to be acceptable from the critical-speed standpoint. A steep positive pressure gradient downstream of the negative pressure peak, however, has been shown in reference 3 to be associated with high drag.

Pressure distributions over the modified canopy (fig. 8) are presented in figure 36. Peak negative

pressures occurred at the top of the canopy and varied from $-0.67q_0$ at $\alpha = -2.5^\circ$ to $-0.87q_0$ at $\alpha = 5^\circ$.

These negative peak pressures correspond to critical speeds, in standard air at 16,000 feet, of 472 and 438 miles per hour. It is noted that the pressures on the sides of the canopy are nearly equal to those on the top and that the slope of the adverse pressure gradient downstream of the negative peak was substantially reduced.

Drag Results

A summary of the drag data obtained during the investigation is presented in table I. The drag increments shown are based on a 3/10-scale wing area of 54.5 square feet. These increments were obtained by subtracting the drag of the basic model and the drag chargeable to the decrease in momentum of the carburetor air along the x-axis from the measured drag of the complete installation. The drag coefficient of the basic model was obtained from tests of the original model with the inlet and bypass of carburetor scoop A faired over and with cowl flaps flush. The drag coefficients given in the table are somewhat erratic; however, the following trends are observed consistently:

- (1) The drag of the scoops increased with increases in α and with decreases in $Q_i/A_i V_o$.
- (2) Replacing scoop A and the original canopy with scoop H and the modified canopy reduced the drag.
- (3) At angles of attack less than 5° , replacing scoop A with scoop I-1 decreased the drag coefficient of the model at high inlet-velocity ratios but increased it at low values of $Q_i/A_i V_o$.
- (4) Fairing out the bypasses of configurations A and H reduced the drag coefficients of the model by about 0.0002 and 0.0004, respectively.
- (5) The drag of the model with the modified canopy and scoop H with a sealed inlet was slightly lower than that of the basic model.

(6) Opening the cowl flaps increased the drag coefficient of the model by 0.0063 at $\alpha = -2.5^\circ$ and 0.0048 at $\alpha = 10^\circ$.

SUMMARY OF RESULTS

The principal results of the propeller-off tests are summarized as follows:

1. The original scoop, configuration A, had an average ramming pressure at the carburetor flange of $0.60q_0$ over the range of high-speed flight conditions.

2. A high-speed ramming pressure of $0.91q_0$ and a more uniform flow at the carburetor flange were obtained by configuration H-4 without increasing the drag of the model. The increase in pressure over that obtained by configuration A is equivalent to an increase in critical altitude of the airplane of approximately 1200 feet and a corresponding increase in top speed of about 5.6 miles per hour.

3. Adequate boundary-layer removal must be provided to obtain a high ramming pressure and uniform flow conditions into the scoop.

4. Maximum carburetor-deck pressure recoveries for those scoops without bypasses appeared to occur at inlet-velocity ratios between 0.3 and 0.5. Optimum inlet-velocity ratios for configurations with adequate boundary-layer removal were somewhat lower.

5. The internal duct losses were decreased by eliminating the expansion in the bend, reducing the angle of the bend of the elbow, and increasing the radius ratio of the elbow.

6. Opening the cowl flaps 16° caused the boundary layer to separate in front of a typical configuration not equipped with a bypass.

7. The drags of scoops A and H were decreased approximately 0.0002 and 0.0004, respectively, by fairing out the bypasses.

8. Scoops extending to the front of the cowl were less sensitive to changes in angle of attack than scoops located at the rear of the cowl.

9. Stagnant or reversed flow was noted at the spinner surface at the top of the cowl inlet for the low-angle-of-attack, low-inlet-velocity-ratio condition; at approximately the same inlet-velocity ratio, an unusually rapid upsweep in the flow in front of the inlet was also observed at high angles of attack. The pressure recovery at the top and bottom of the cowl orifice plate was very sensitive to changes in angle of attack.

10. The critical speed of the cowling was well above the maximum speed of the airplane.

11. A steep adverse pressure gradient was measured at the top of the original canopy.

12. Substitution of the modified canopy for the original canopy increased the critical speed and reduced the drag a small amount.

Langley Memorial Aeronautical Laboratory
National Advisory Committee for Aeronautics
Langley Field, Va., June 7, 1944

REFERENCES

1. Corson, Blake W., Jr.: The Belt Method for Measuring Pressure Distribution. NACA RB, Feb. 1943.
2. von Kármán, Th.: Compressibility Effects in Aerodynamics. Jour. Aero. Sci., vol. 8, no. 9, July 1941, pp. 337-356.
3. Delano, James B., and Wright, Ray H.: Investigation of Drag and Pressure Distribution of Windshields at High Speeds. NACA ARR, Jan. 1942.

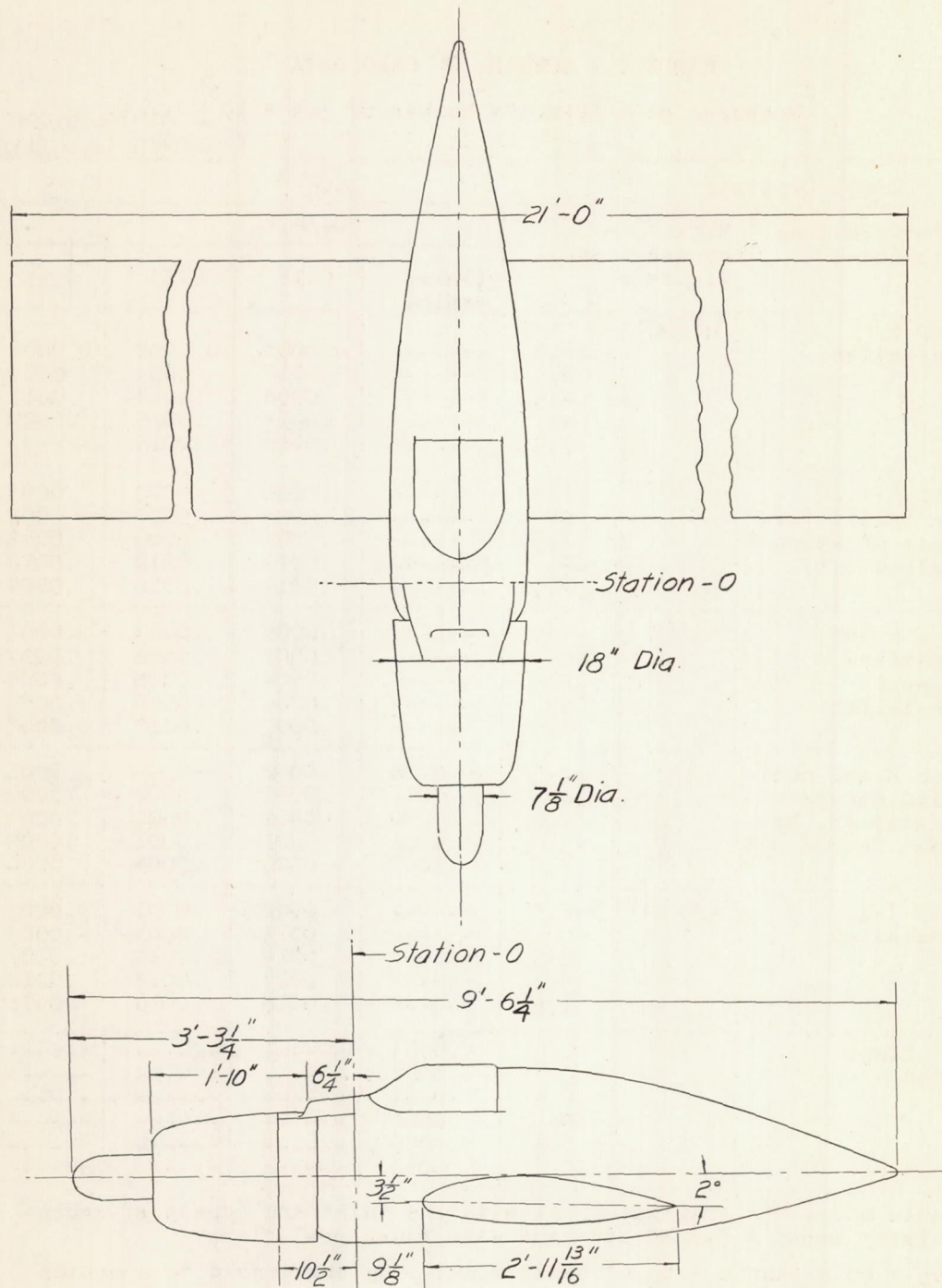
TABLE I.- SUMMARY OF DRAG DATA

Measured at a Reynolds number of 3.4×10^6 NATIONAL ADVISORY
COMMITTEE FOR AERONAUTICS

Model Condition	Ref- erence figure	α (deg)	ΔC_D ^b	$Q_1/A_1 V_0$		
				0 (inlet sealed)	0.18	0.33
Scoop A installed	3, 5(a)	-2.5	-----	0.0008	0.0008	0.0006
		0	-----	.0010	.0009	.0007
		2.5	-----	.0008	.0012	.0011
		5	-----	.0013	.0010	.0007
		7.5	-----	.0016	.0015	-----
Scoop A-1 installed (by- pass of scoop A faired out)	5(b)	-2.5	-----	.0006	.0003	.0003
		0	-----	.0008	.0007	.0005
		2.5	-----	.0007	.0006	.0006
		5	-----	.0011	.0012	.0012
		7.5	-----	.0014	.0016	.0004
Scoop H and modified canopy installed	5(i)	-2.5	-----	.0002	.0003	.0001
		0	-----	.0007	.0008	.0007
		2.5	-----	.0004	.0008	.0004
		5	-----	.0006	.0009	.0004
		7.5	-----	.0007	.0012	.0003
Scoop H and modi- fied canopy installed, by- pass faired out	-do-	-2.5	-0.0008	.0002	-.0004	-.0001
		0	-.0001	.0005	.0002	.0006
		2.5	.0000	.0002	.0000	.0003
		5	-.0001	.0001	.0001	.0005
		7.5	-.0001	.0006	.0004	.0000
Scoop I-1 installed	5(j), 5(k)	-2.5	-----	.0002	.0001	-.0003
		0	-----	.0013	.0004	-.0003
		2.5	-----	.0019	.0010	.0007
		5	-----	.0024	.0018	.0012
		7.5	-----	.0018	.0016	.0011
Cowl flaps opened	4(c)	-2.5	.0063	-----	-----	-----
		0	.0063	-----	-----	-----
		2.5	.0063	-----	-----	-----
		5	.0060	-----	-----	-----
		7.5	.0056	-----	-----	-----
		10	.0048	-----	-----	-----

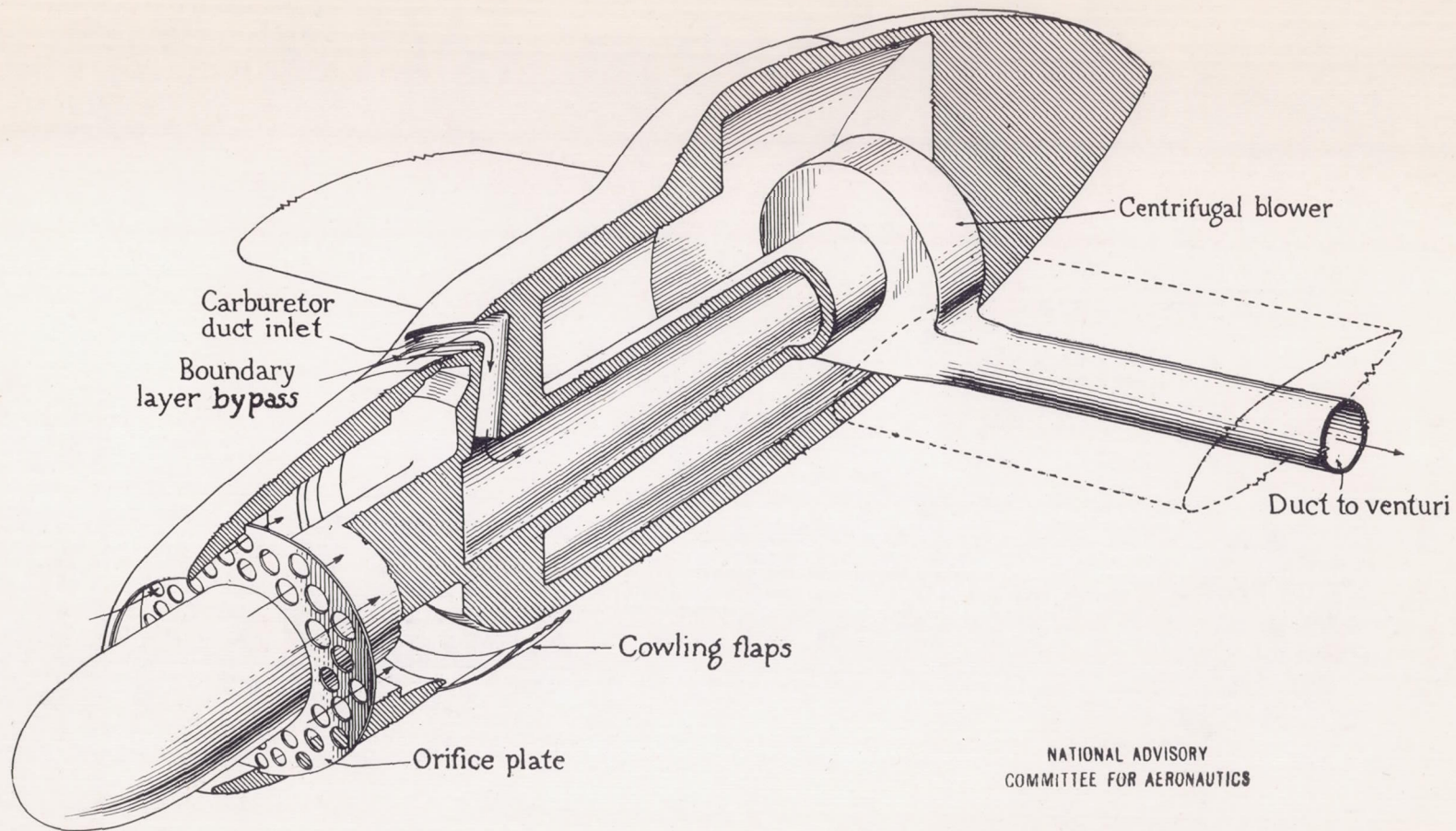
^a Basic model was original model with the inlet and bypass of carburetor scoop A faired over and with flush cowl flaps.

^b $\Delta C_D = C_D \text{ measured} - C_D \text{ of basic model} - C_D \text{ chargeable to momentum decrease of carburetor air.}$



NATIONAL ADVISORY
COMMITTEE FOR AERONAUTICS

Figure 1 .- General arrangement and basic dimensions
of model.



NATIONAL ADVISORY
COMMITTEE FOR AERONAUTICS

Figure 2.-Interior arrangement of model.

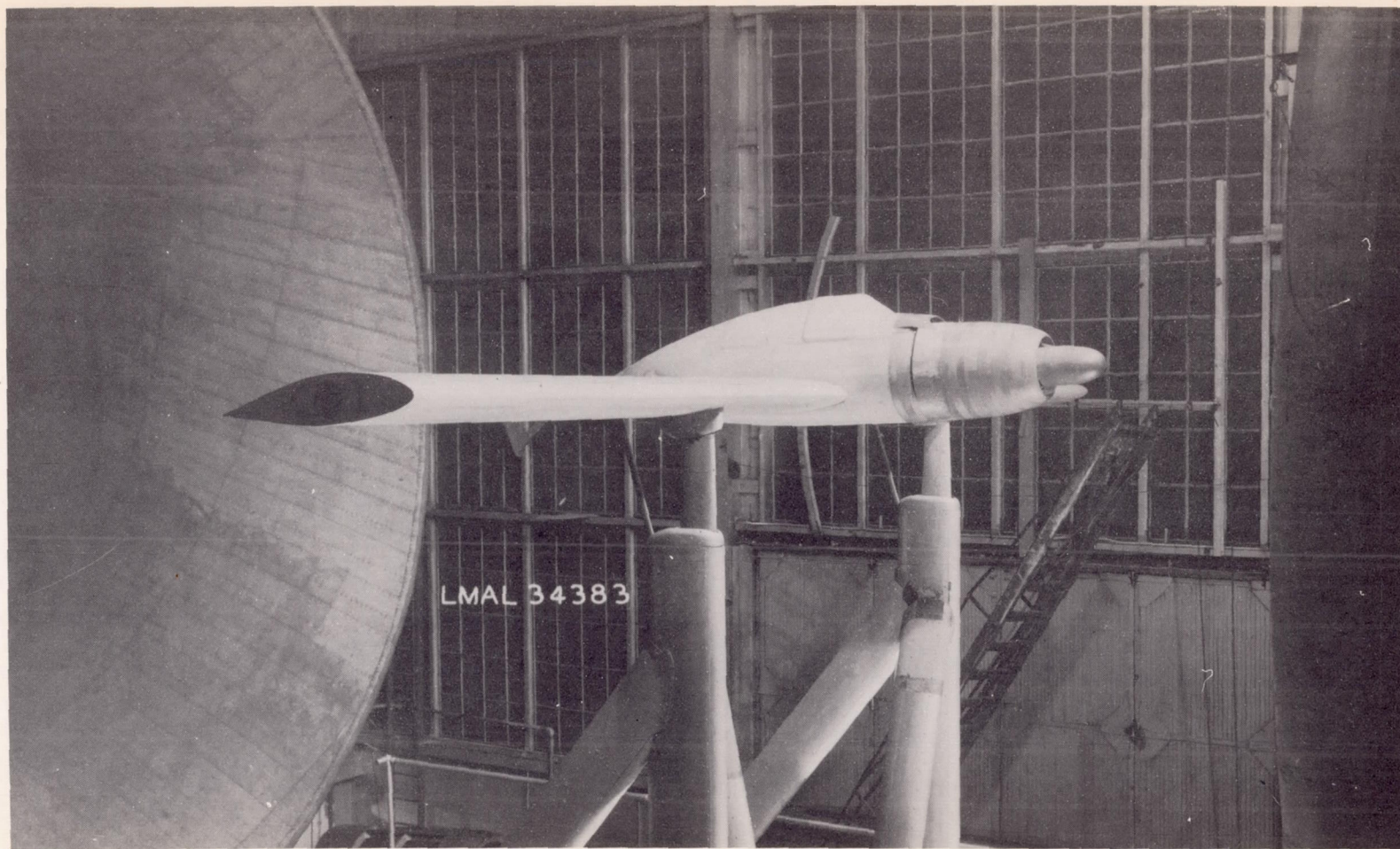
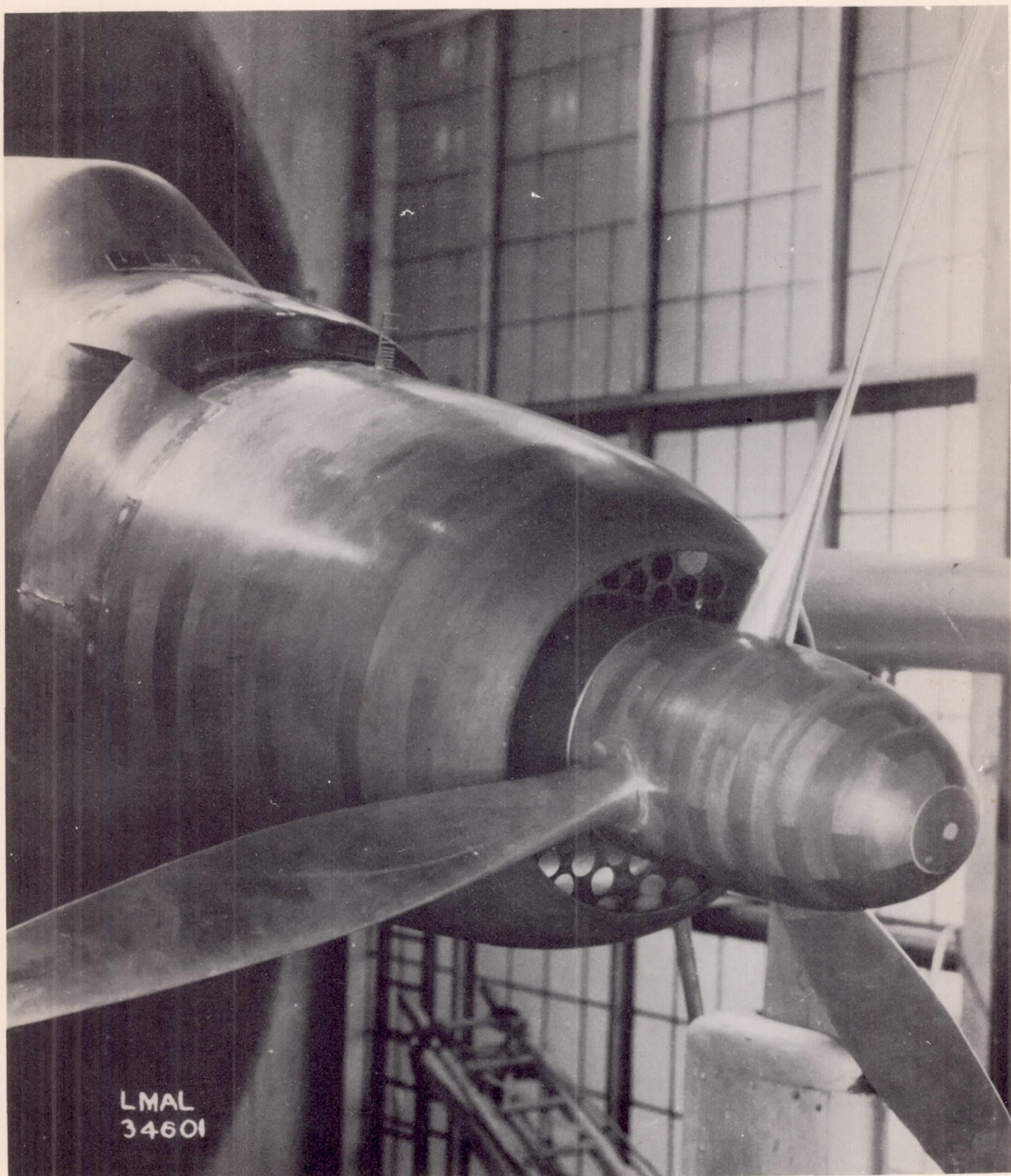


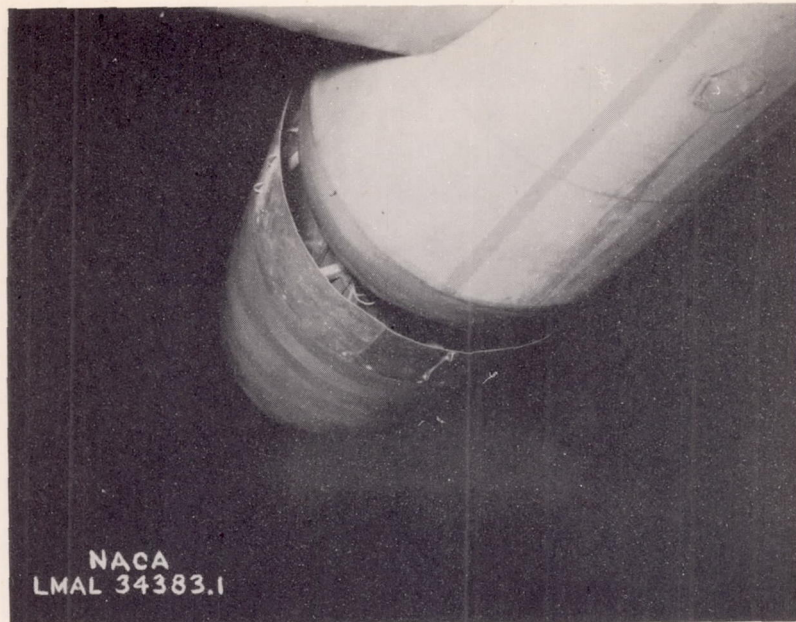
Figure 3.- General view of XTB2D-1 carburetor-ram model mounted in the propeller-research tunnel.



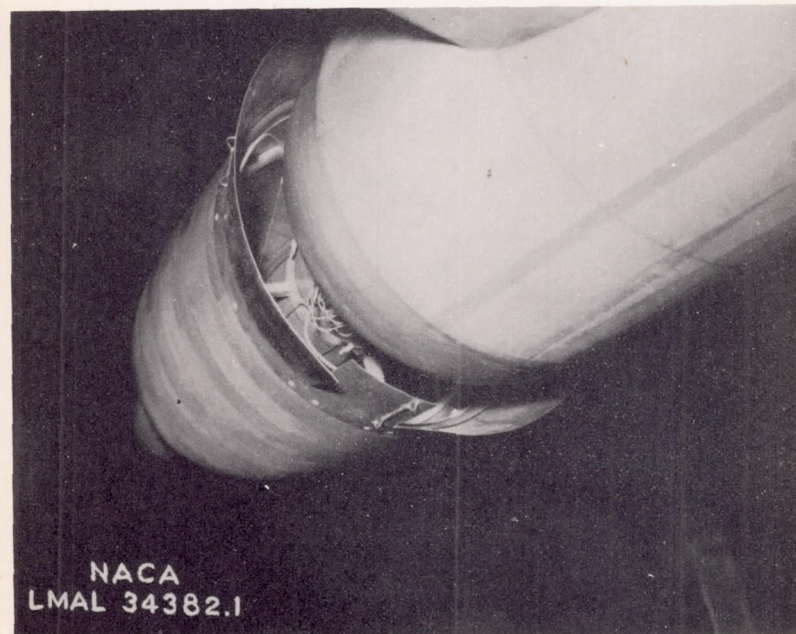
(a) Inlet.

Figure 4.- Detailed views of cowling.

L-751

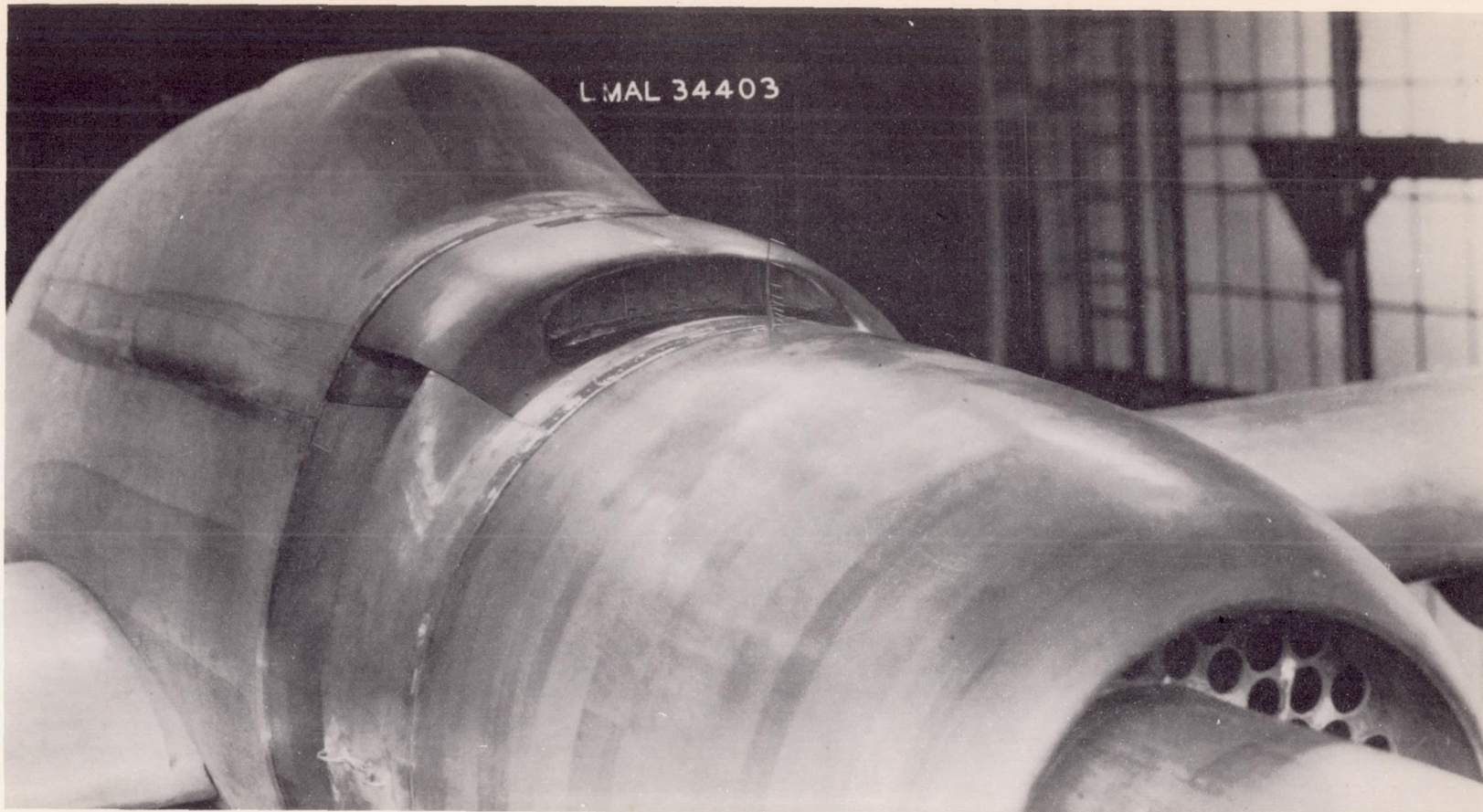


(b) Outlet with flaps at 0° .



(c) Outlet with flaps at 16° .

Figure 4.- Concluded.



(a) Carburetor-duct configuration A.

Figure 5.- Views of the several carburetor air duct configurations installed on the model.



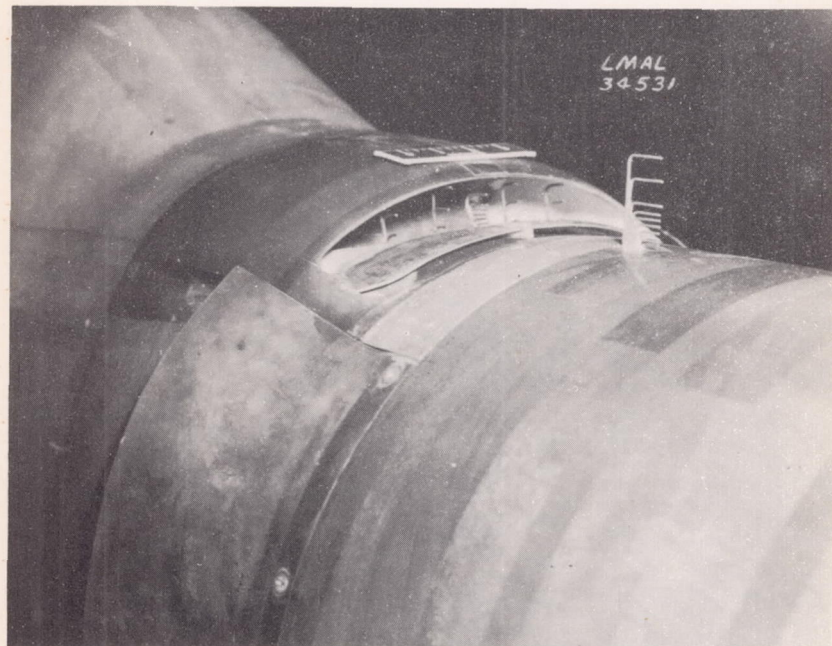
(b) Carburetor-duct configuration A-1.

Figure 5.- Continued.



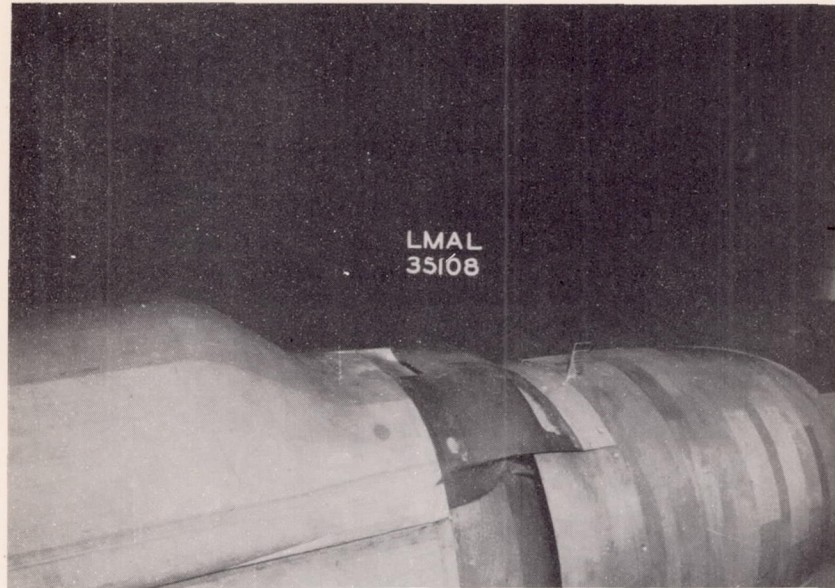
(c) Carburetor-duct configuration B.

Figure 5.- Continued.

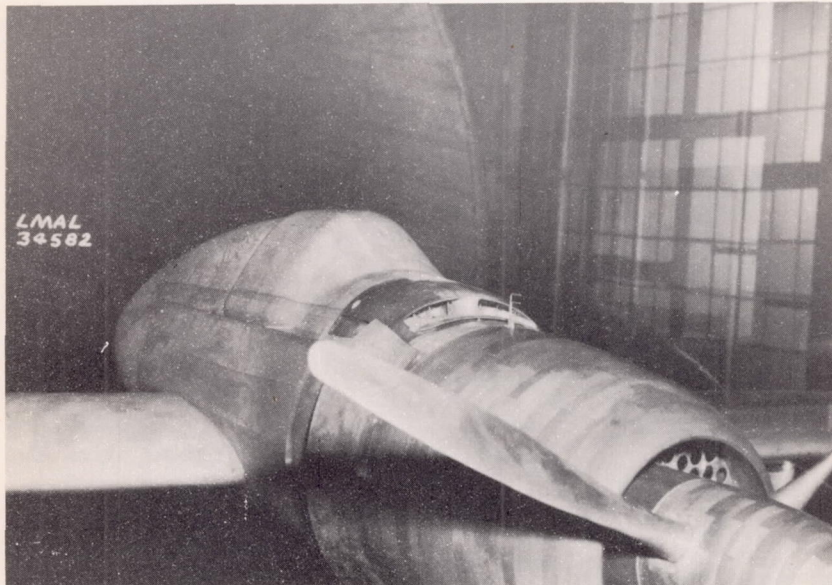


(d) Carburetor-duct configuration C.

Figure 5.- Continued.



(1) Three-quarter rear view.



(2) Three-quarter front view.

(e) Carburetor-duct configuration D.

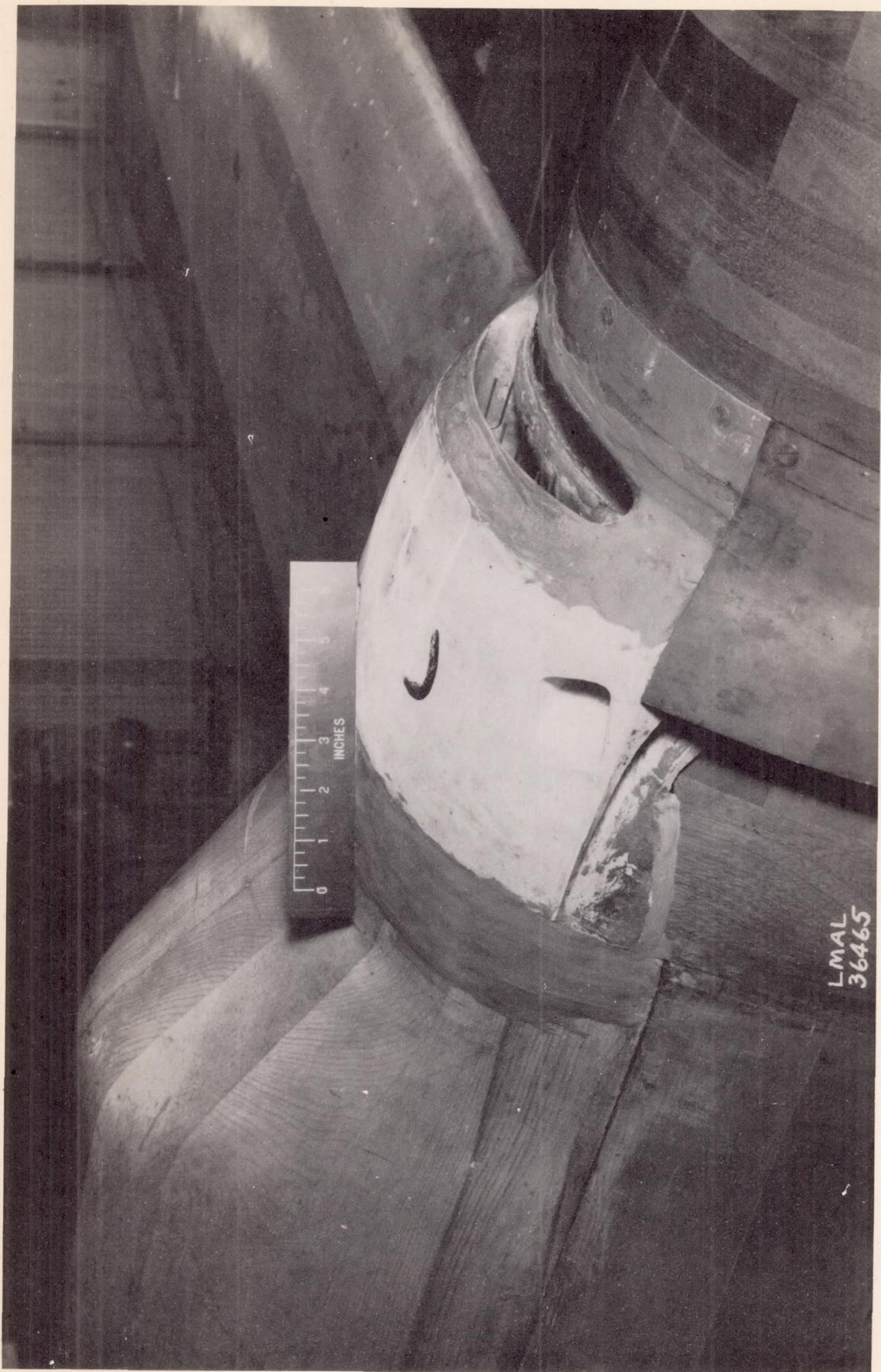
Figure 5.- Continued.



(f) Carburetor-duct configuration E.

Figure 5.- Continued.

L-751



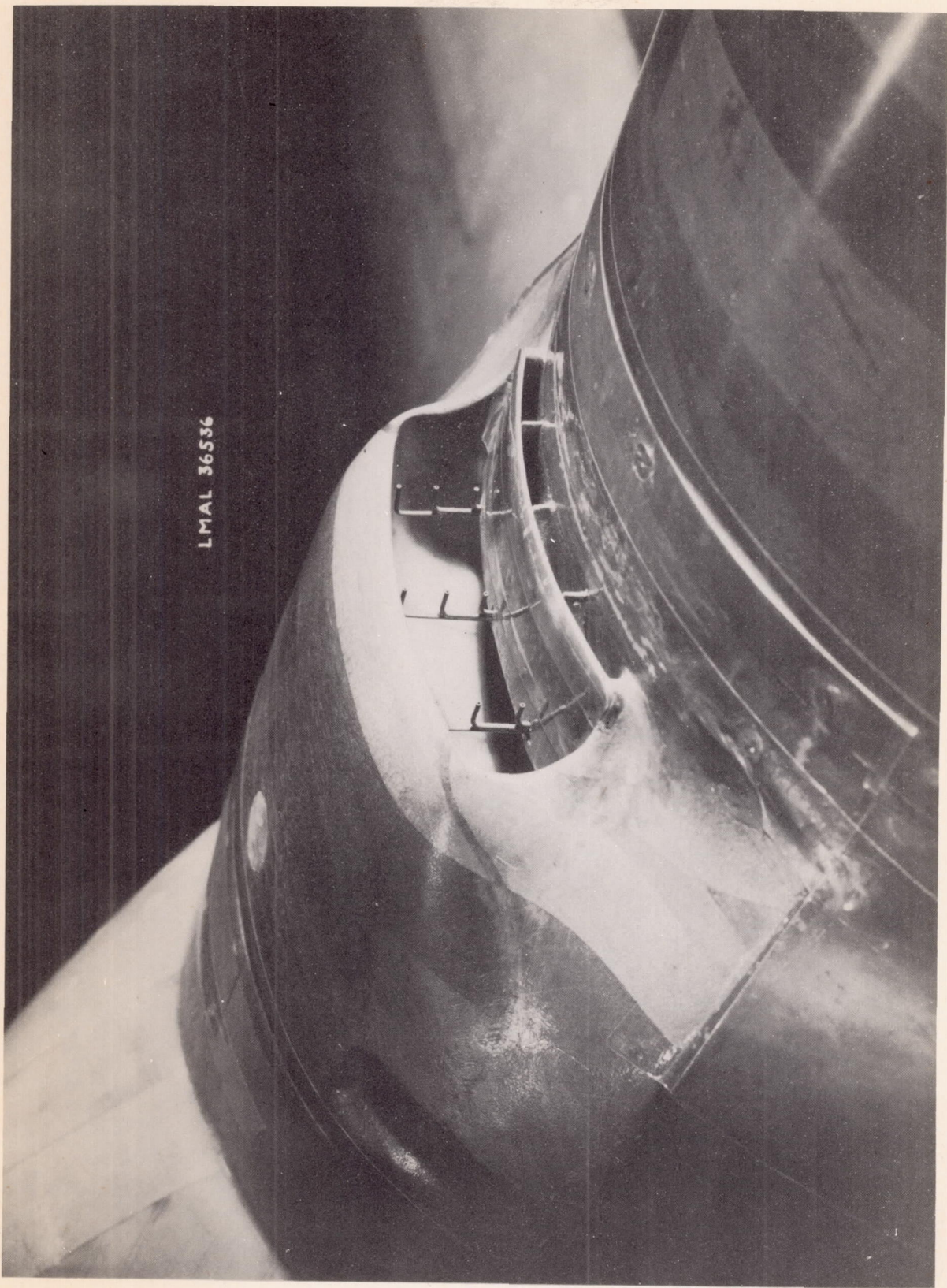
(g) Carburetor-duct configuration F.

Figure 5.- Continued.



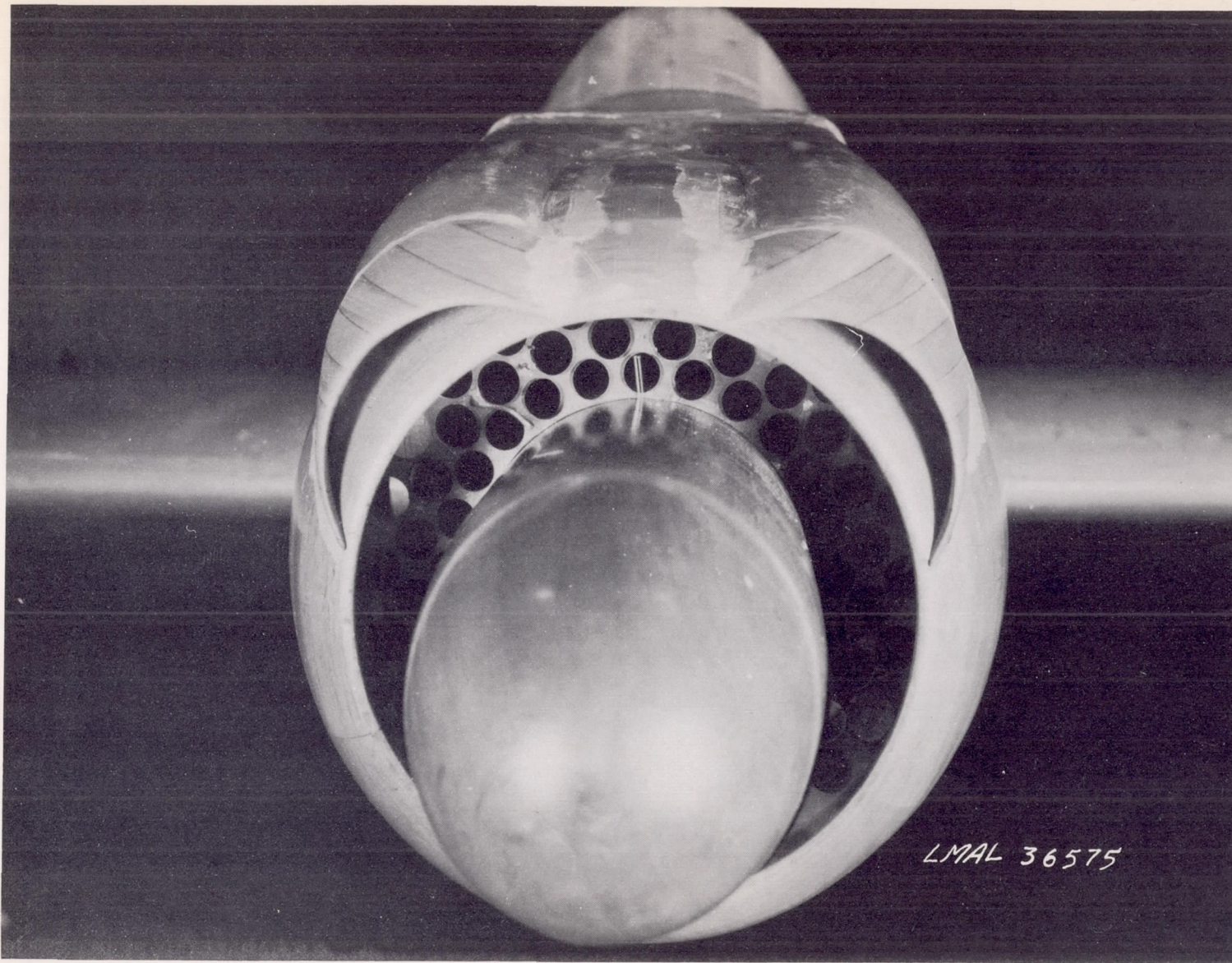
(h) Carburetor-duct configuration G.

Figure 5.- Continued.



(i) Carburetor-duct configuration H.

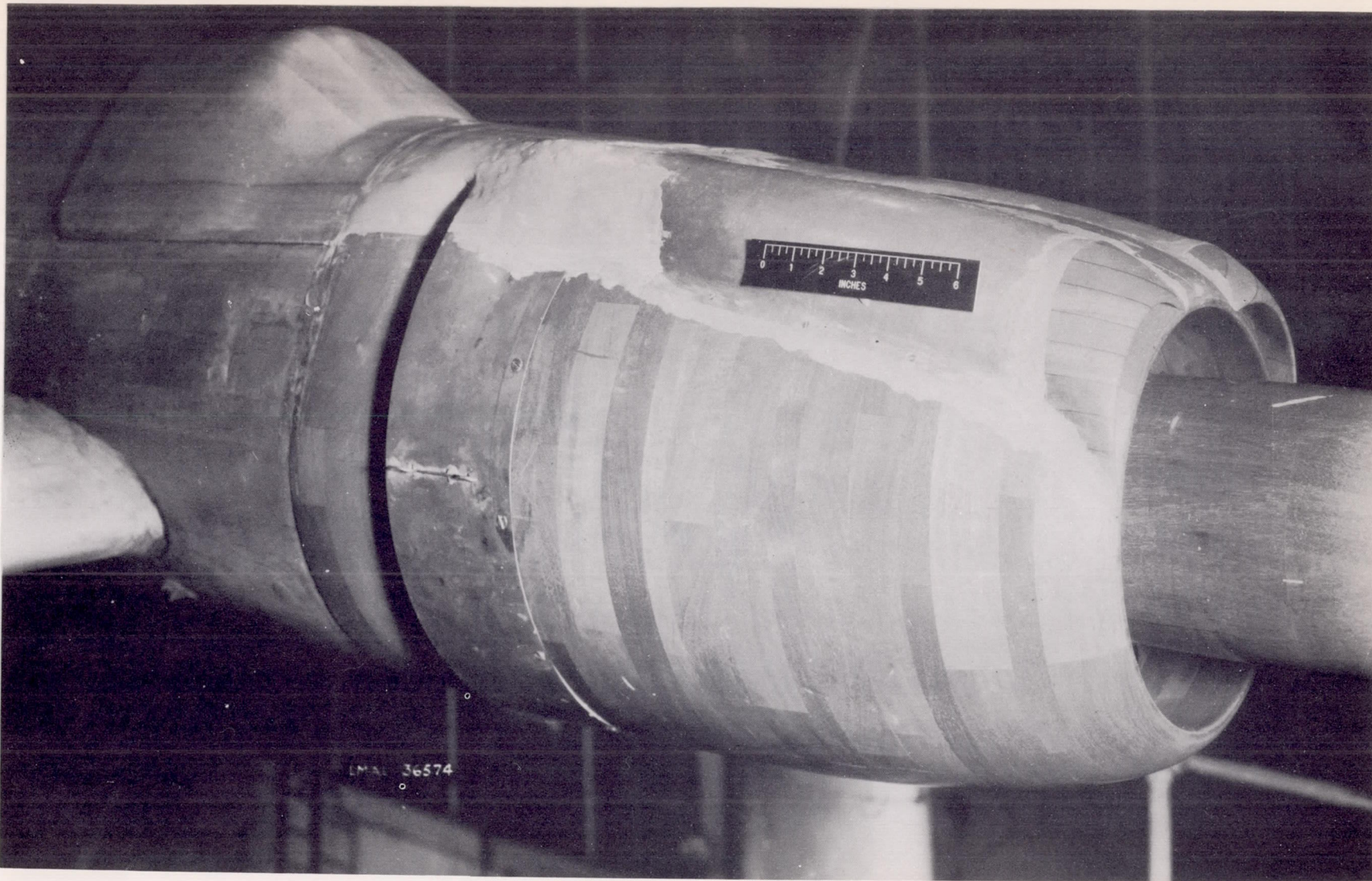
Figure 5.- Continued.



LMAL 36575

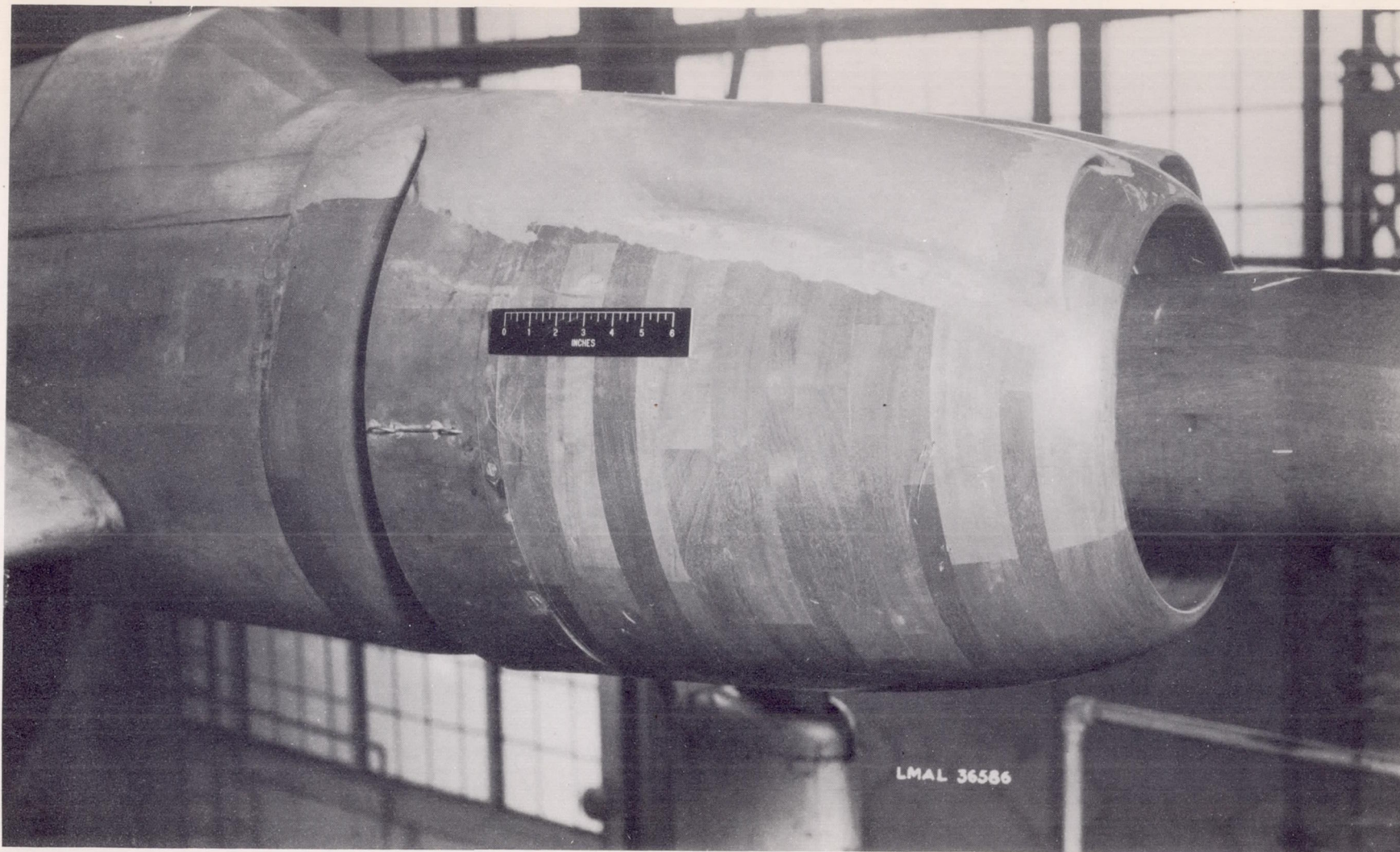
(j) Carburetor-duct configuration I, front view.

Figure 5.- Continued.



(k) Carburetor-duct configuration I, three-quarter side view.

Figure 5.- Continued.



(1) Carburetor-duct configuration I-1, three-quarter side view.

Figure 5.- Concluded.

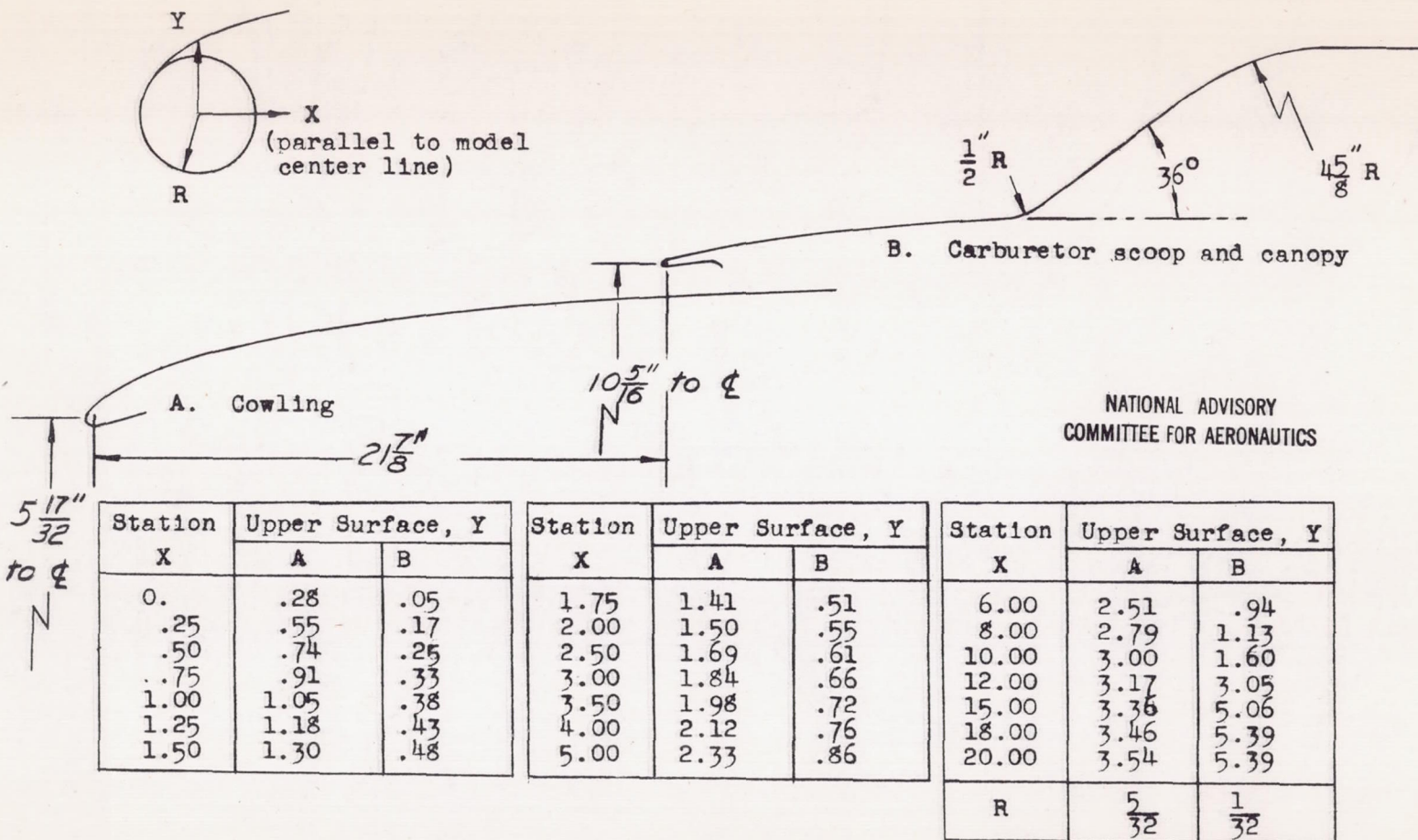
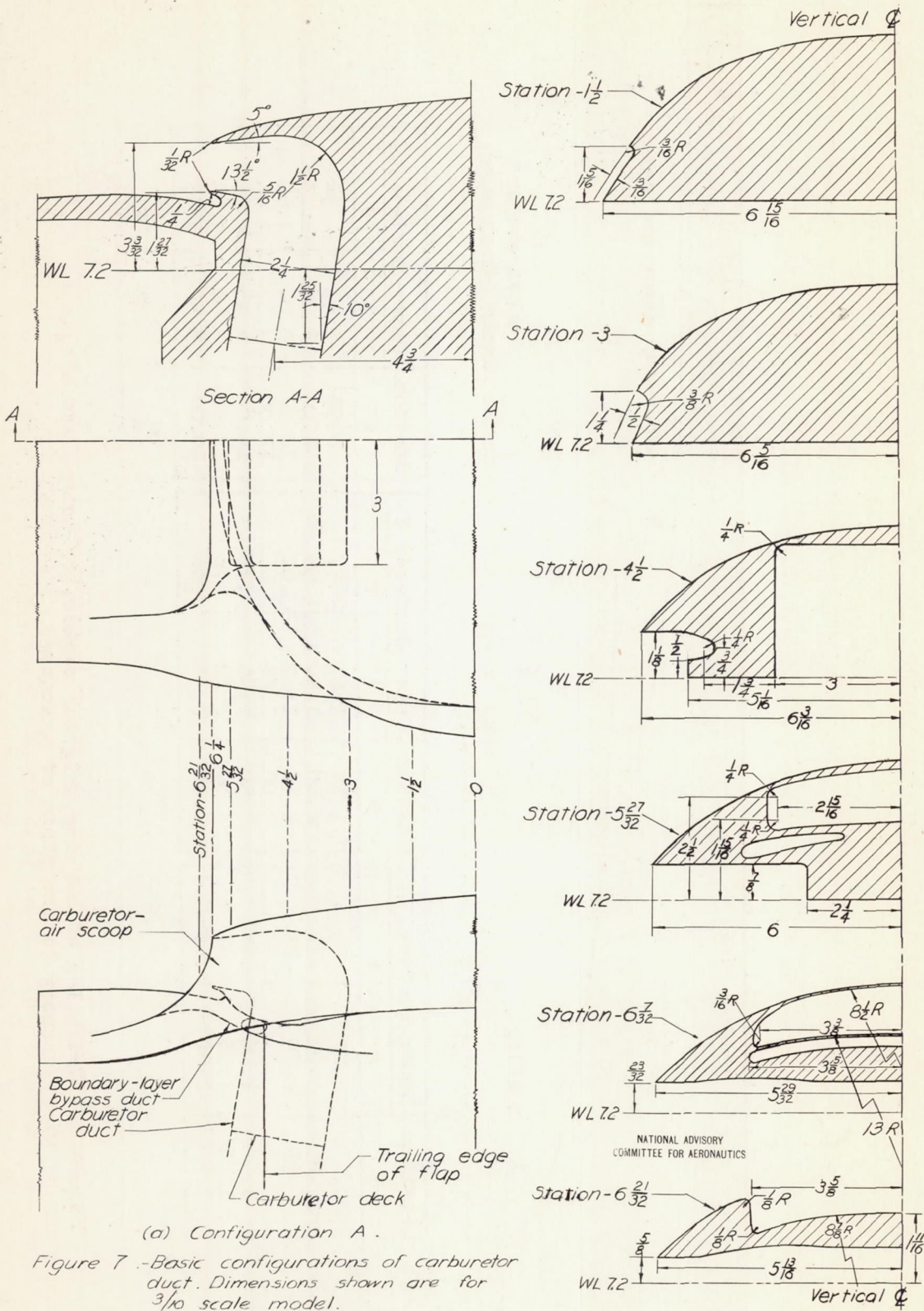
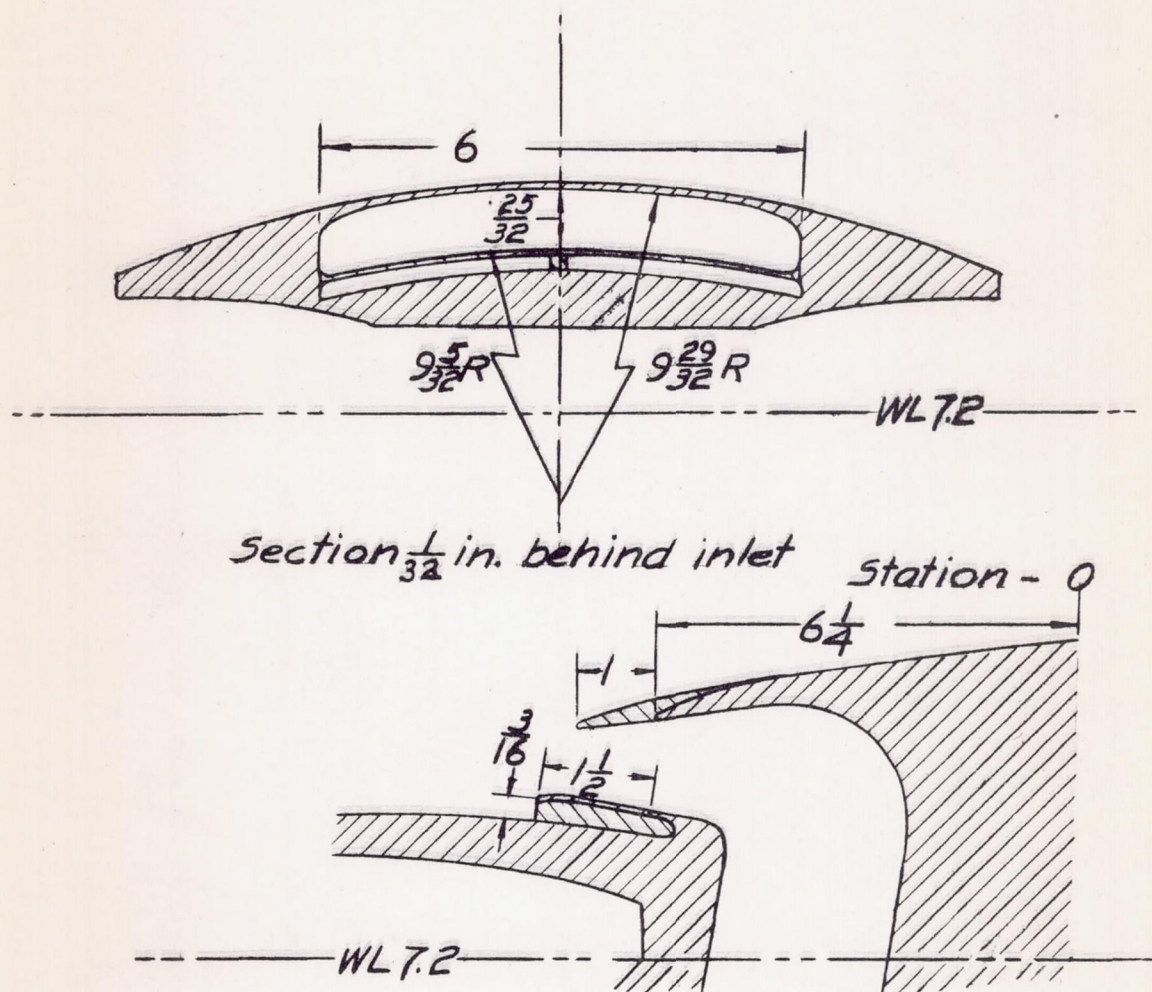


Figure 6.- Ordinates of cowling, original carburetor scoop, and original canopy in the plane of symmetry.



(a) Configuration A.

Figure 7.-Basic configurations of carburetor duct. Dimensions shown are for $\frac{3}{10}$ scale model.



Note : Interior lines and bypass same as for configuration A. See figure 7 (a)

(b) Configuration B

NATIONAL ADVISORY
COMMITTEE FOR AERONAUTICS

Figure 7.-Continued.

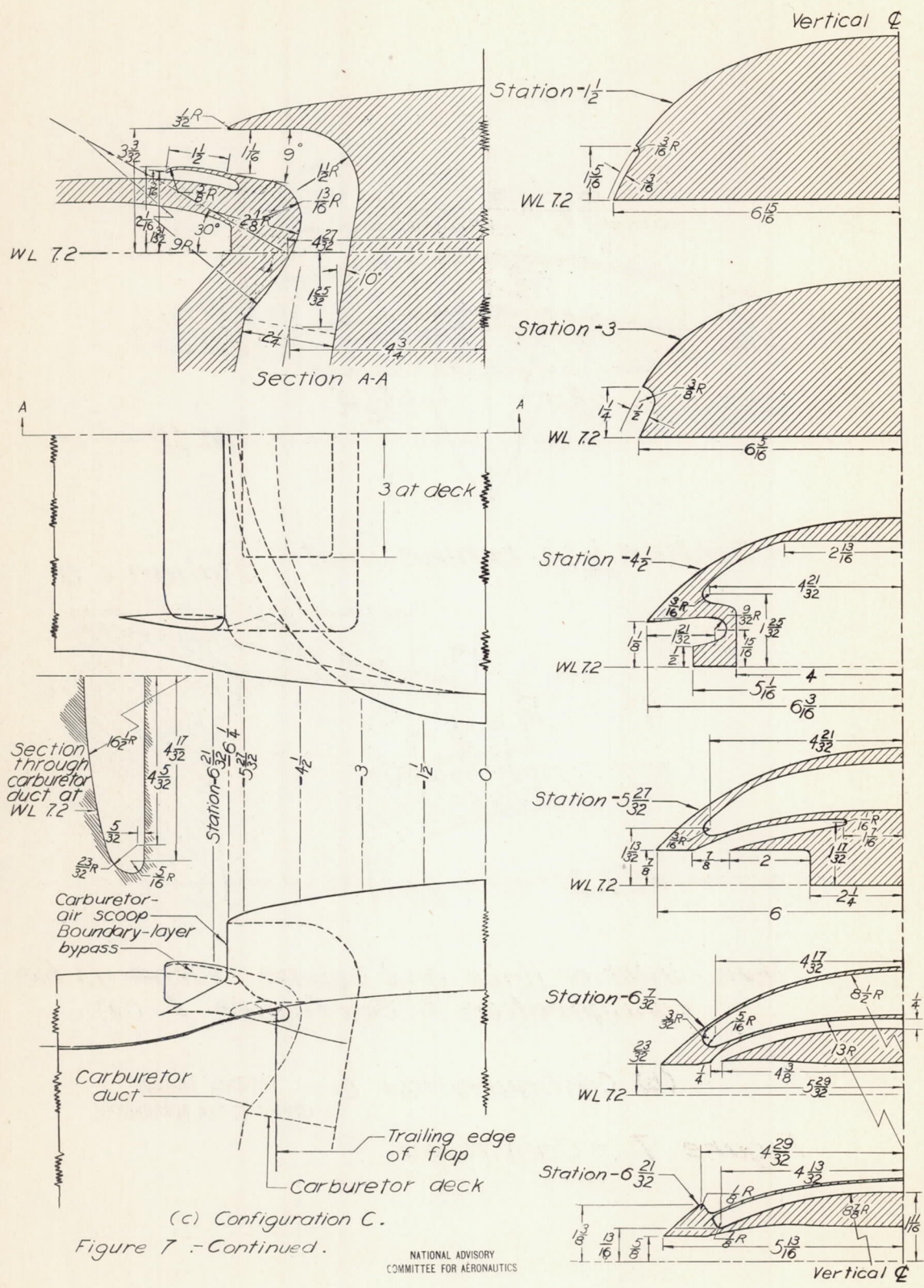
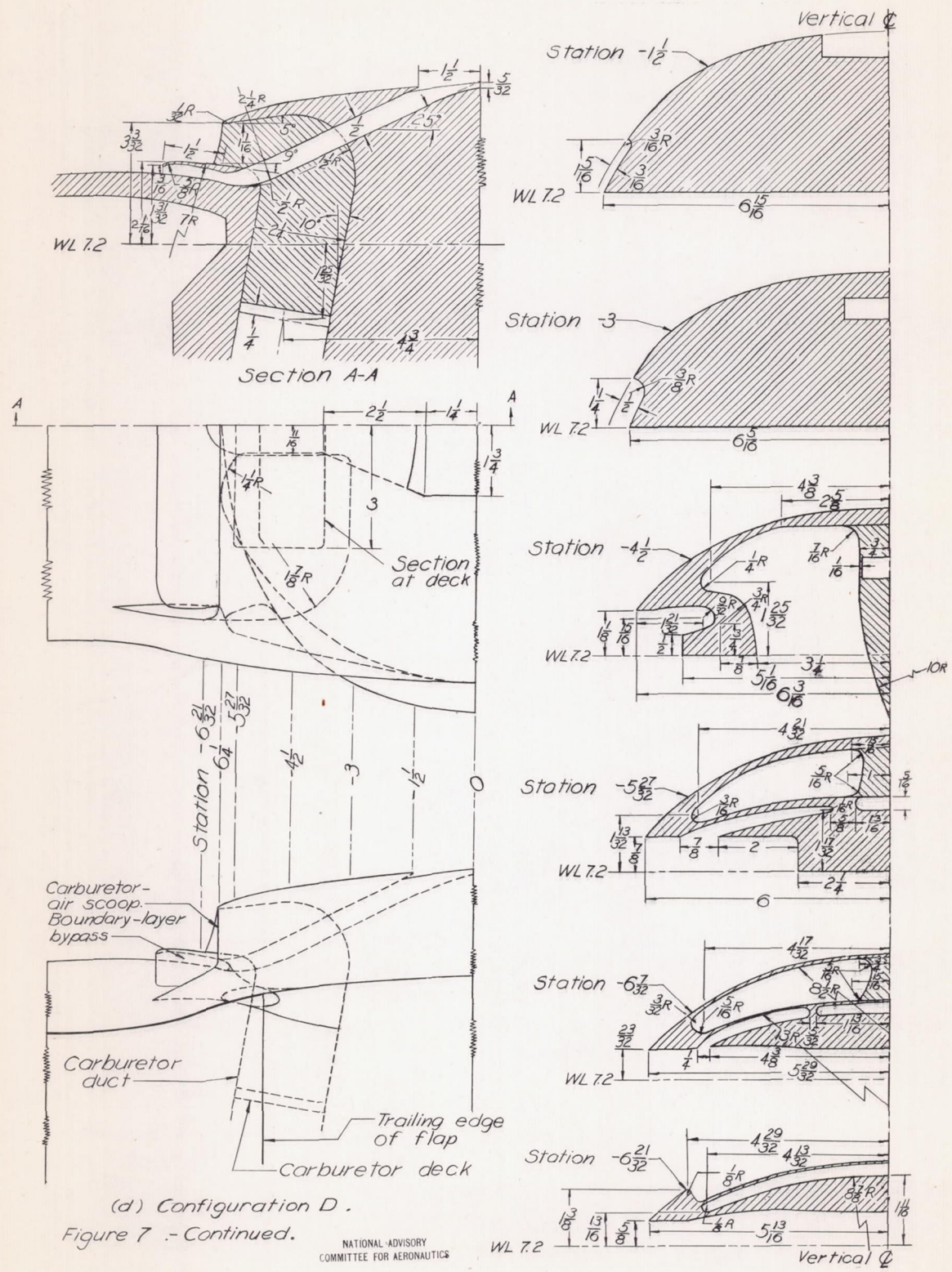
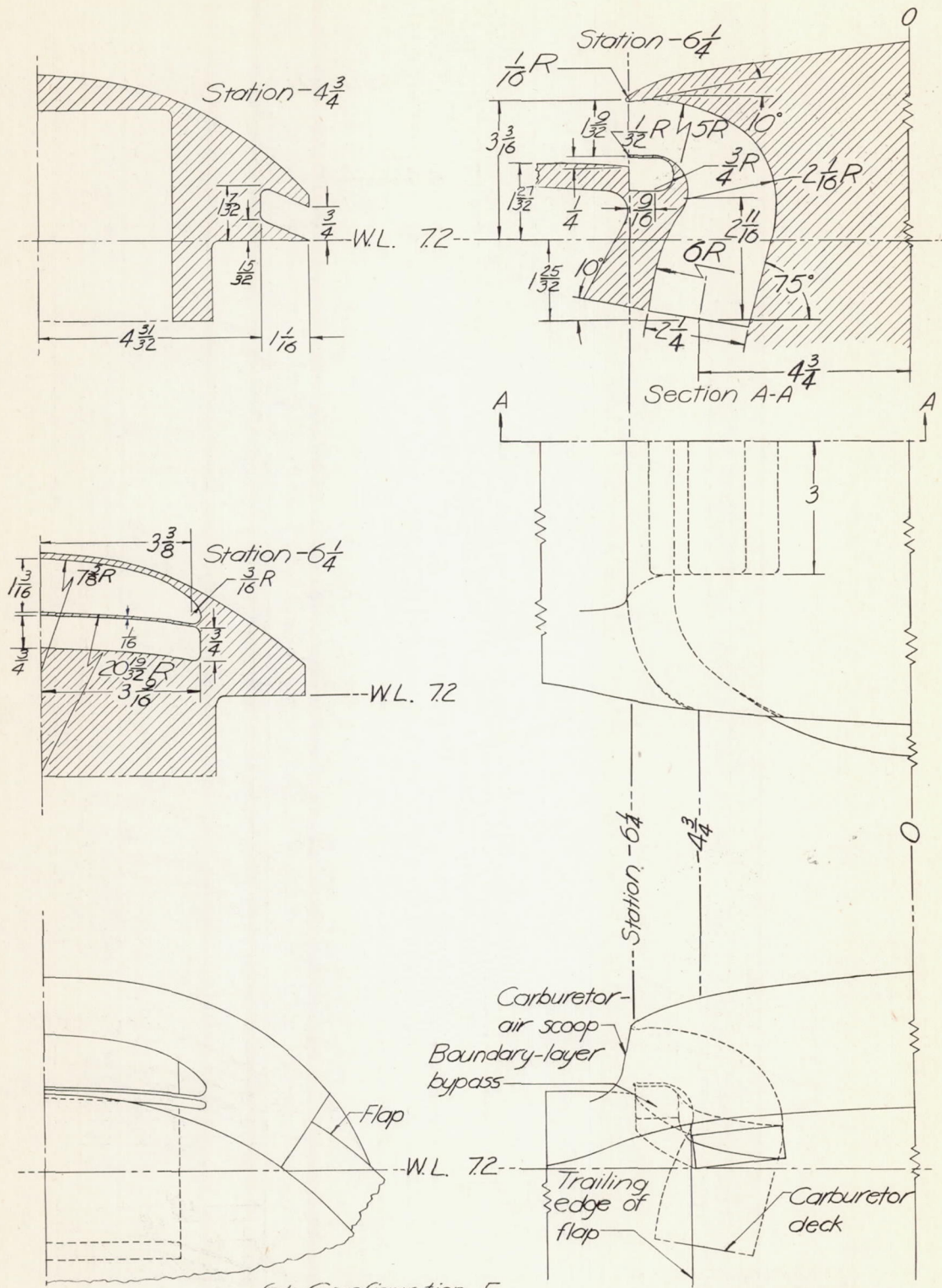


Figure 7 -Continued.

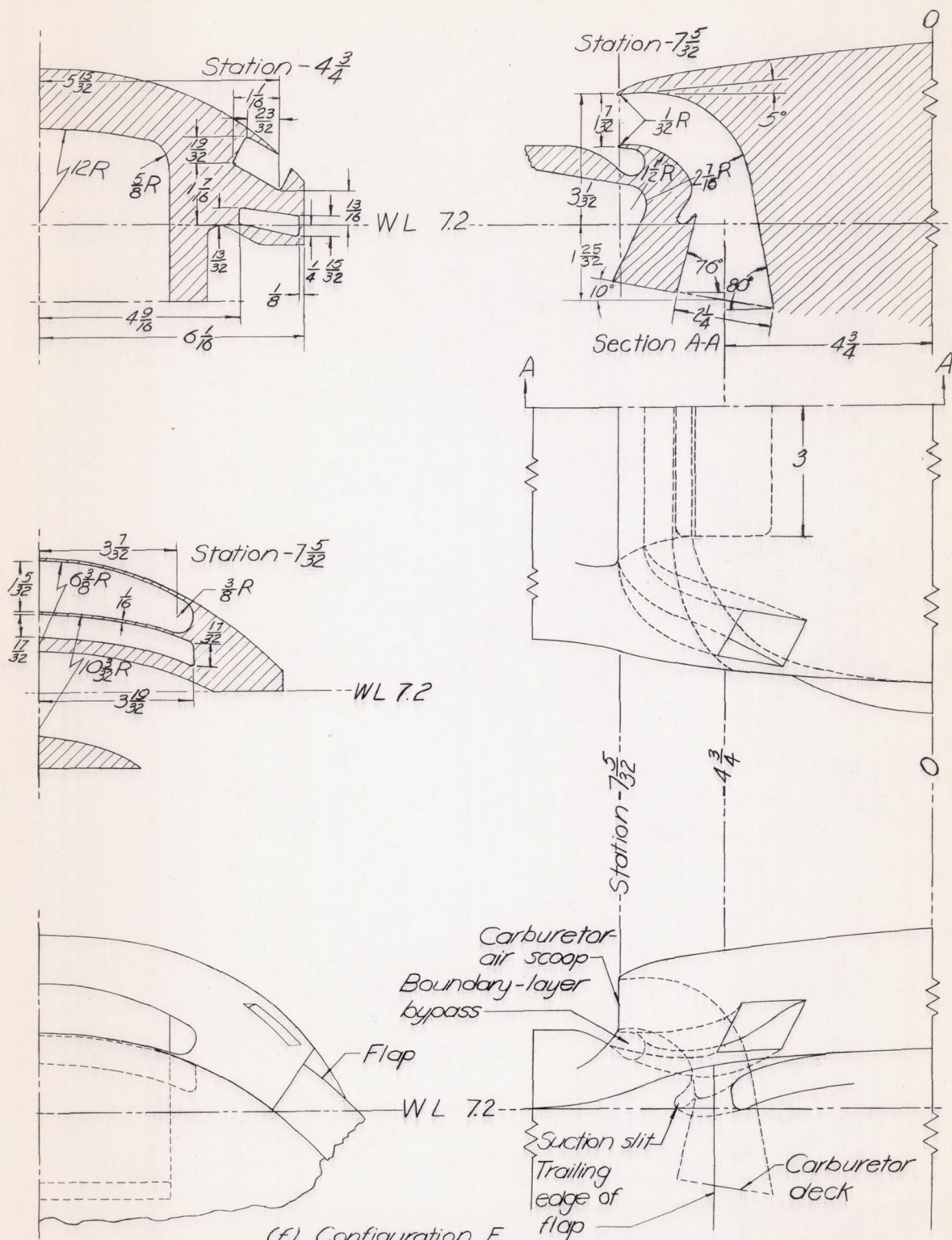
NATIONAL ADVISORY
COMMITTEE FOR AERONAUTICS





(e) Configuration E.
Figure 7.-Continued.

NATIONAL ADVISORY
COMMITTEE FOR AERONAUTICS



(F) Configuration F.
Figure 7.—Continued.

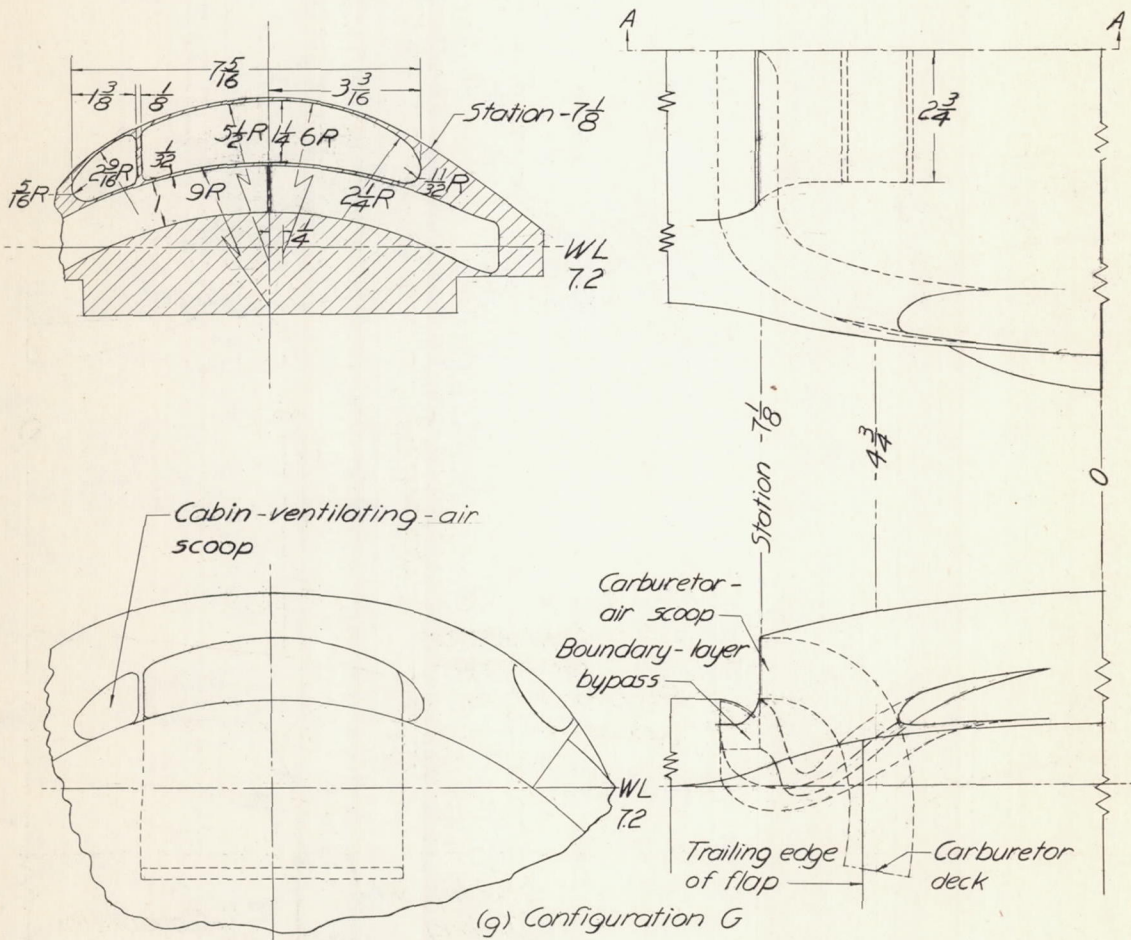
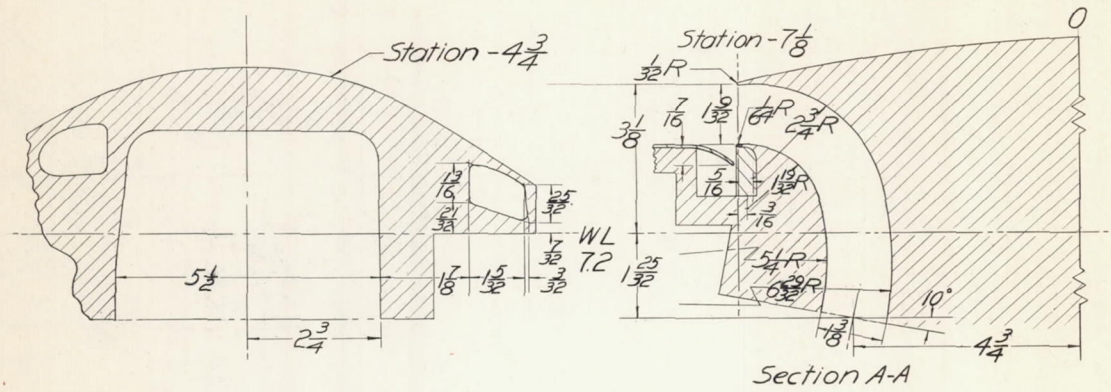
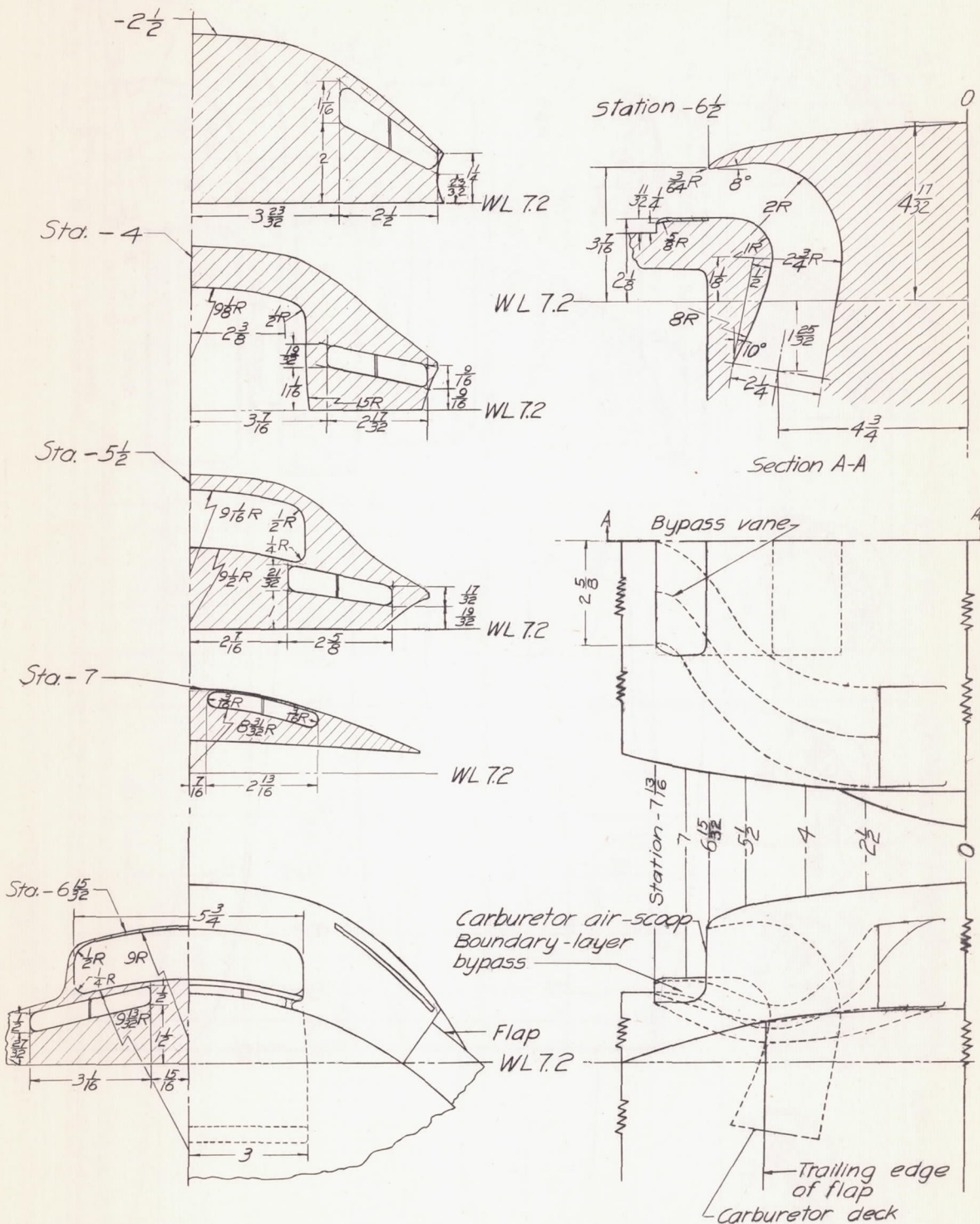
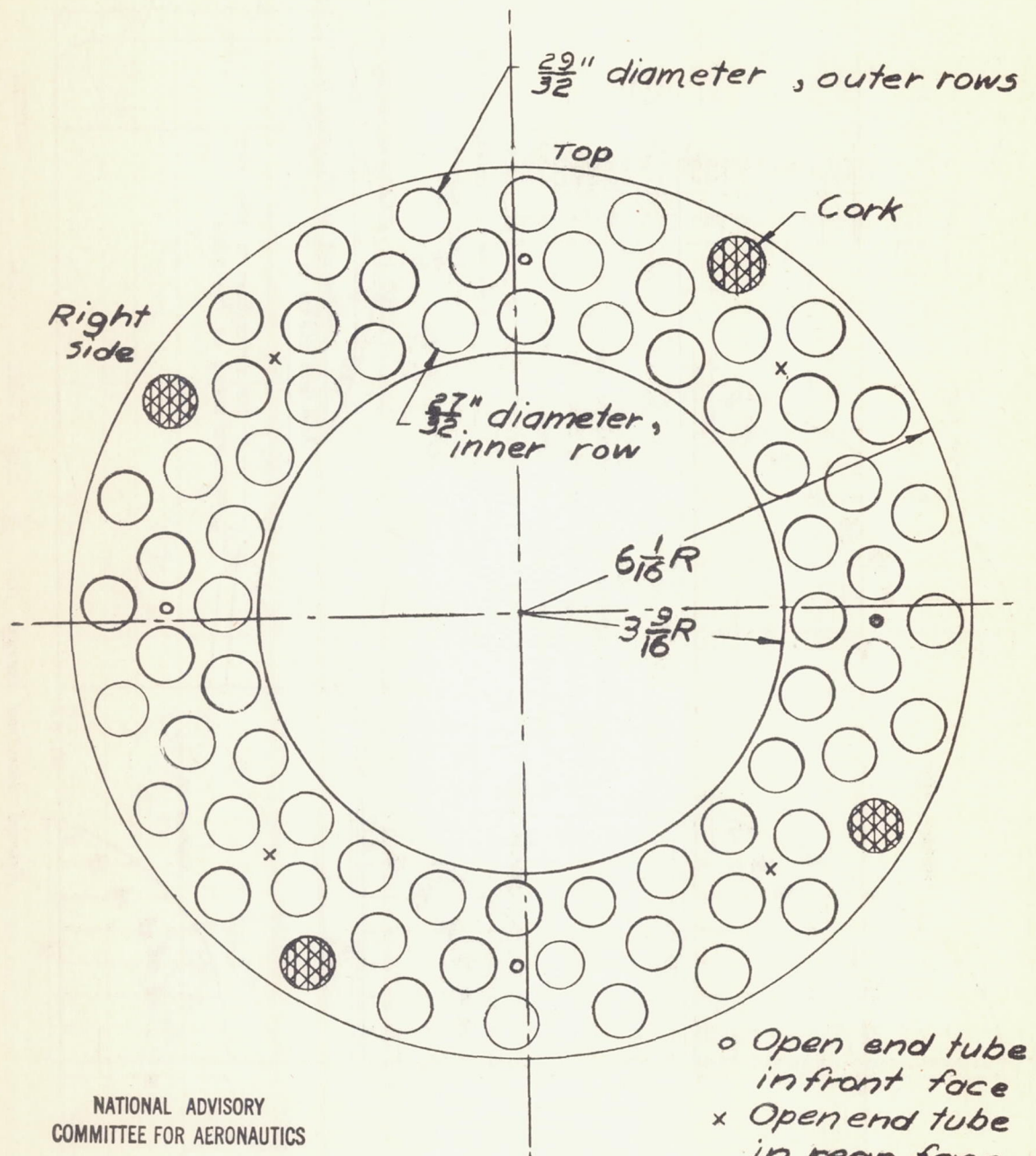


Figure 7.-Continued

NATIONAL ADVISORY
COMMITTEE FOR AERONAUTICS

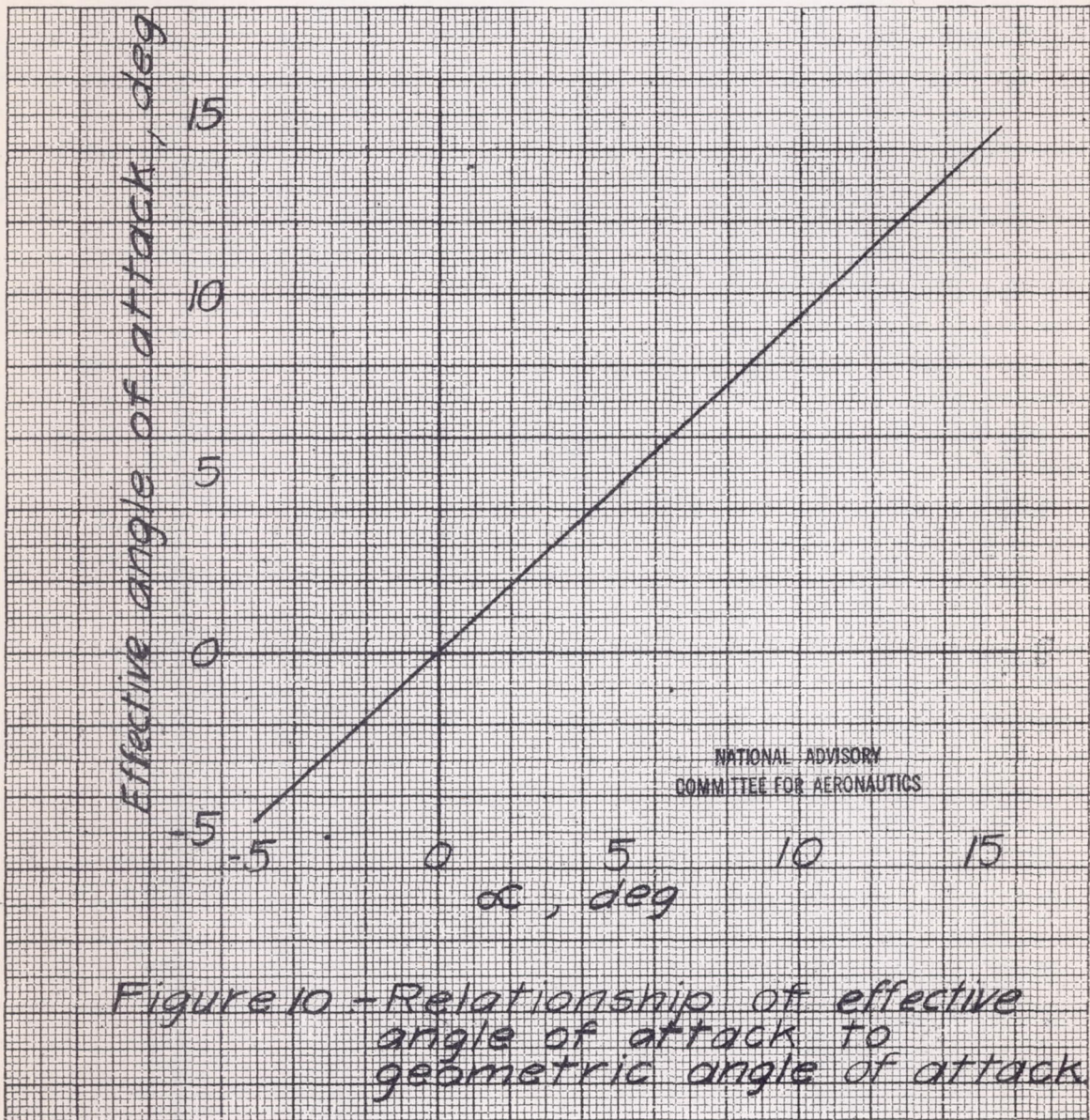


(h) Configuration H
Figure 7 - Continued.



NATIONAL ADVISORY
COMMITTEE FOR AERONAUTICS

Figure 9 .- Engine orifice plate and instrumentation. Effective area , 0.206 sq ft.



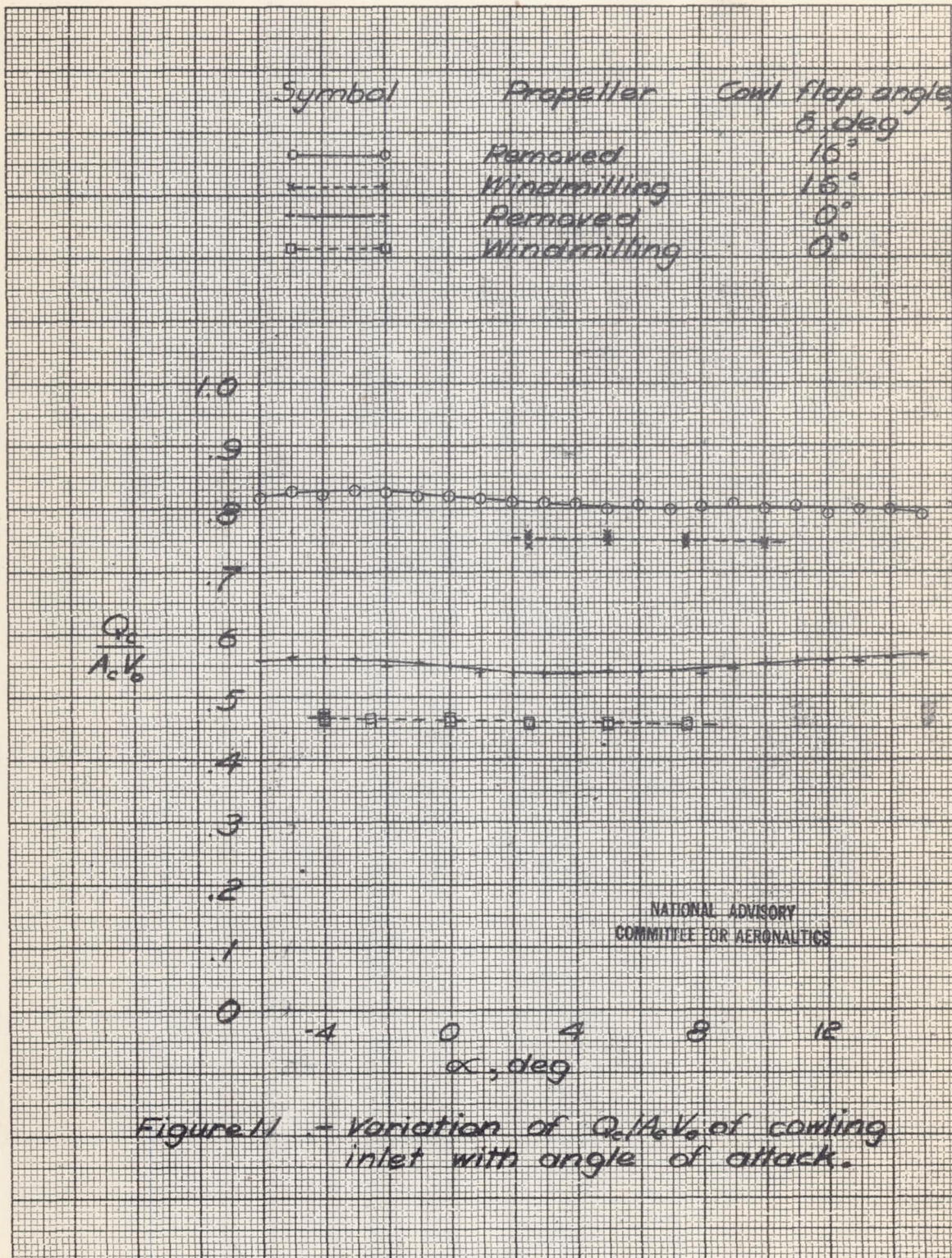
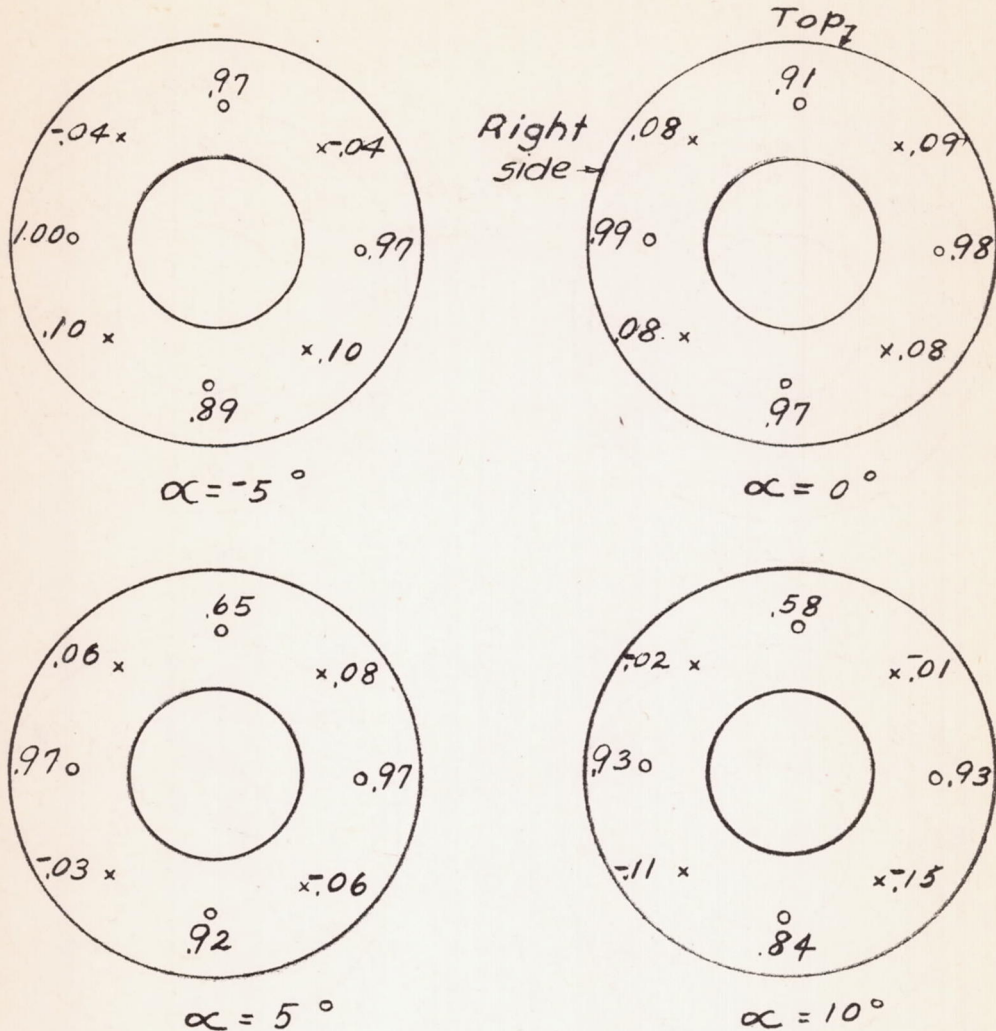


Figure 11. - Variation of $Q_c/A_e V_0$ of cooling inlet with angle of attack.



$$\circ \frac{H - P_0}{g_0}$$

Open end tube in front face.

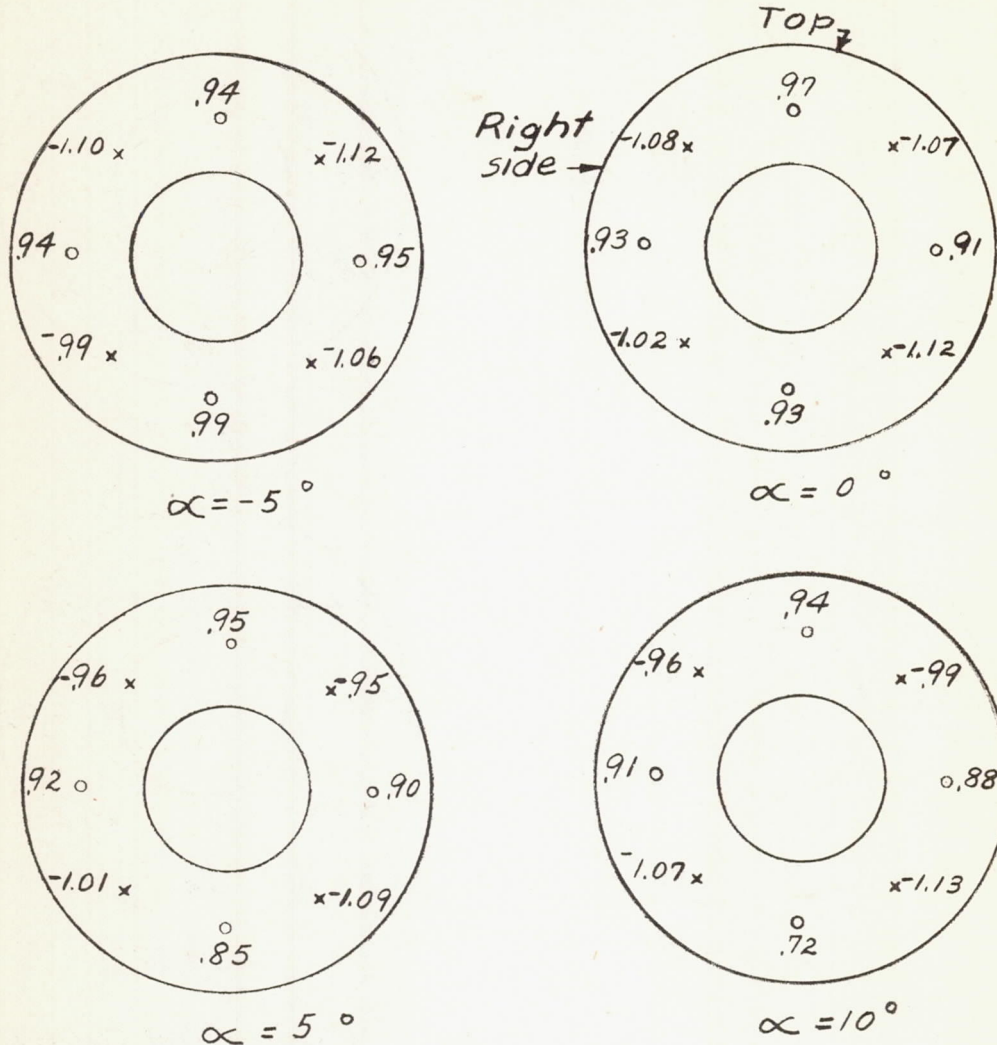
$$\times \frac{P - P_0}{g_0}$$

Open end tube in rear face.

$$(a) \delta = 0^\circ, Q_c/A_c V_0 = 0.55.$$

NATIONAL ADVISORY
COMMITTEE FOR AERONAUTICS

Figure 12.- Pressure distribution at orifice plate. Propeller removed.

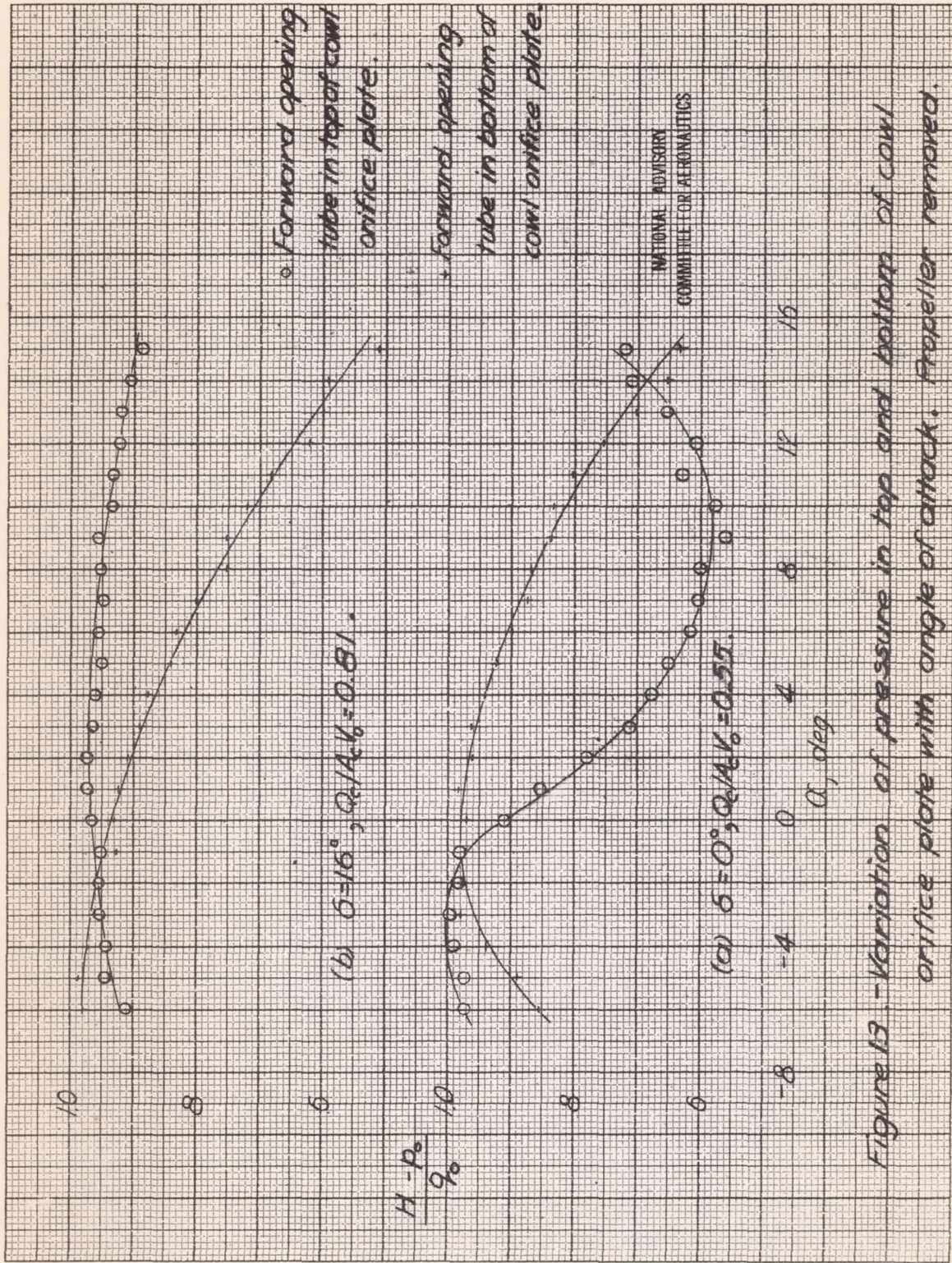


- $\frac{H - P_0}{P_0}$ Open end tube in front face.
- × $\frac{P - P_0}{P_0}$ Open end tube in rear face.

$$(b) \delta = 16^\circ, Q_c/A_c V_0 = 0.81.$$

Figure 12. -- Concluded.

NATIONAL ADVISORY
COMMITTEE FOR AERONAUTICS



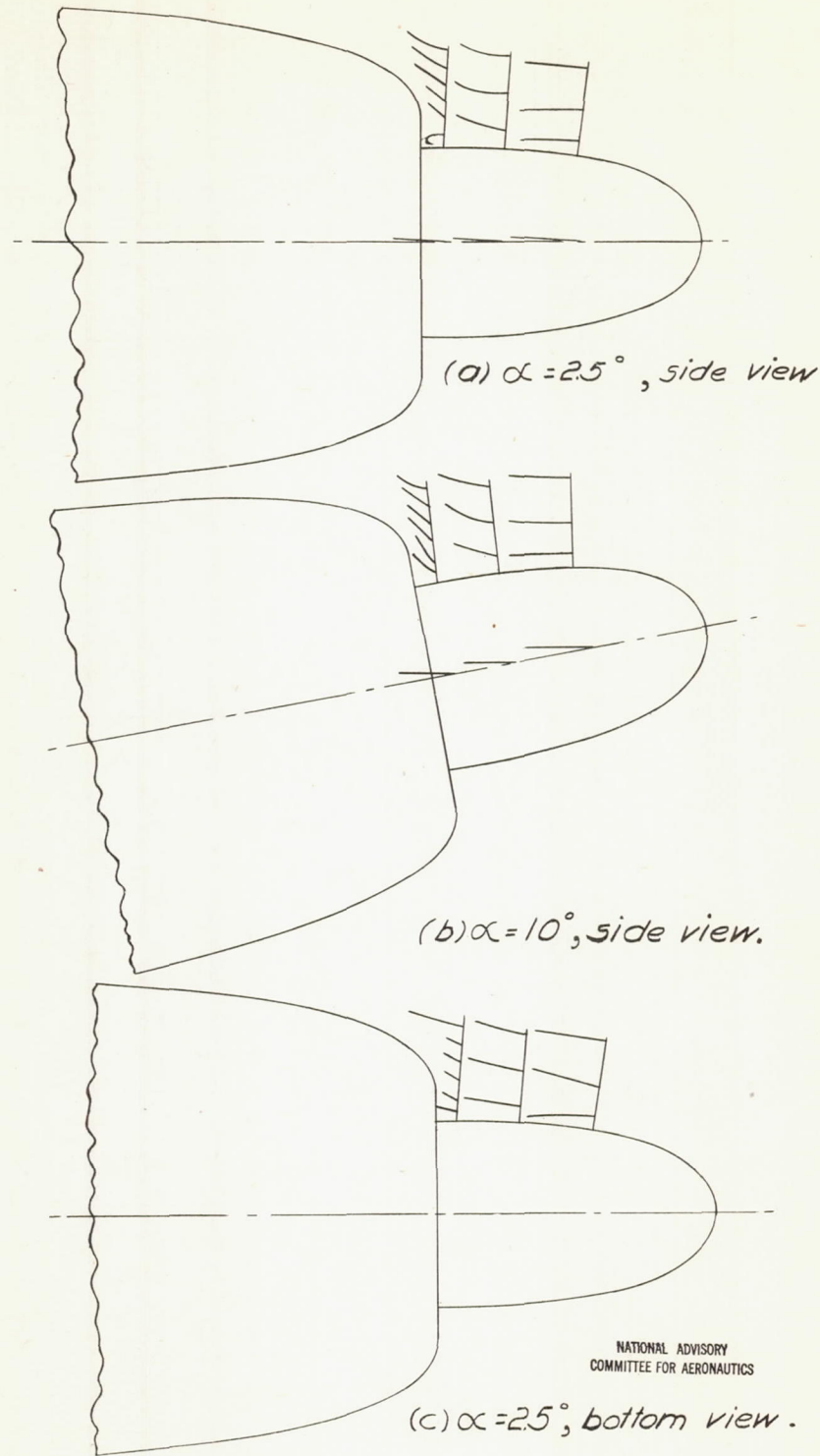


Figure 14.-Tuft observations of flow into
cowl inlet. $\delta=0^\circ$, $Q_c/A_c V_0 = 0.55$.

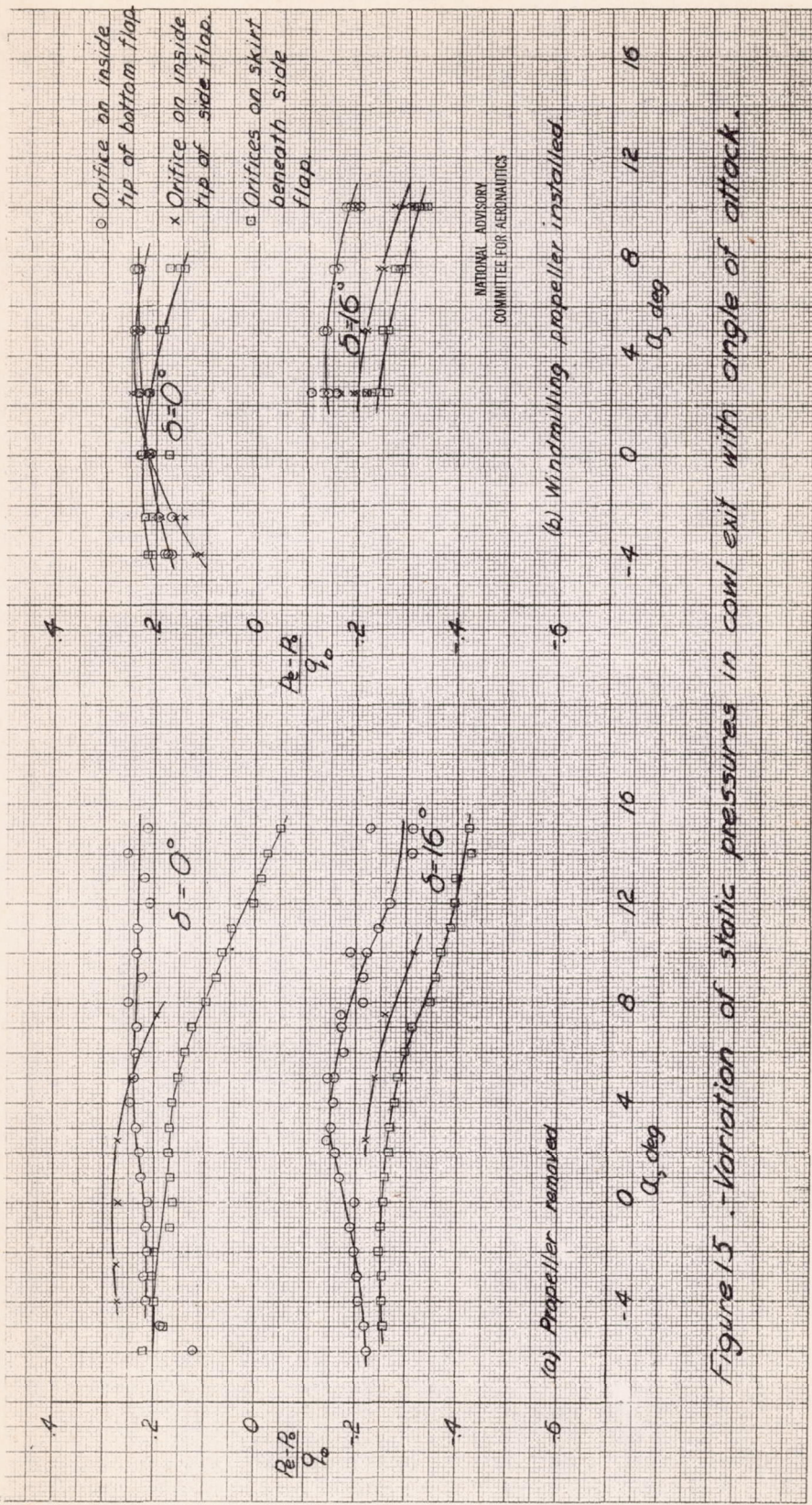
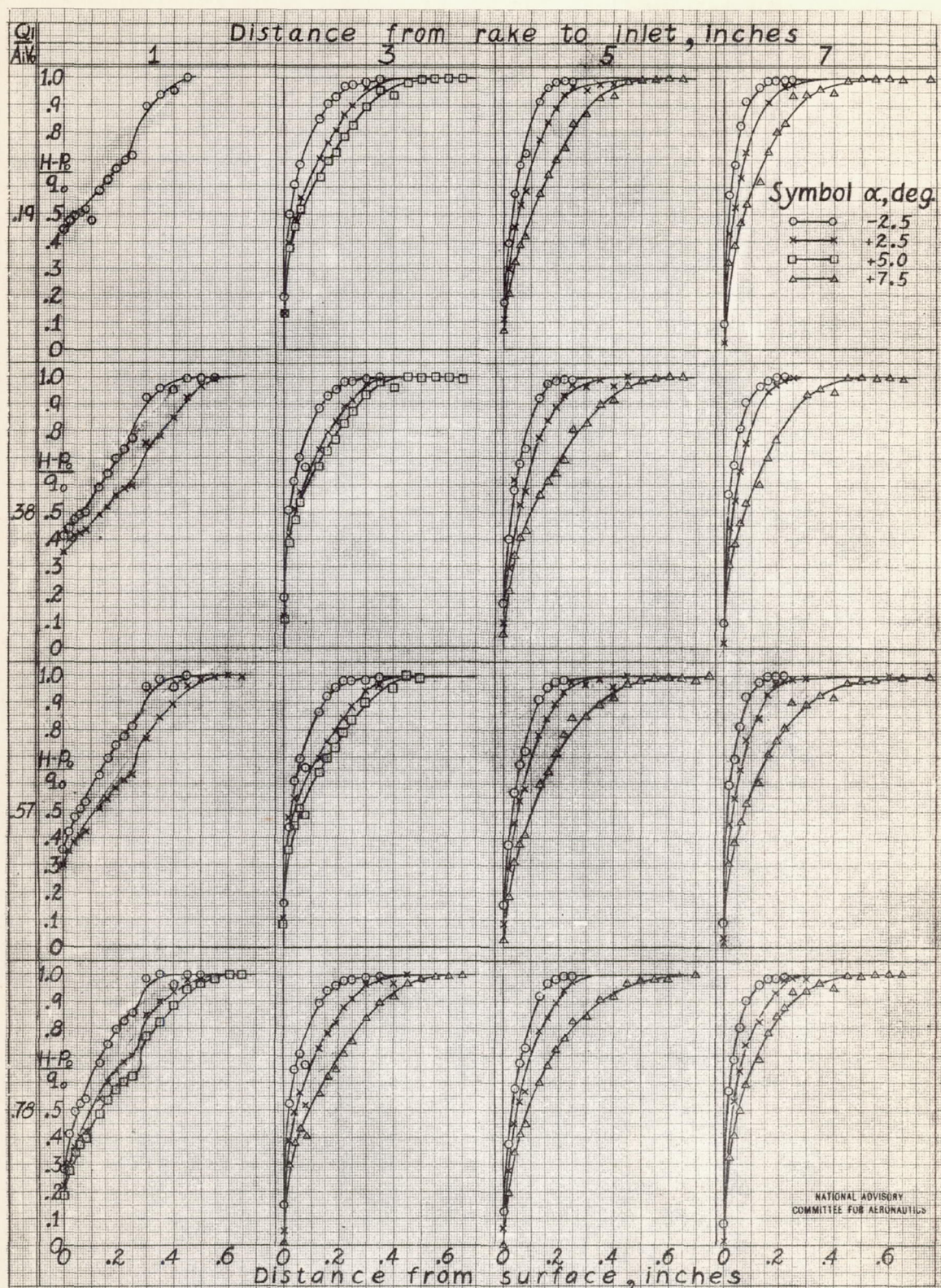


Figure 15. Variation of static pressures in cowl exit with angle of attack.



(a) Cowl flaps flush, $\delta = 0^\circ$.

Figure 16. - Total pressure distribution in cooling boundary layer in front of carburetor-duct inlet. Duct configuration A1.

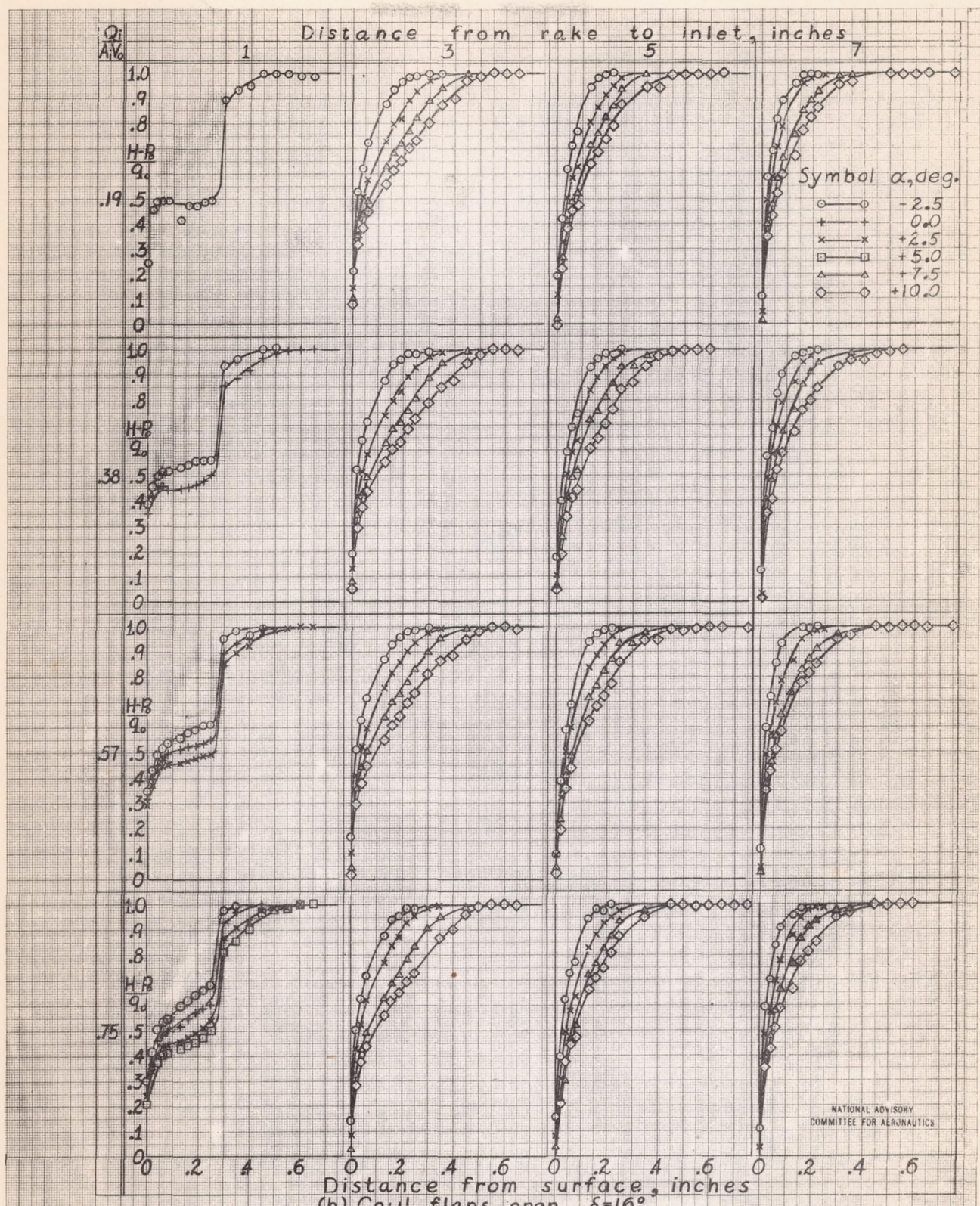


Figure 16 .- Total pressure distribution in cowling boundary layer in front of carburetor-duct inlet. Duct configuration A-1.
(b) Cowl flaps open, $\delta=10^\circ$.

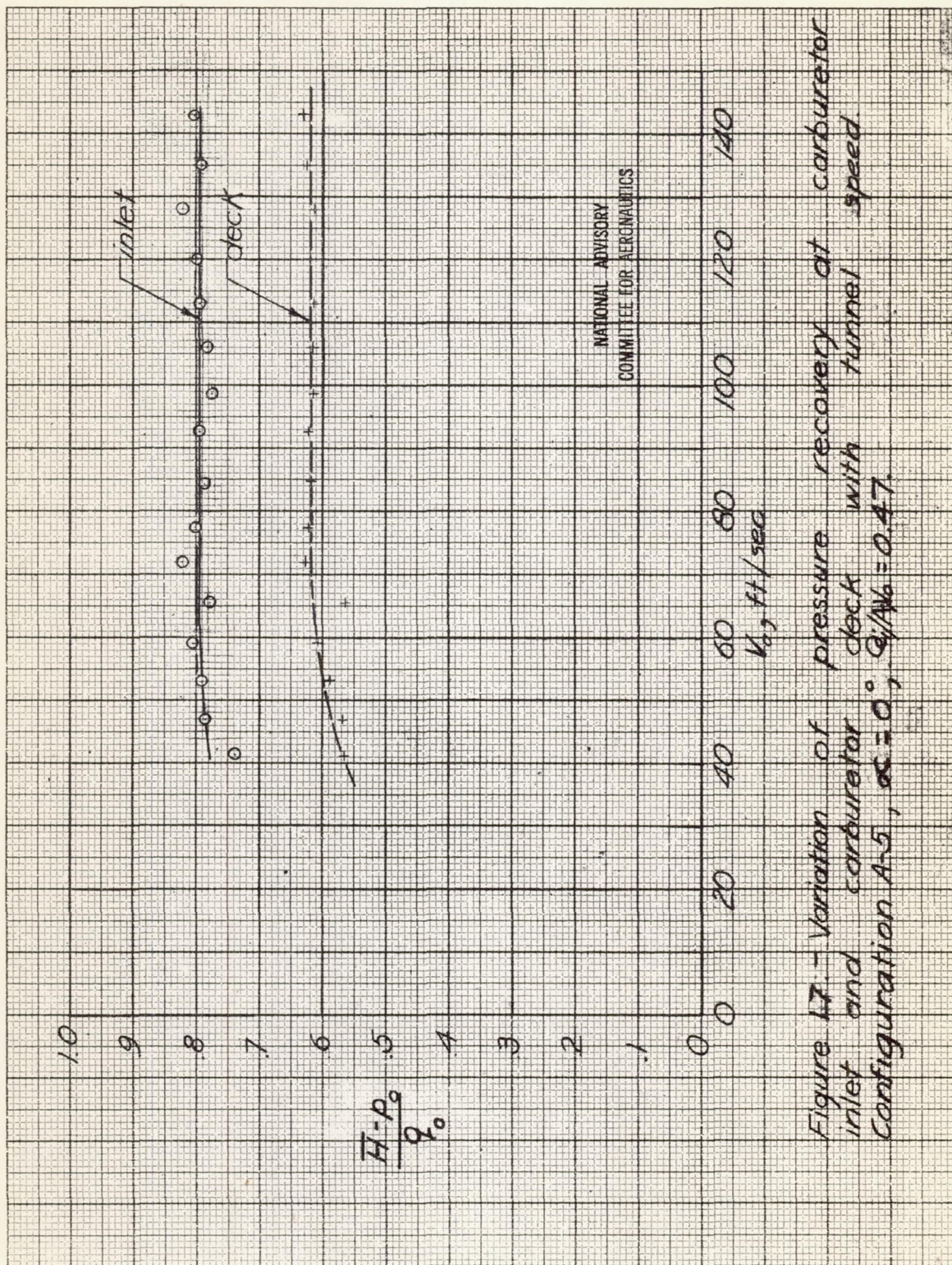


Figure 17 - Variation of pressure recovery at carburetor inlet and carburetor deck with tunnel speed.
configuration A-5, $\alpha = 0^\circ$, $C_{fus} = 0.47$.

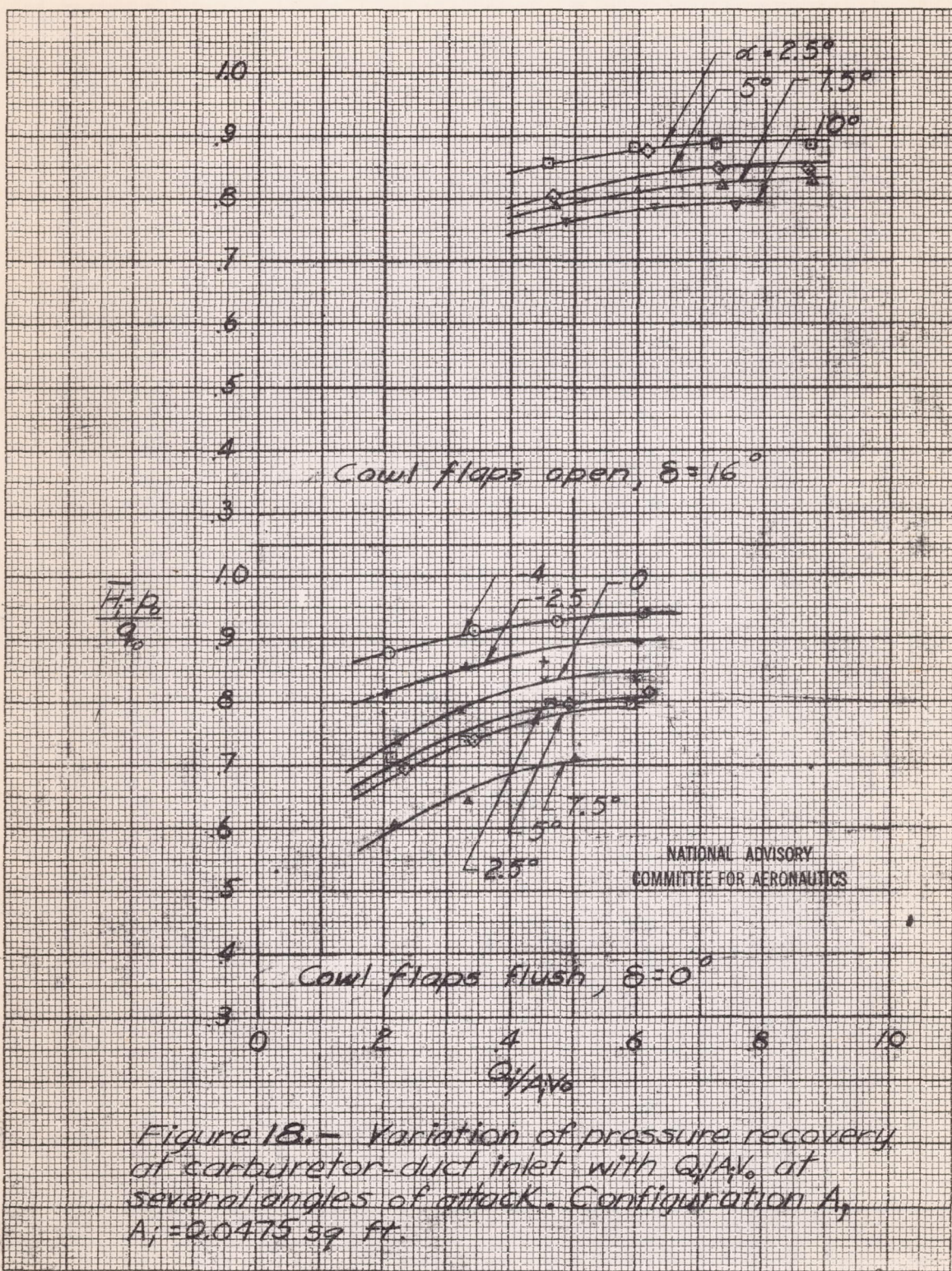


Figure 18.— Variation of pressure recovery of carburetor-duct inlet with A_1/A_0 at several angles of attack. Configuration 1, $A_1 = 0.0475 \text{ sq ft}$.

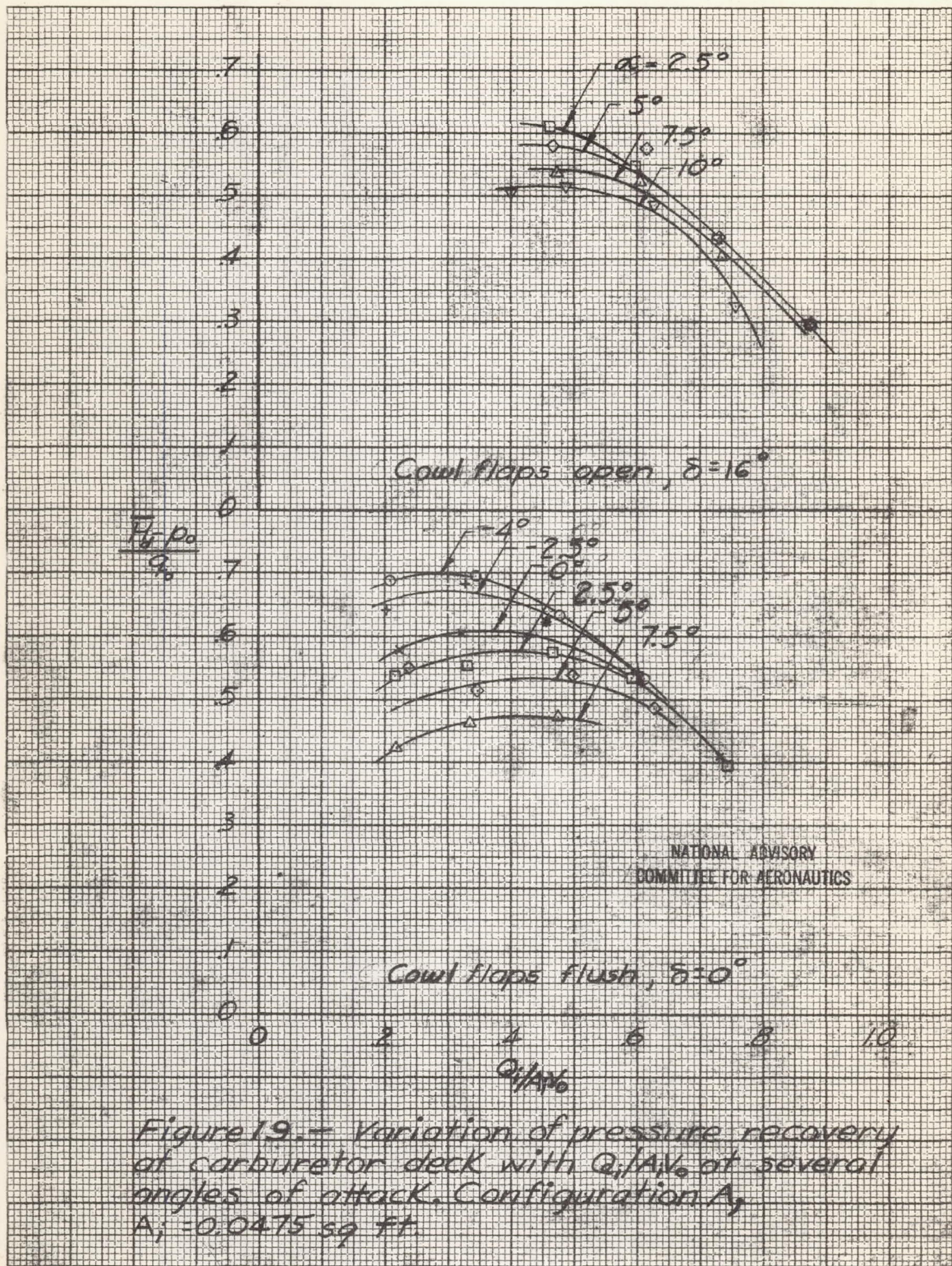


Figure 19 - Variation of pressure recovery at carburetor deck with Q_c/AV_c of several angles of attack. Configuration A,
 $A_1 = 0.0475 \text{ sq ft}$

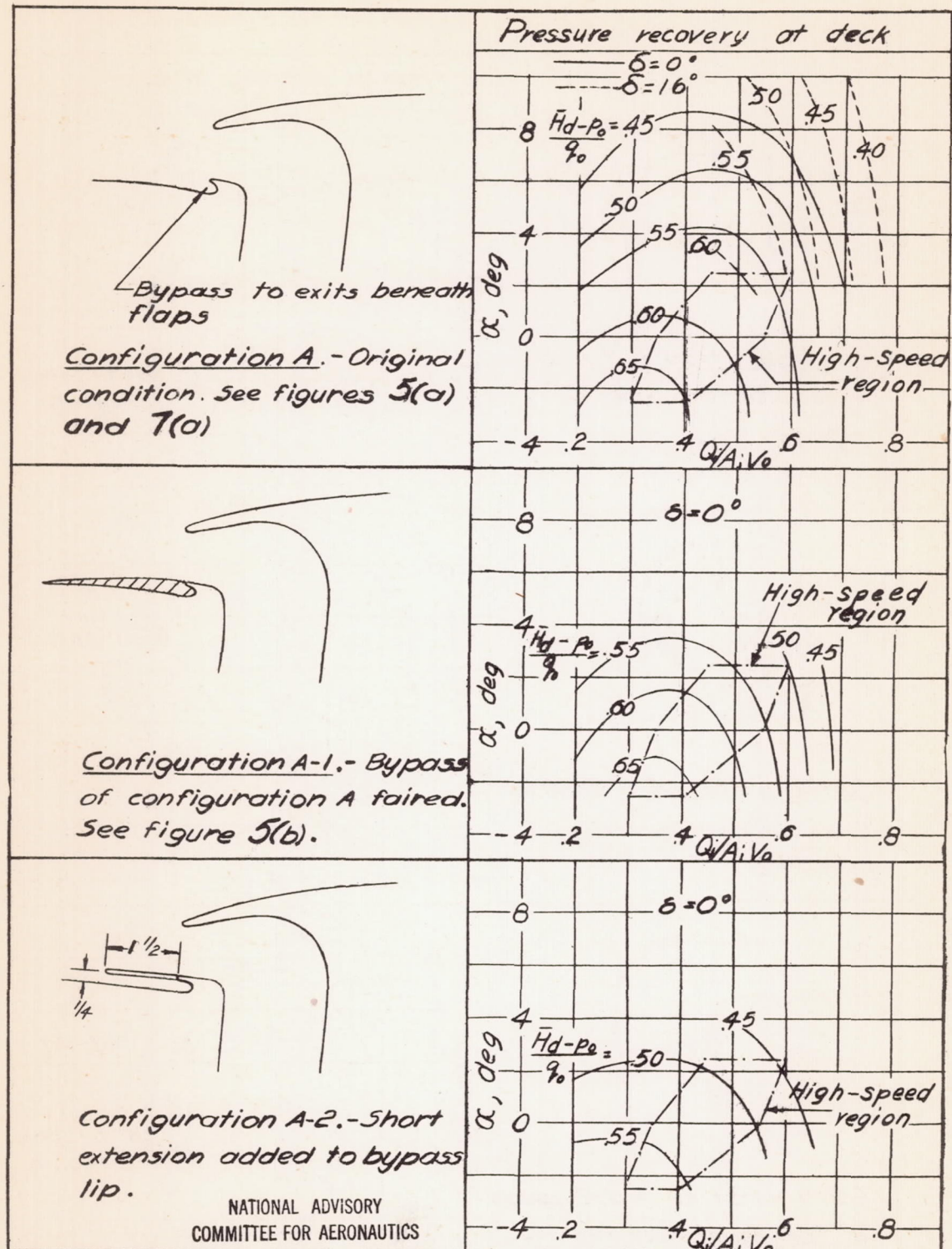
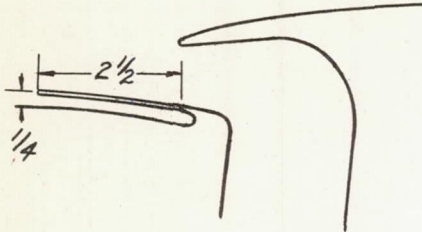
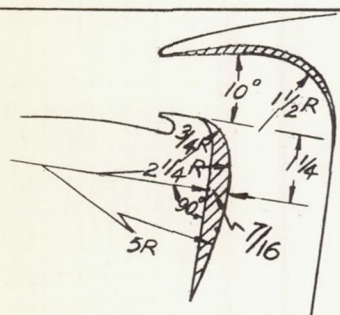


Figure 20.- Pressure recovery at upper deck of carburetor as a function of α and $Q/A_i V_0$ for several duct configurations.

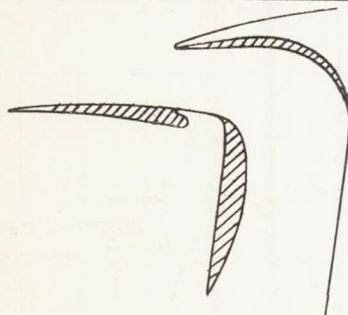
NATIONAL ADVISORY
COMMITTEE FOR AERONAUTICS



Configuration A-3. - Long extension added to bypass lip.

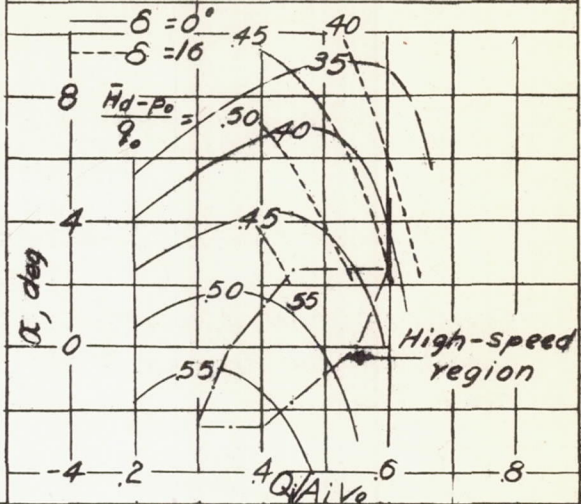


Configuration A-4. - Interior lines of configuration A refaired.

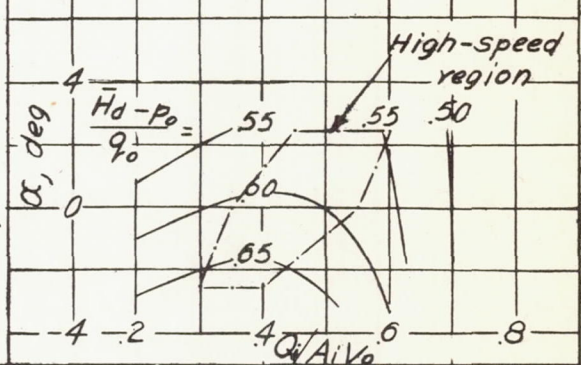


Configuration A-5. - Bypass of configuration A-4 refaired.

Pressure recovery at deck



$\delta = 0^\circ$



$\delta = 0^\circ$

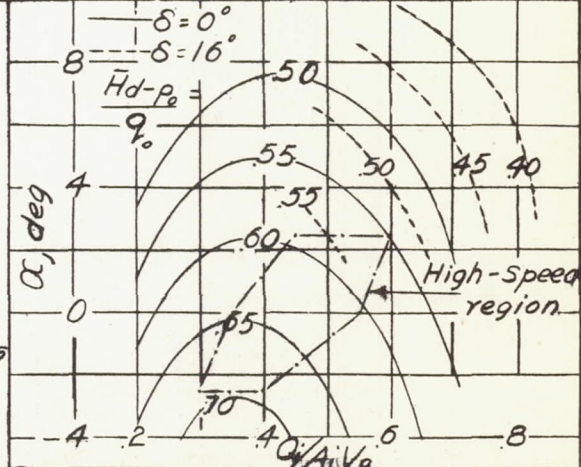


Figure 20 . - Continued.

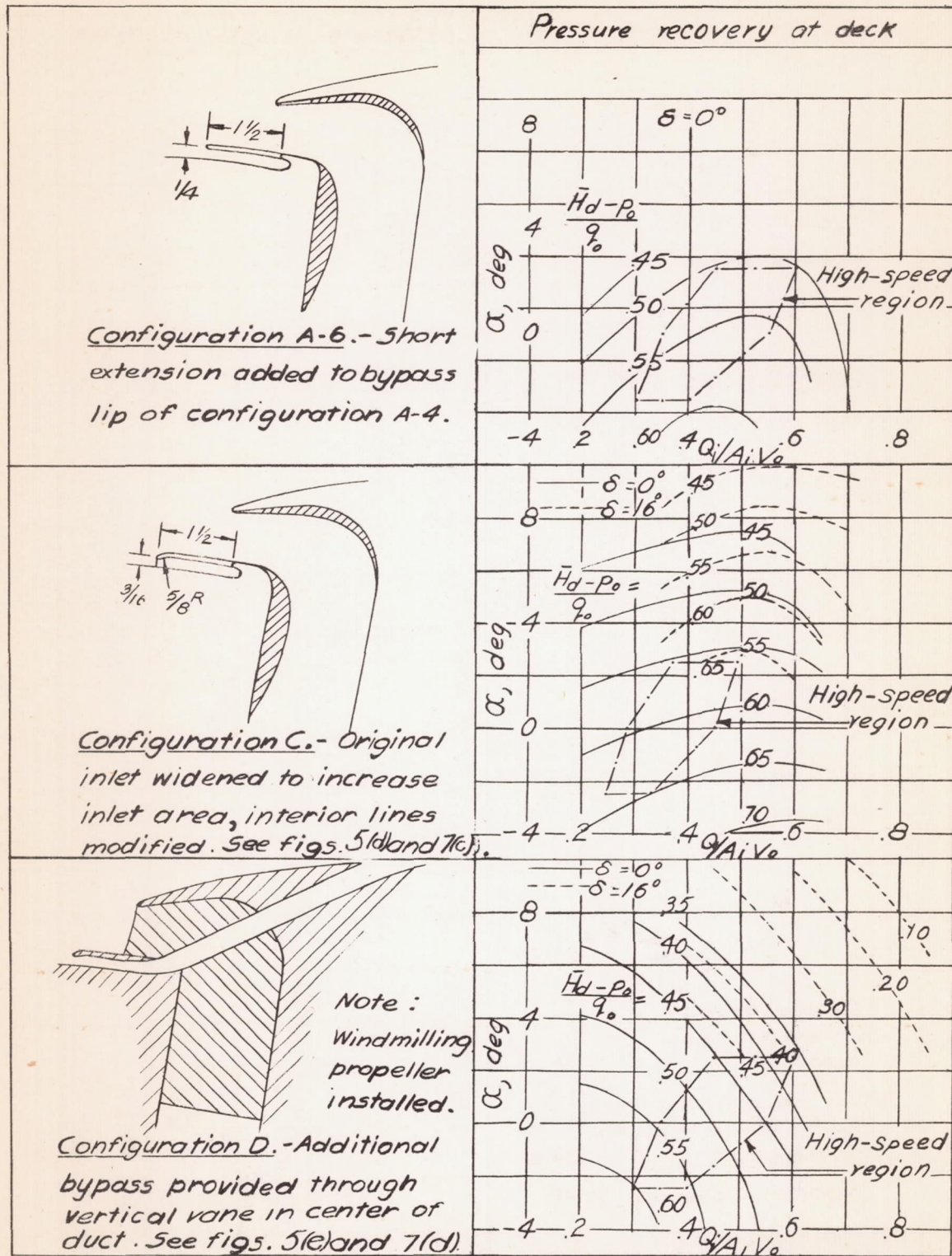
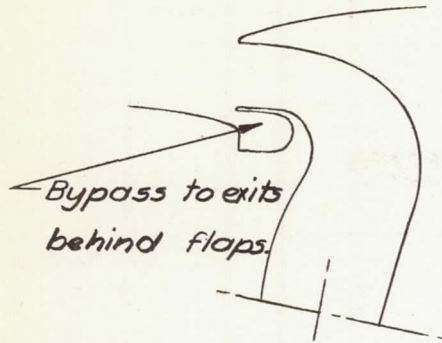


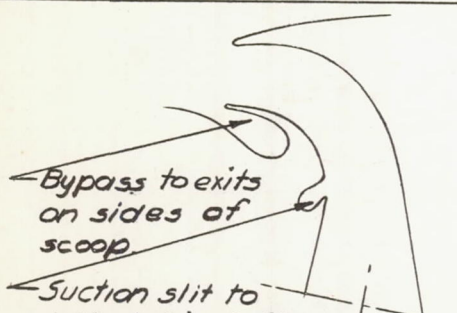
Figure 20 - Continued.



Configuration E. - See
figures 5(f) and 7(e).



Configuration E-1.-Bypass
faired.



Configuration F. - See
figures 5(g) and 7(f).

Pressure recovery at deck

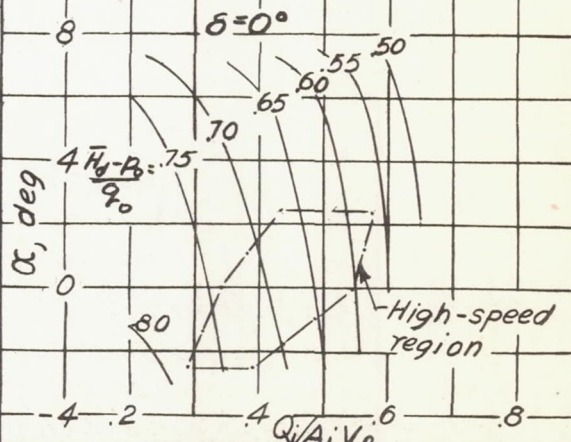
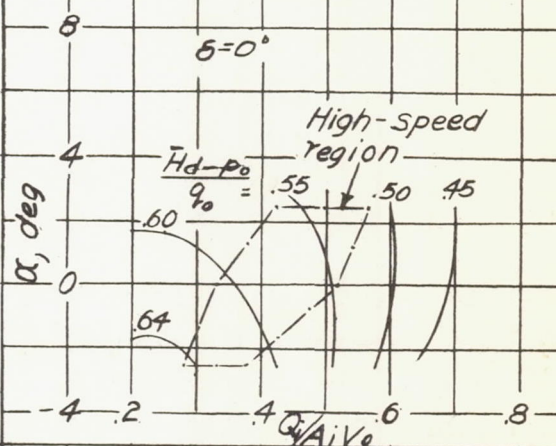
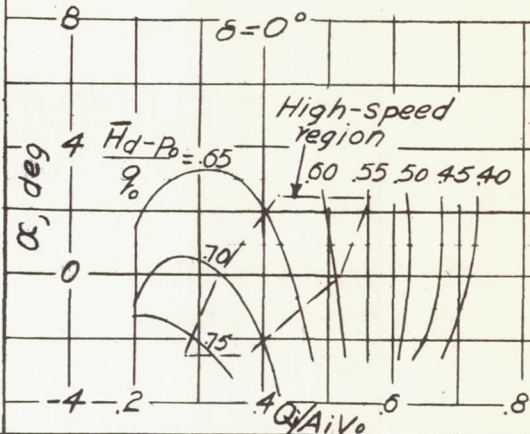


Figure 20.- Continued.

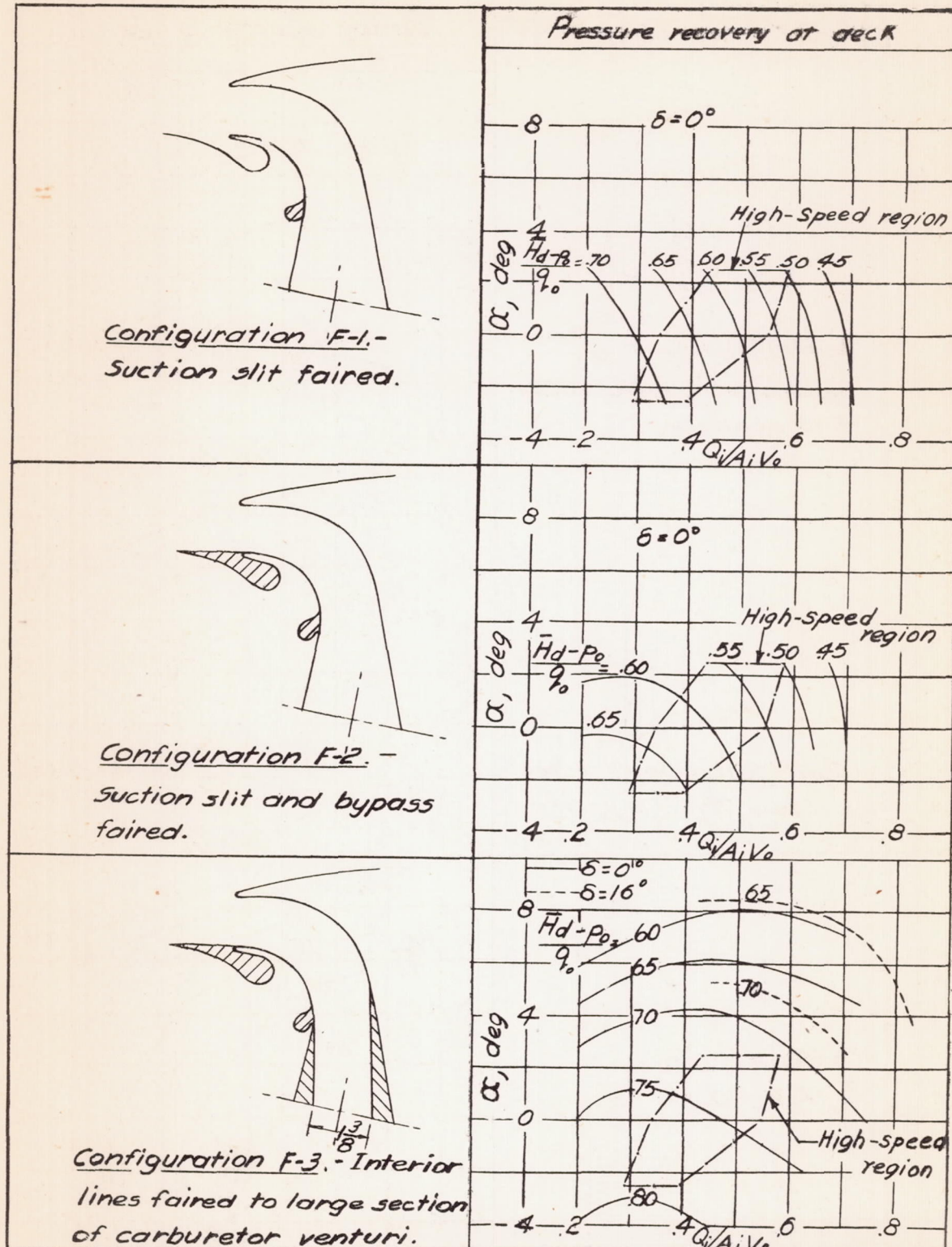
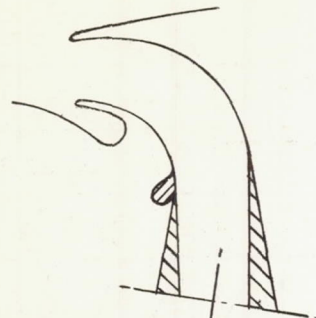
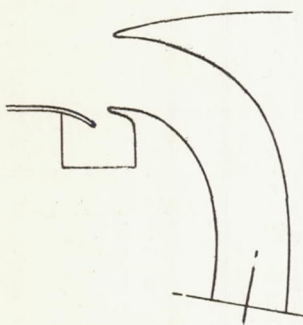


Figure 20.-Continued.



Configuration 'F-4'.

Bypass of configuration
F-3 opened.



Configuration G. - See
figs. 5(h) and 7(g). $\bar{Q}_d/A_d V_0 = 0.55$

Configuration G . -

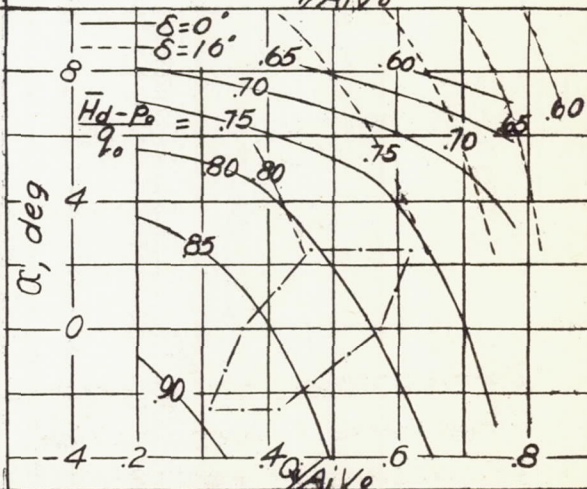
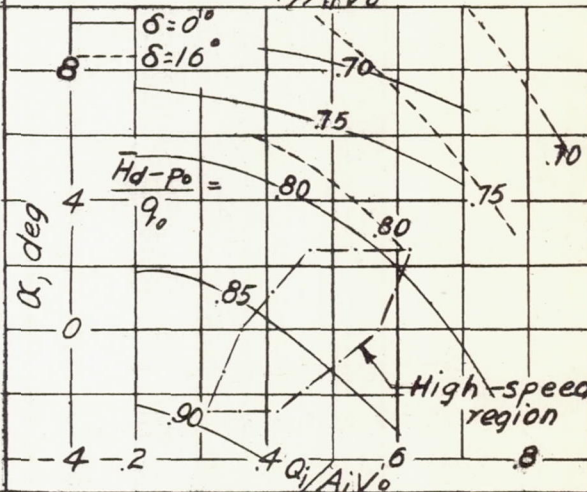
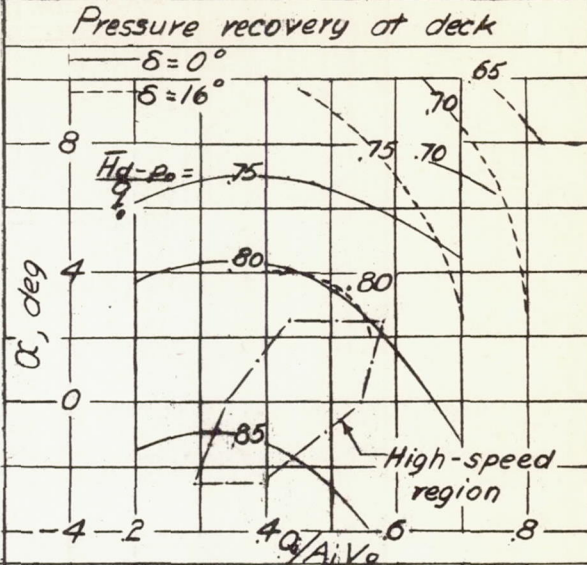


Figure 20 .- Continued

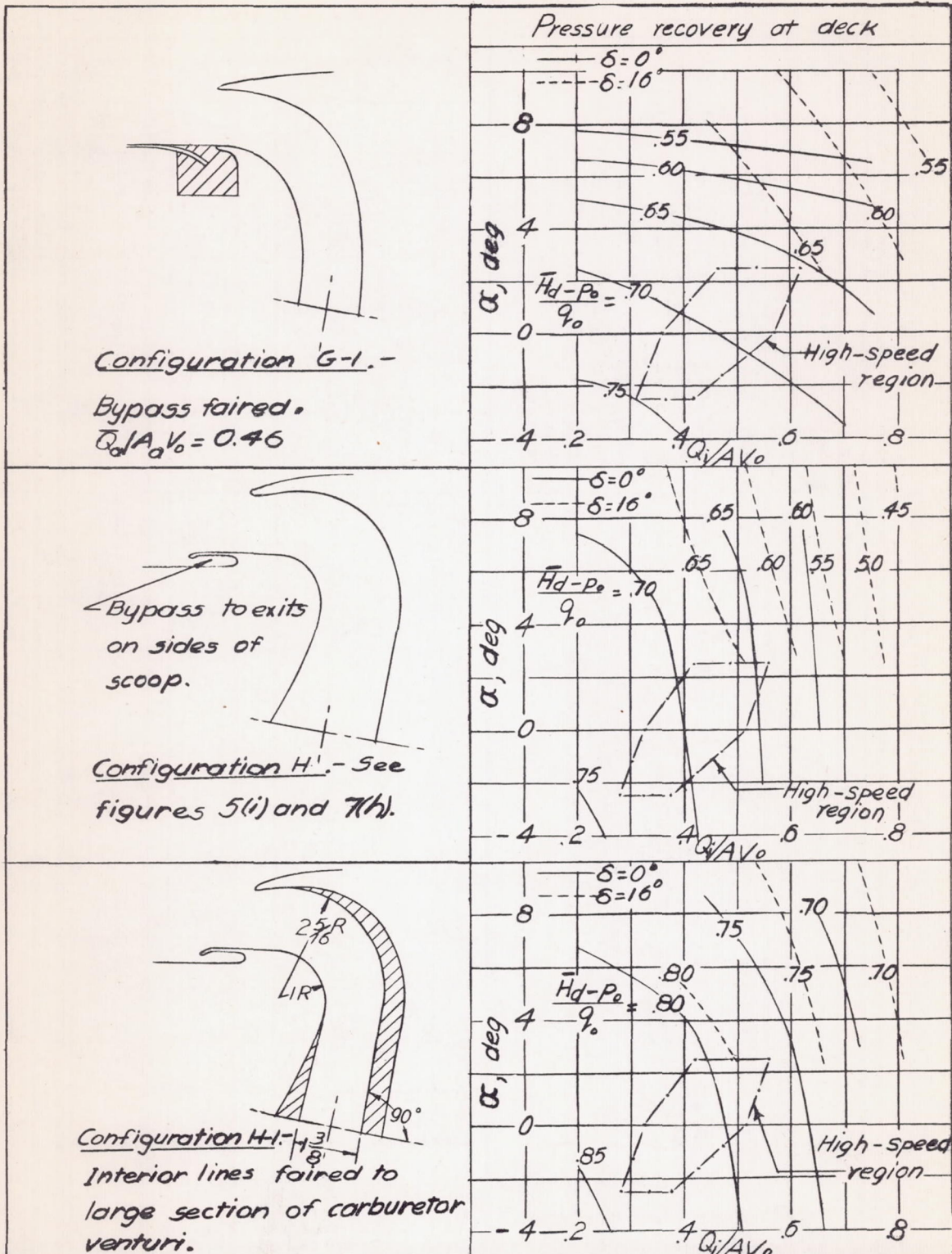
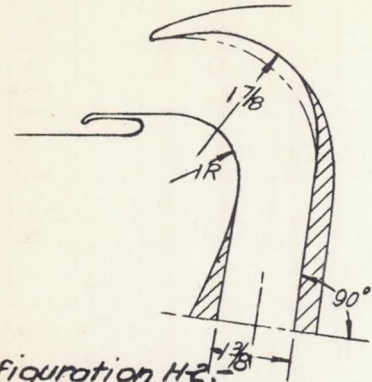
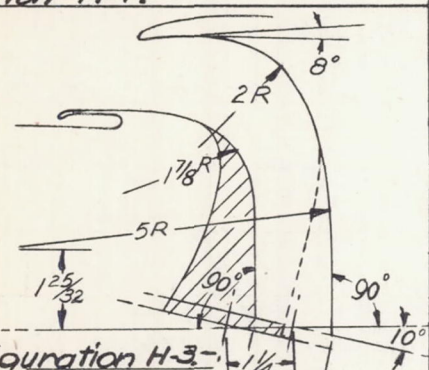


Figure 20. - Continued.

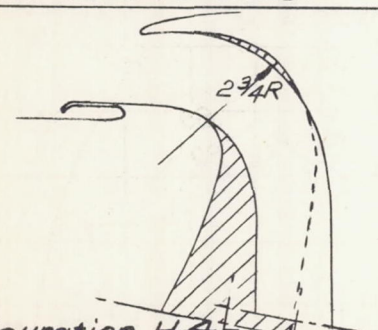


Configuration H-2.

Expansion rate increased in upstream portion of configuration H-1.



Configuration H-3-1/8
Entire scoop moved $\frac{1}{8}$ inch forward, and interior lines refaired.



Configuration H-4-1
Interior lines of configuration H-3 refaired to reduce bend expansion rate.

Pressure recovery at deck

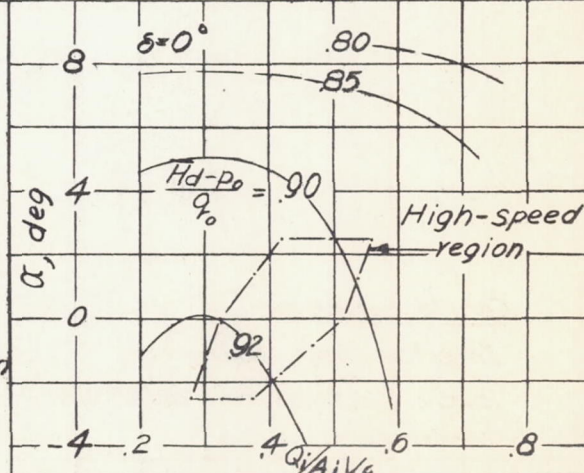
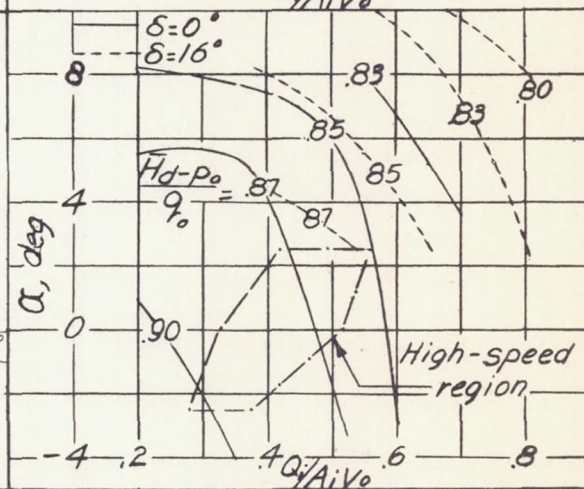
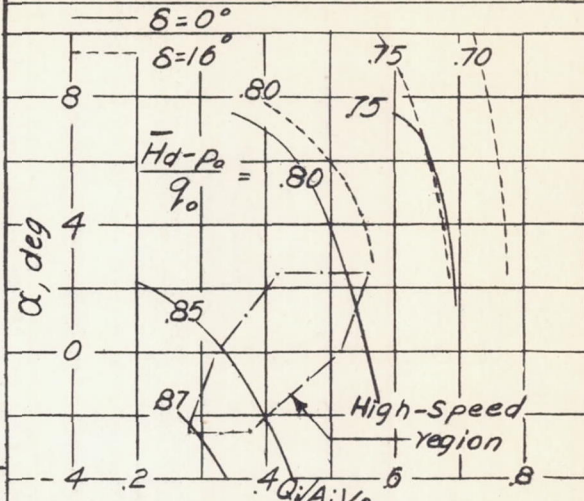
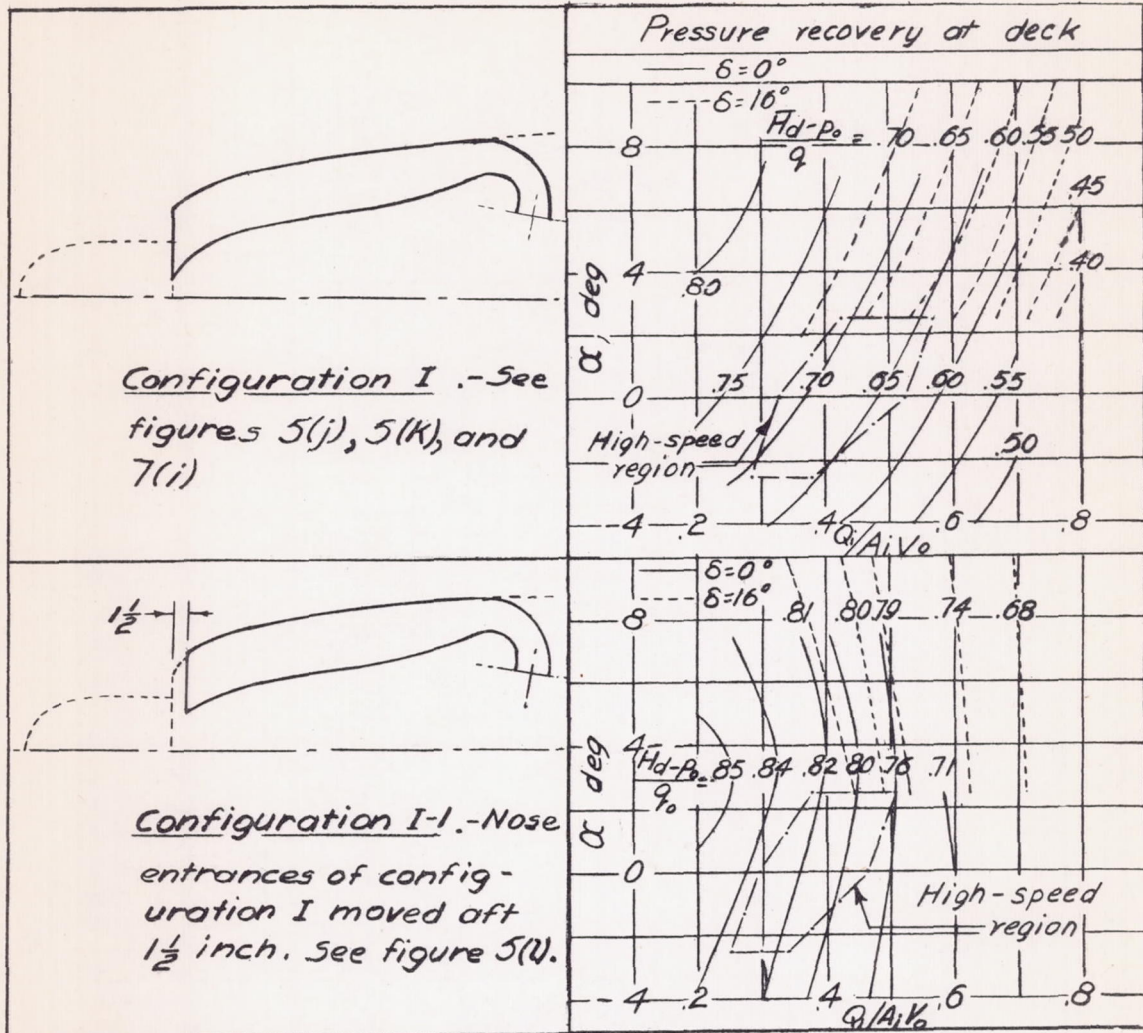


Figure 20.- Continued.



NATIONAL ADVISORY
COMMITTEE FOR AERONAUTICS

Figure 20.-Concluded.

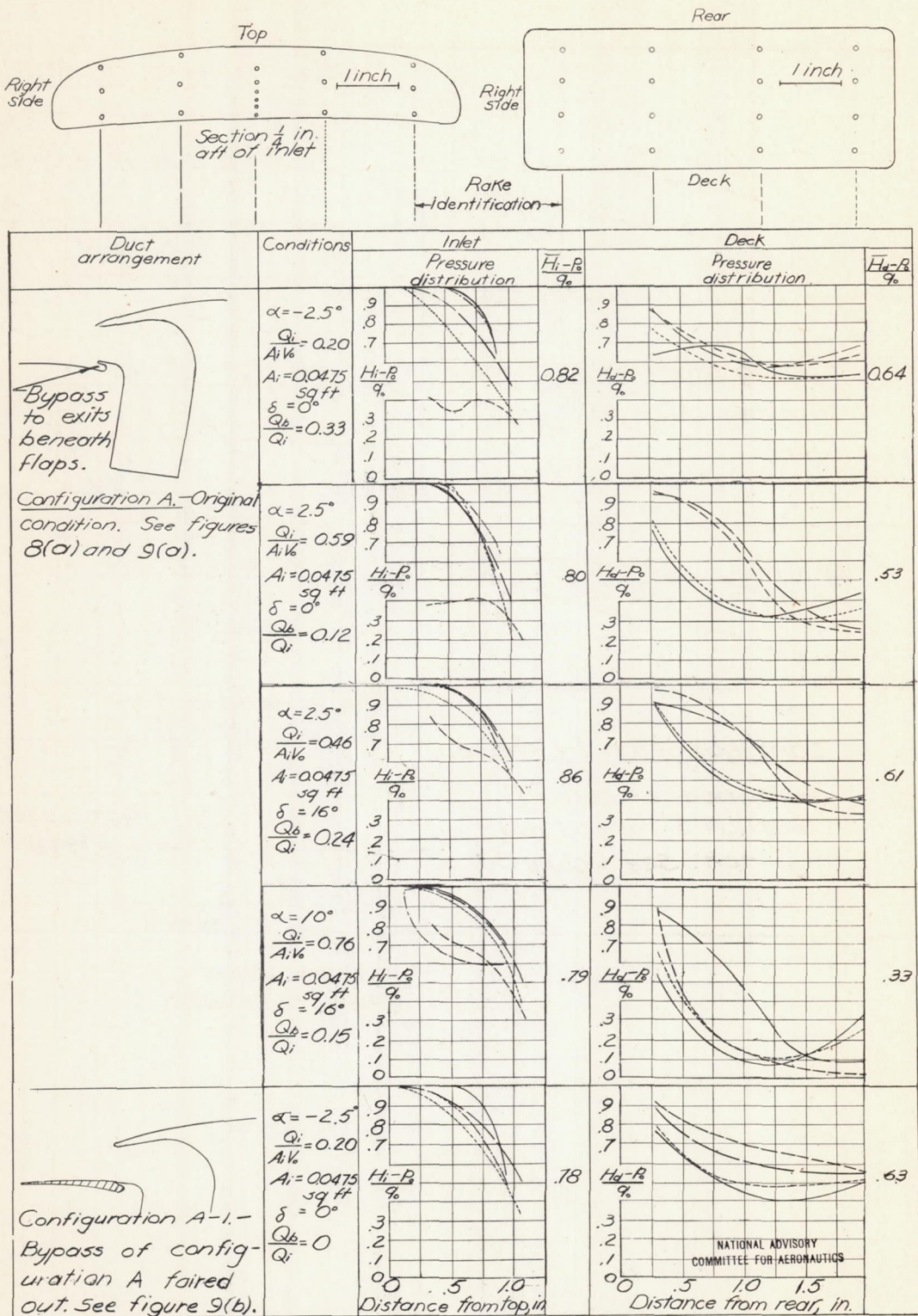


Figure 21.—Pressure distributions and average recoveries for series A carburetor ducts.

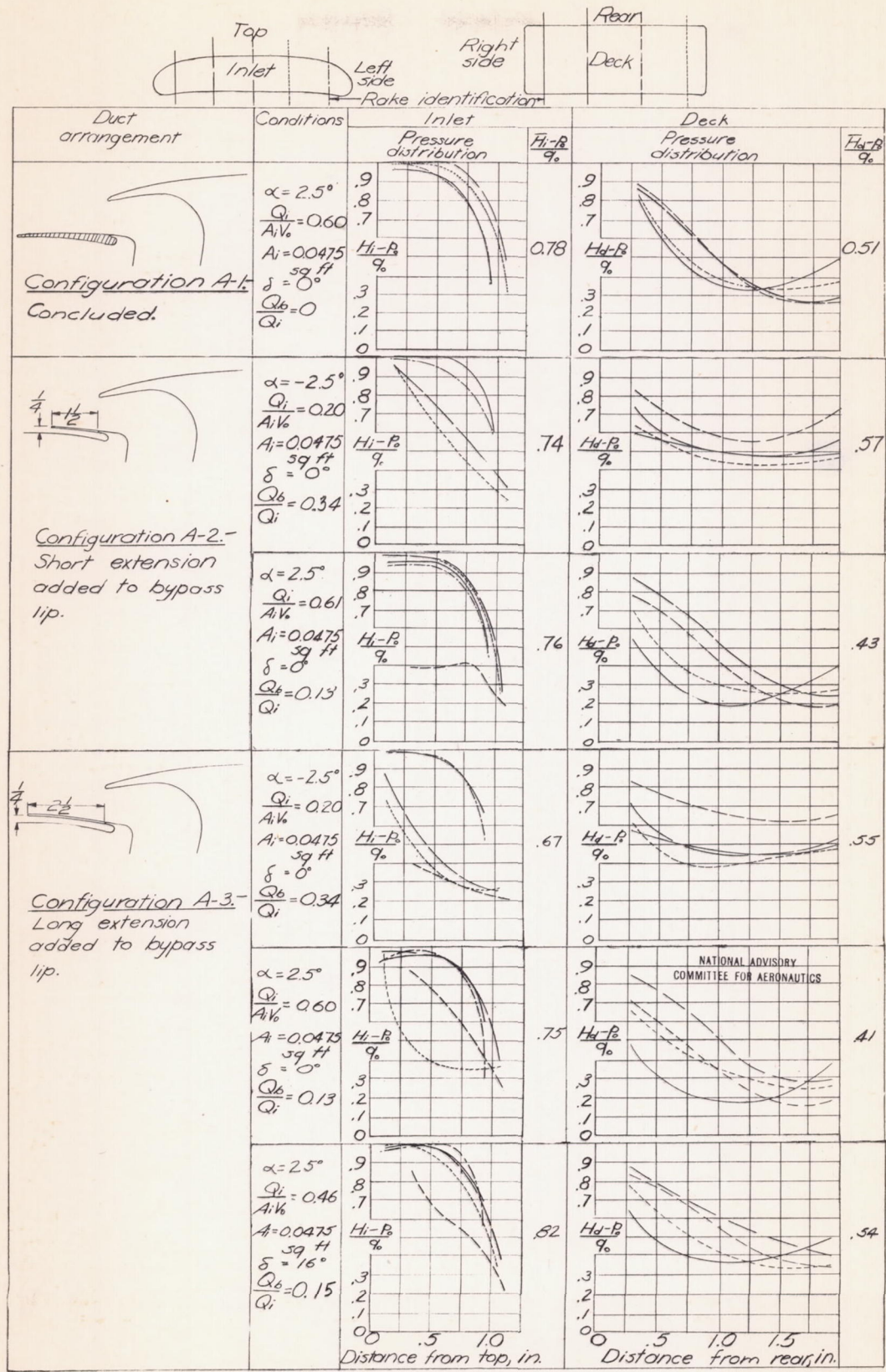


Figure 21.—Continued.

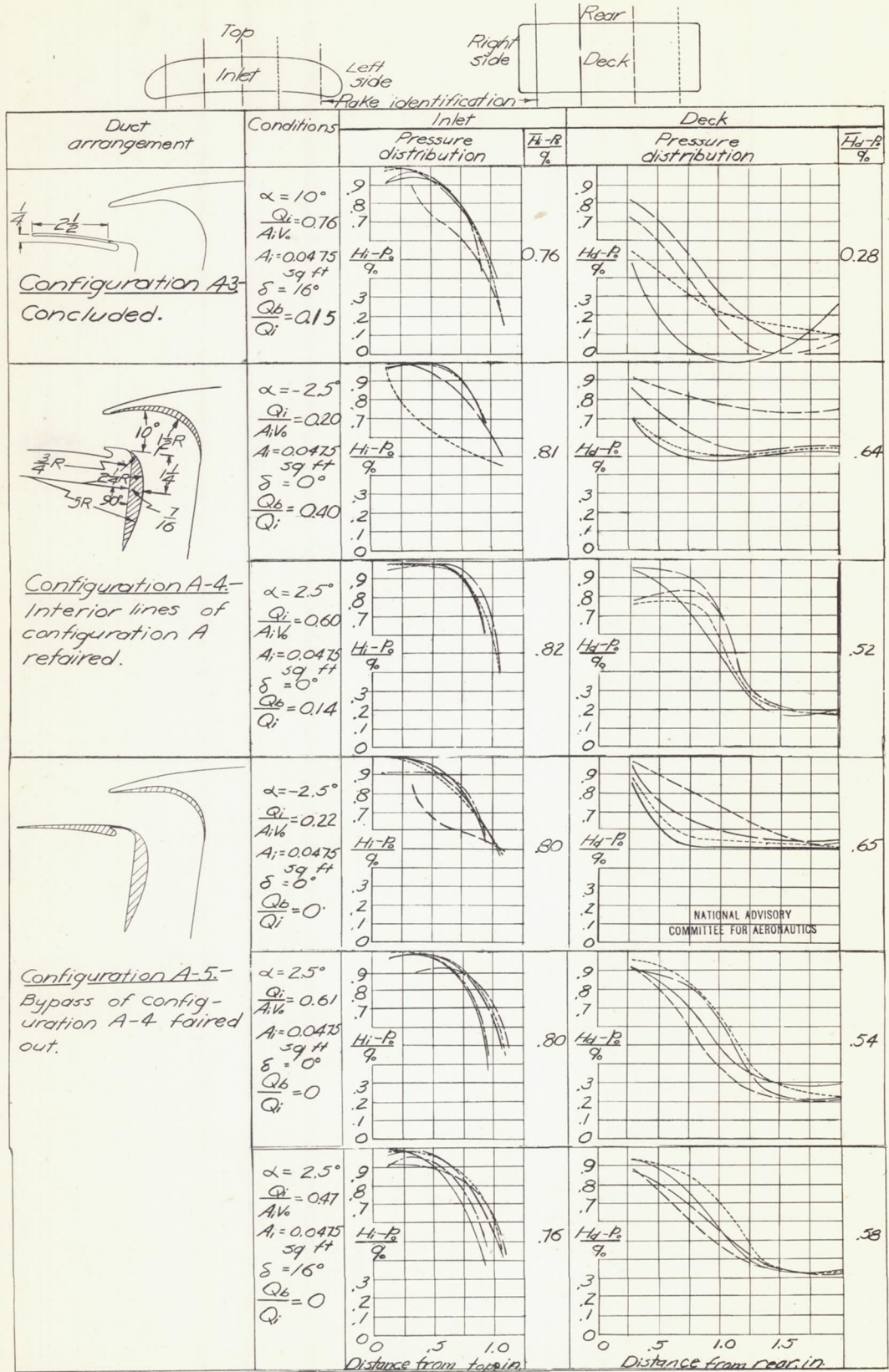


Figure 21.-Continued.

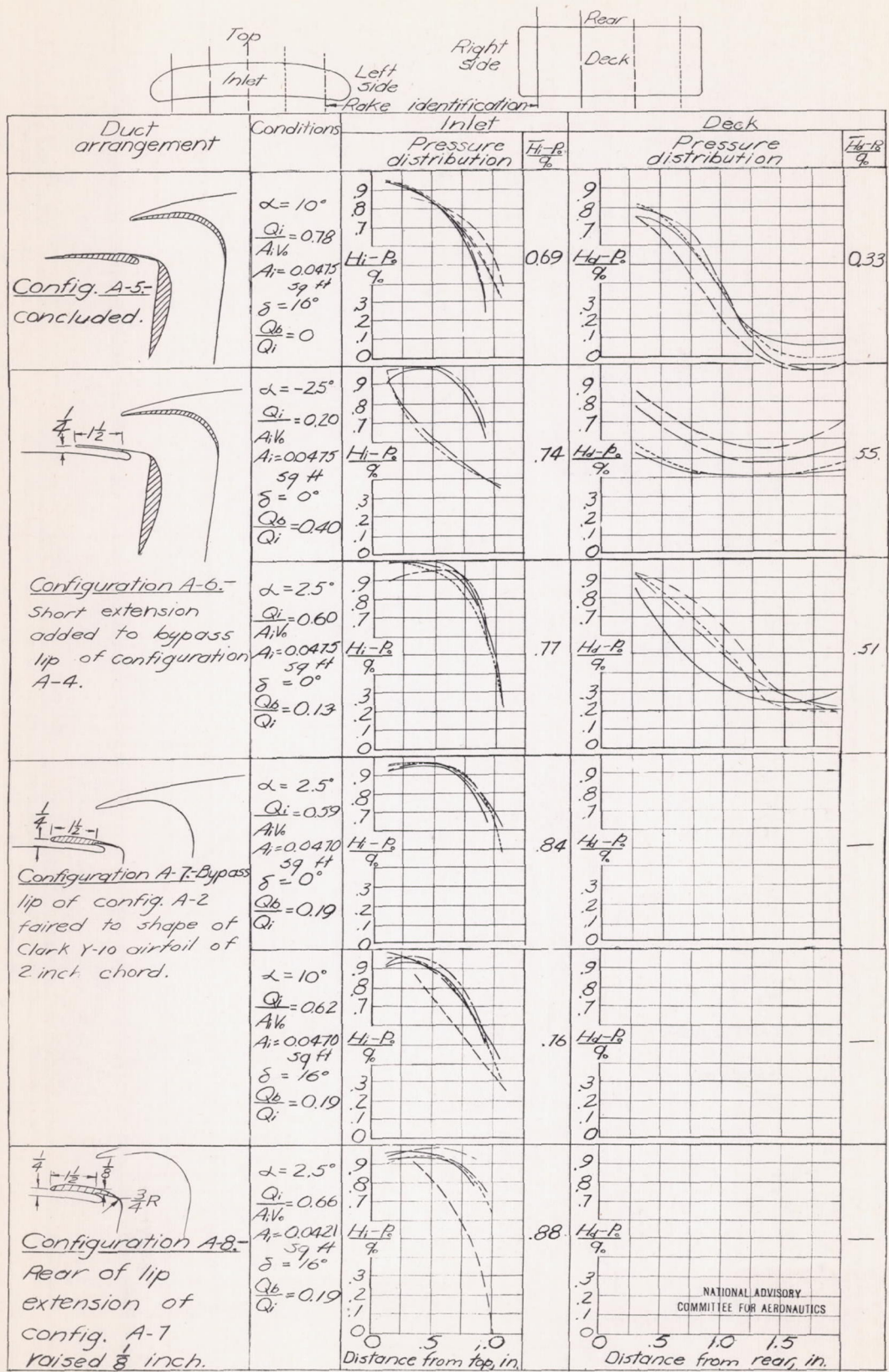


Figure 21. -Continued.

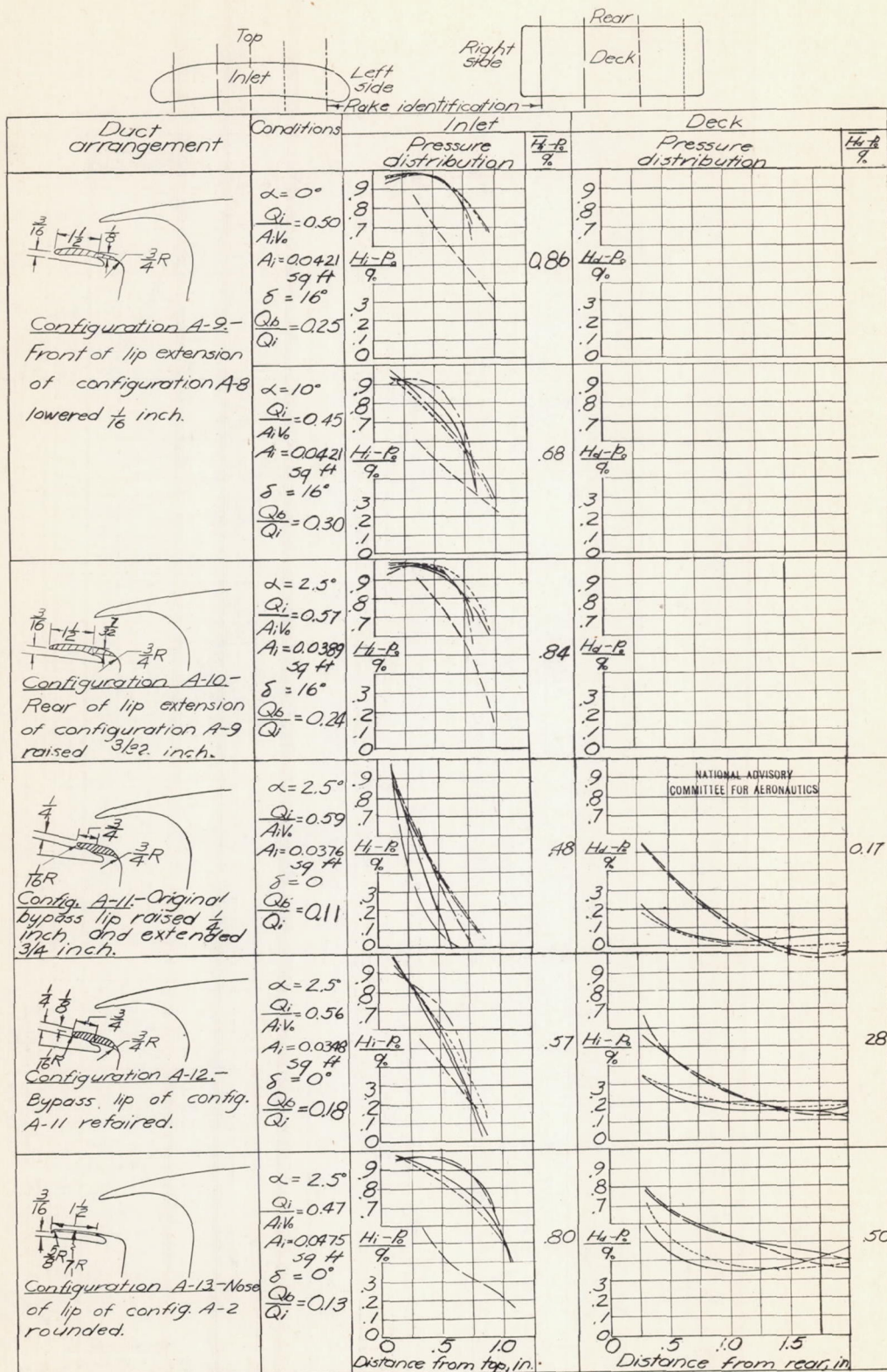


Figure 21. - Continued.

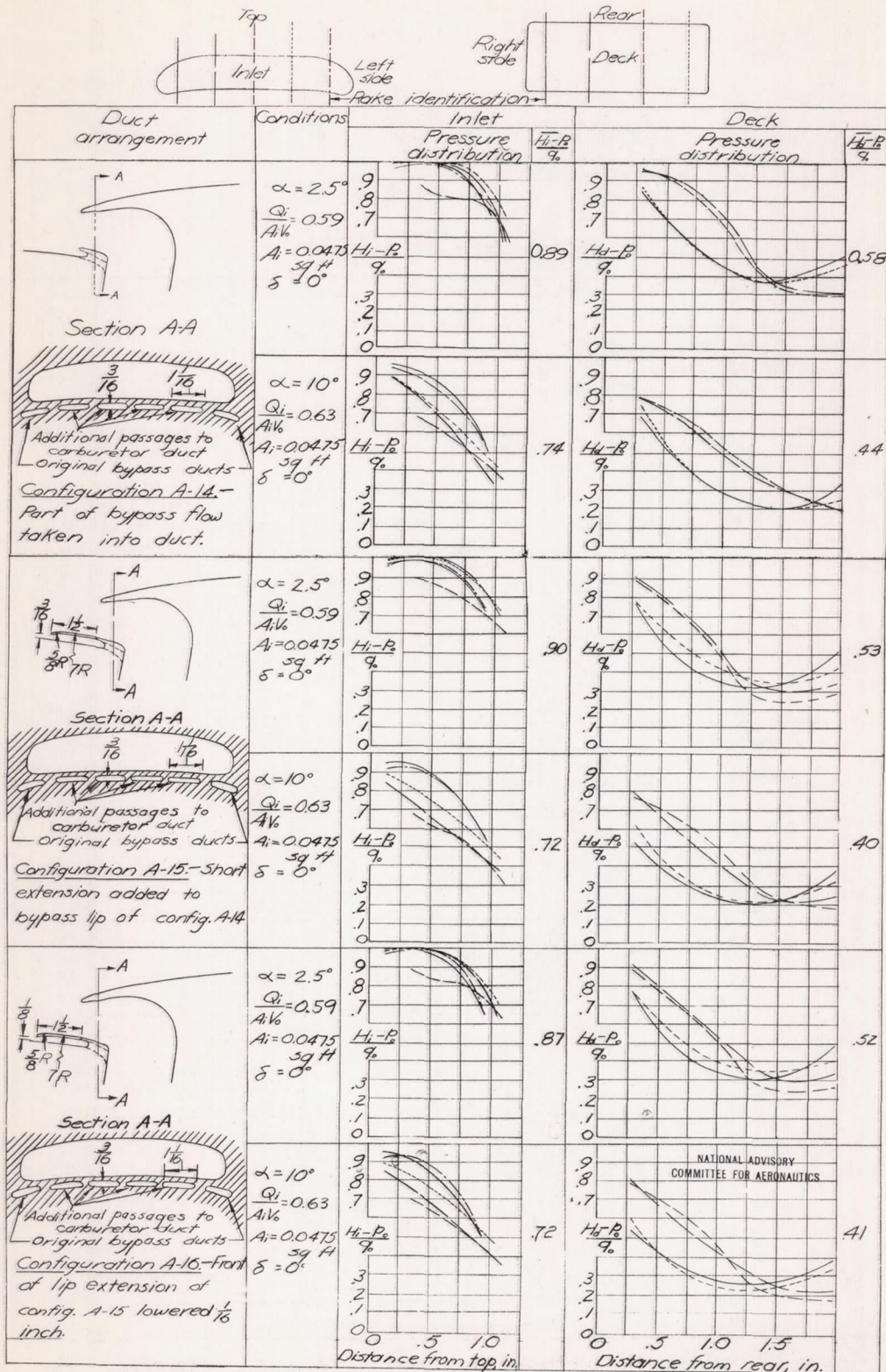


Figure 21 .-Concluded.

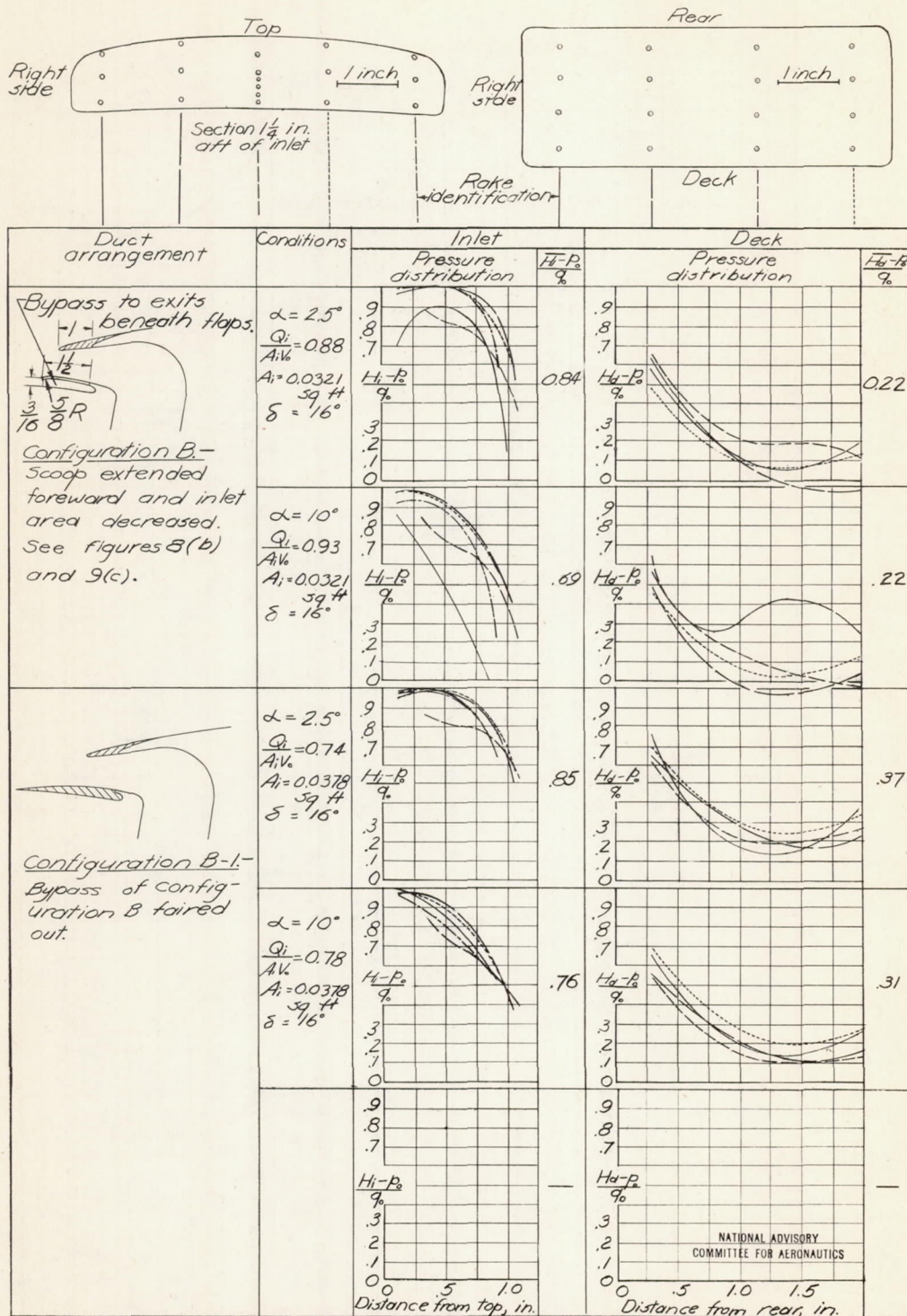


Figure 22.—Pressure distributions and average recoveries for series B carburetor ducts.

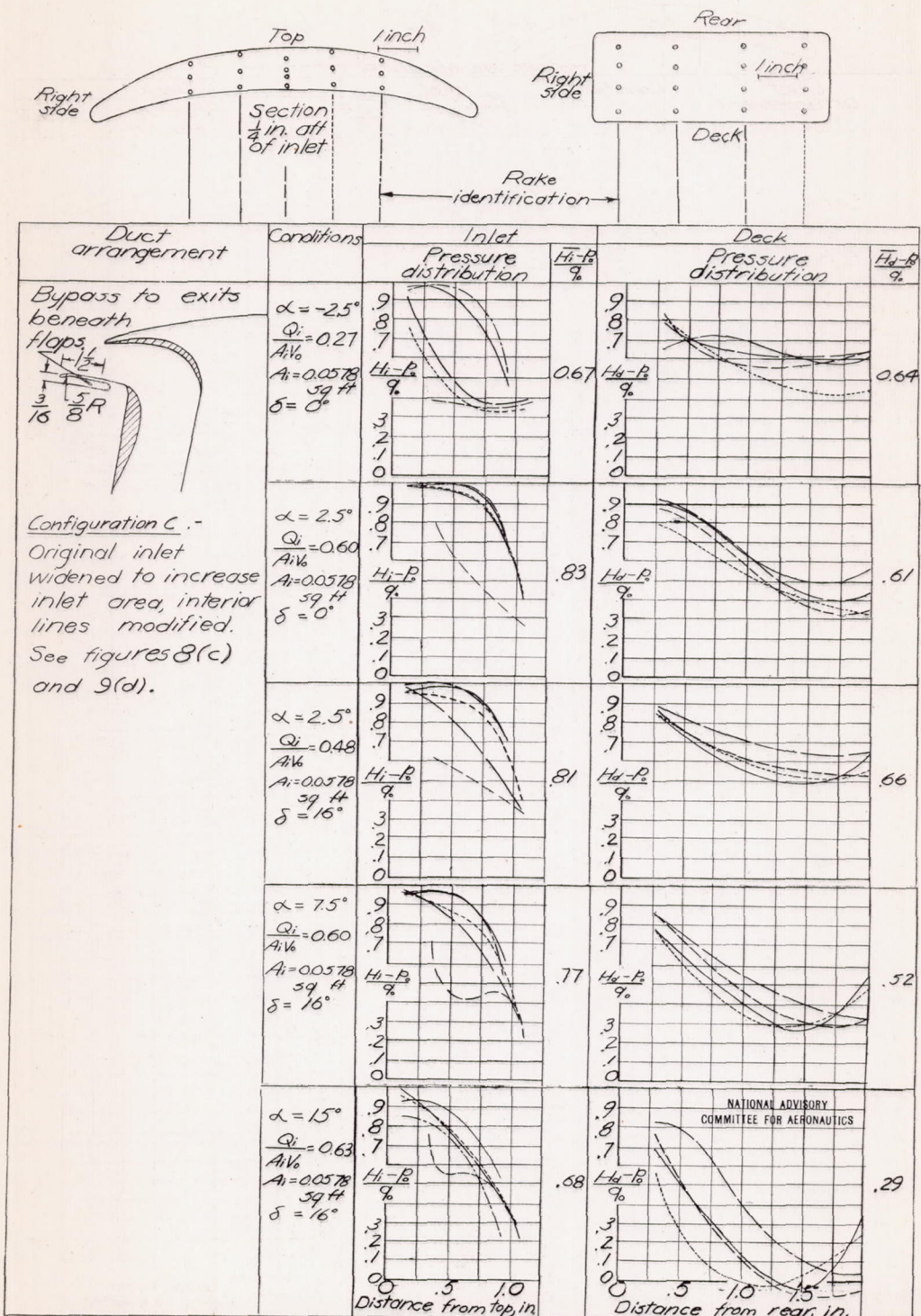


Figure 23. - Pressure distributions and average recoveries for series C carburetor ducts.

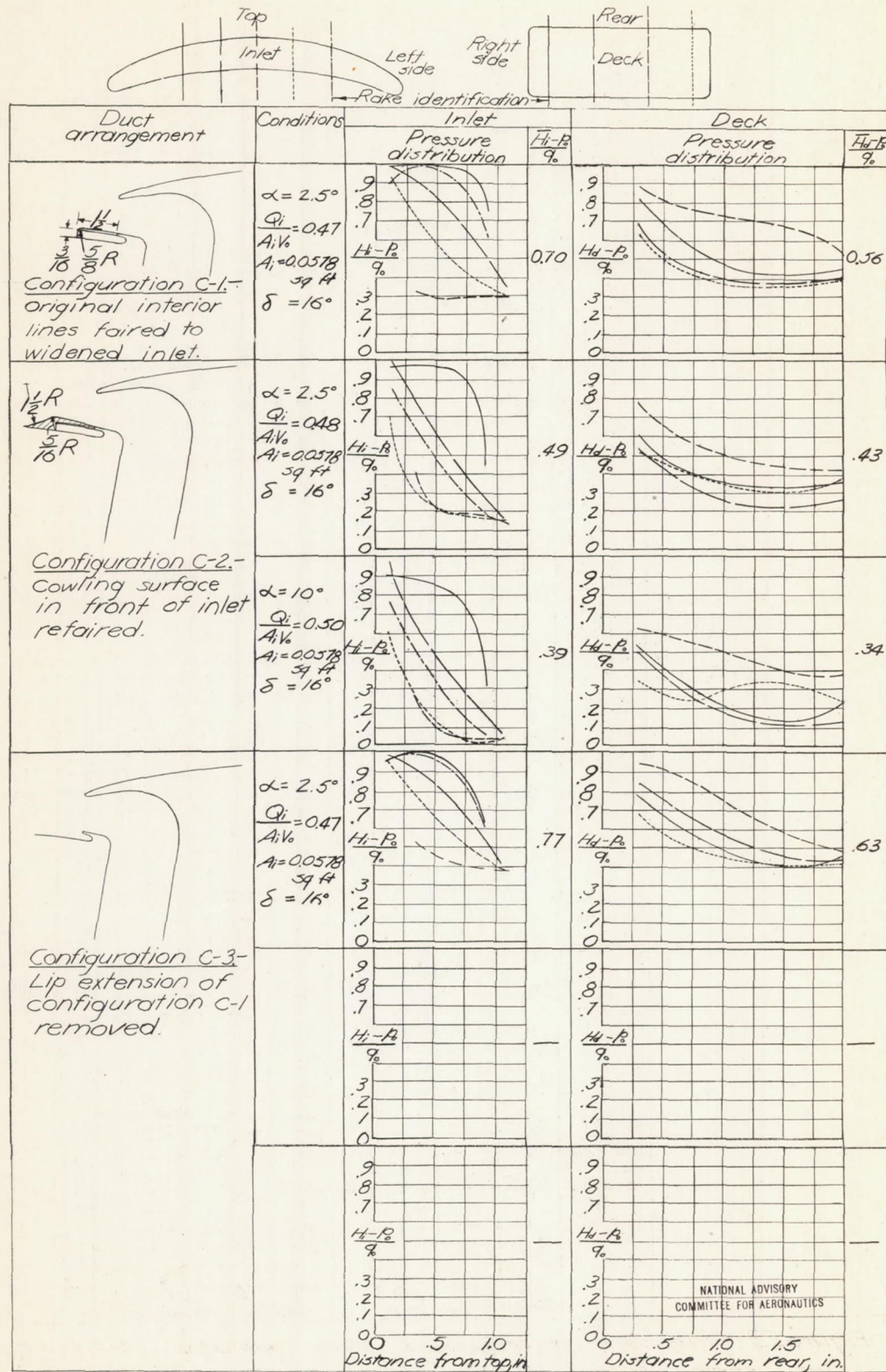


Figure 23. - Concluded.

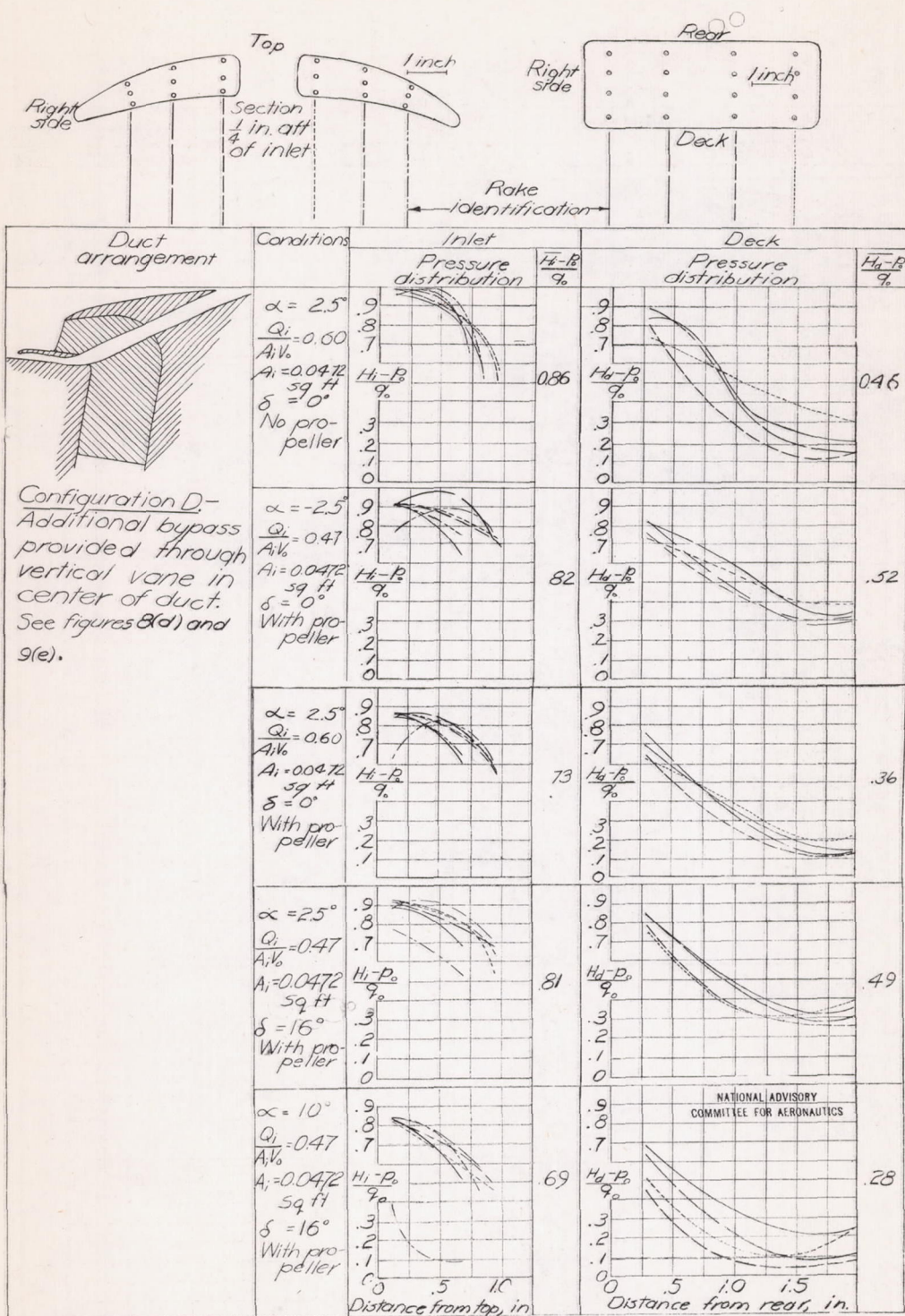


Figure 24.—Pressure distributions and average recoveries for series D carburetor ducts.

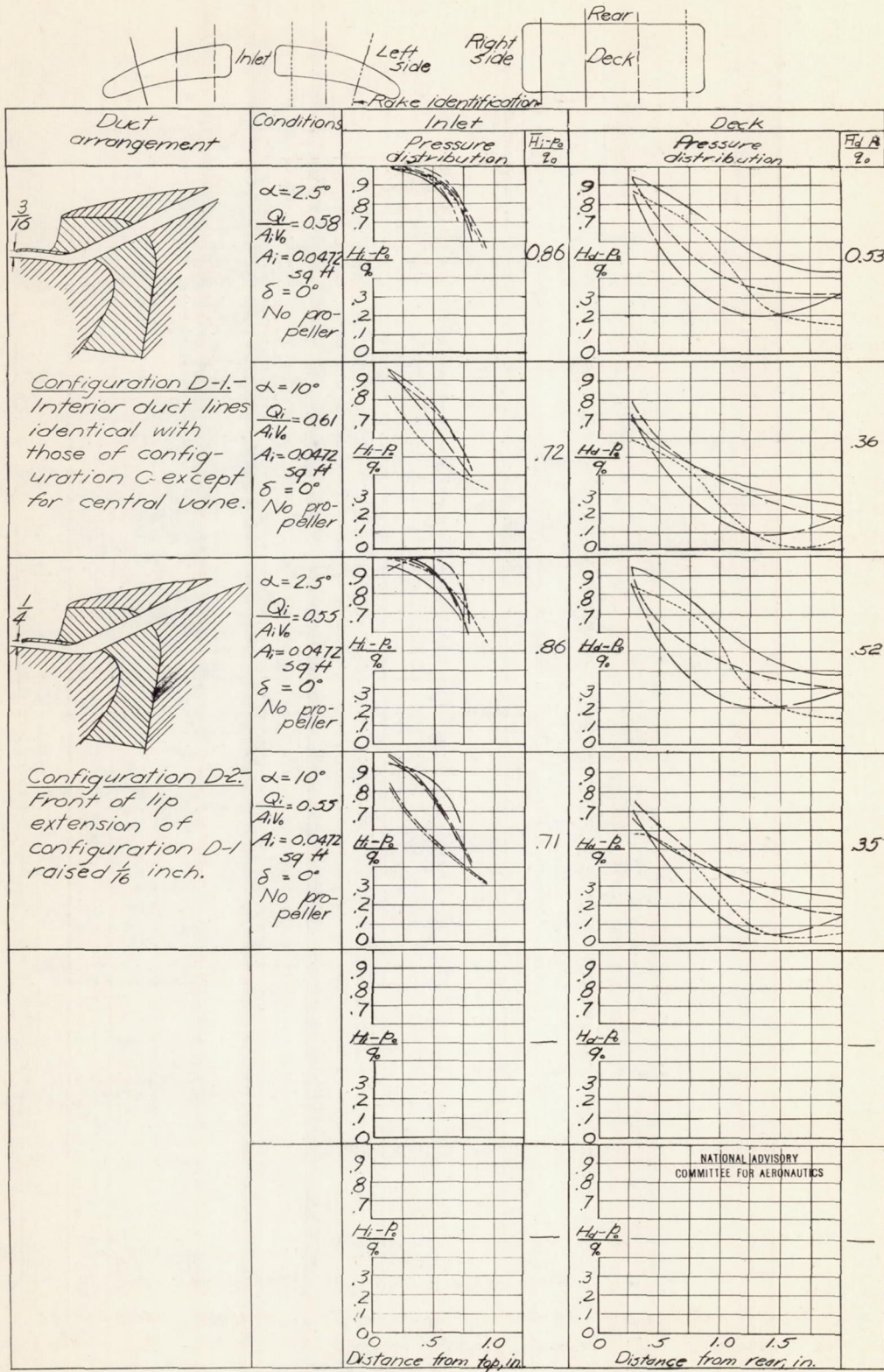


Figure 24. -Concluded.

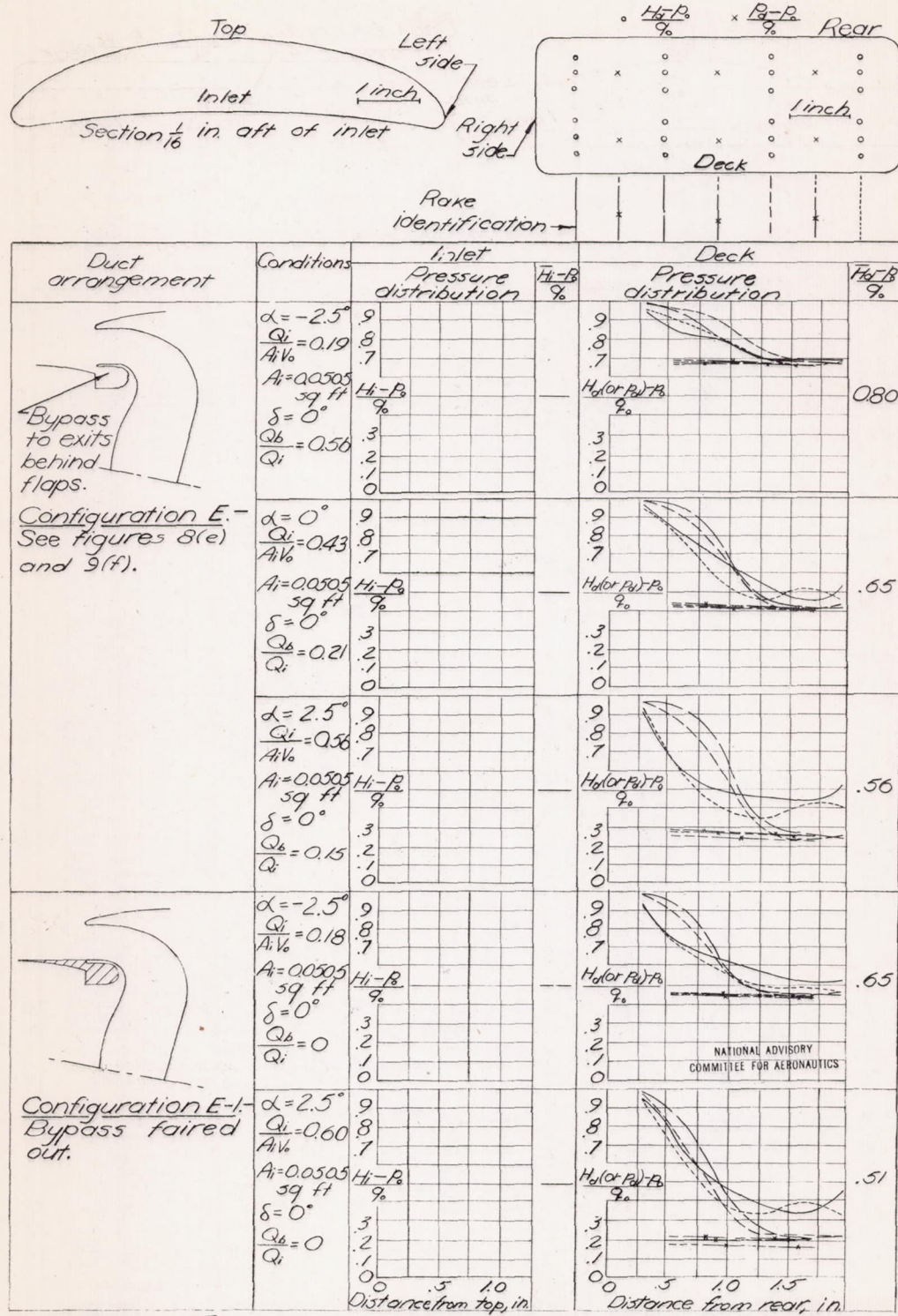


Figure 25.—Pressure distributions and average recoveries for series E carburetor ducts.

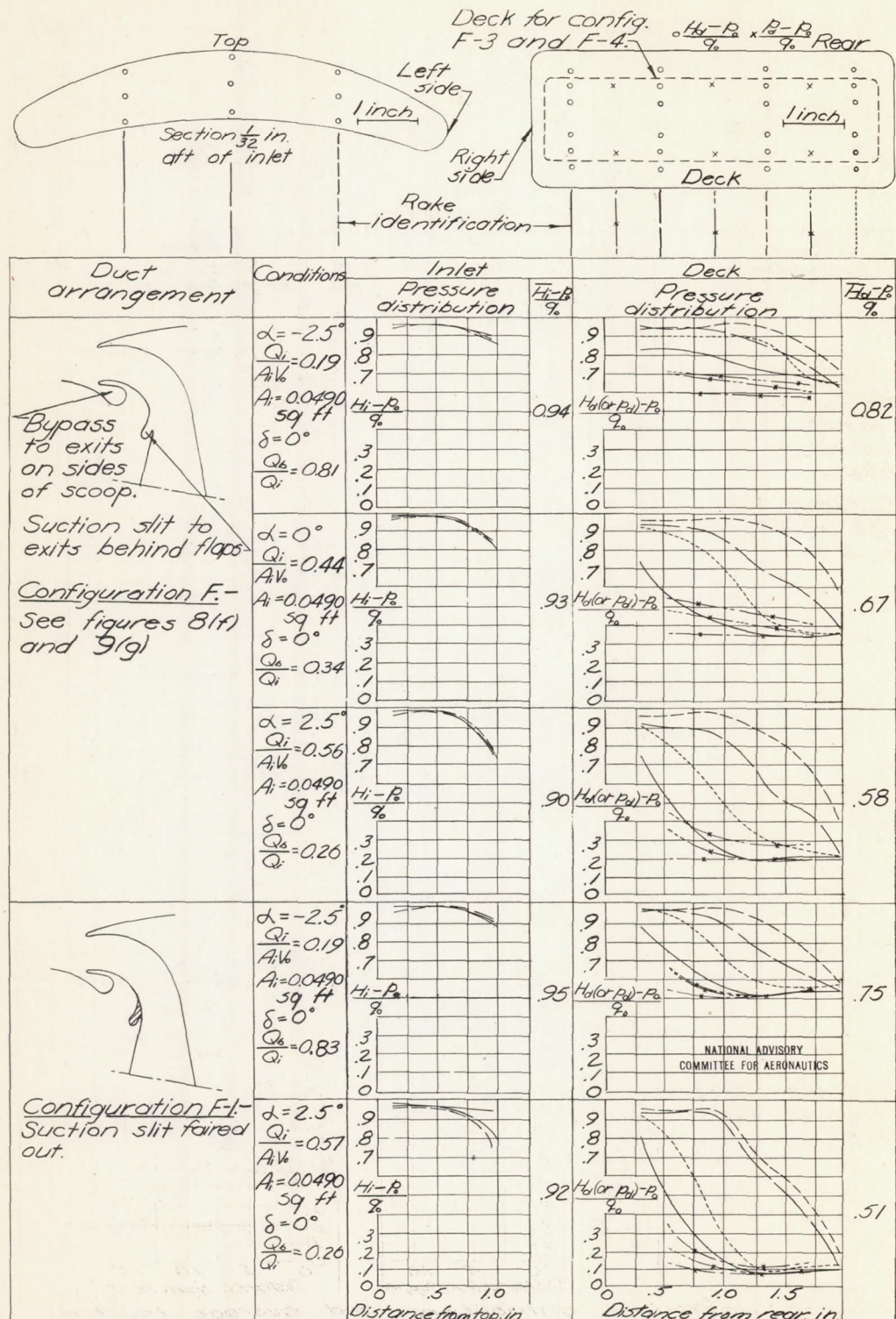


Figure 26.—Pressure distributions and average recoveries for series F carburetor ducts.

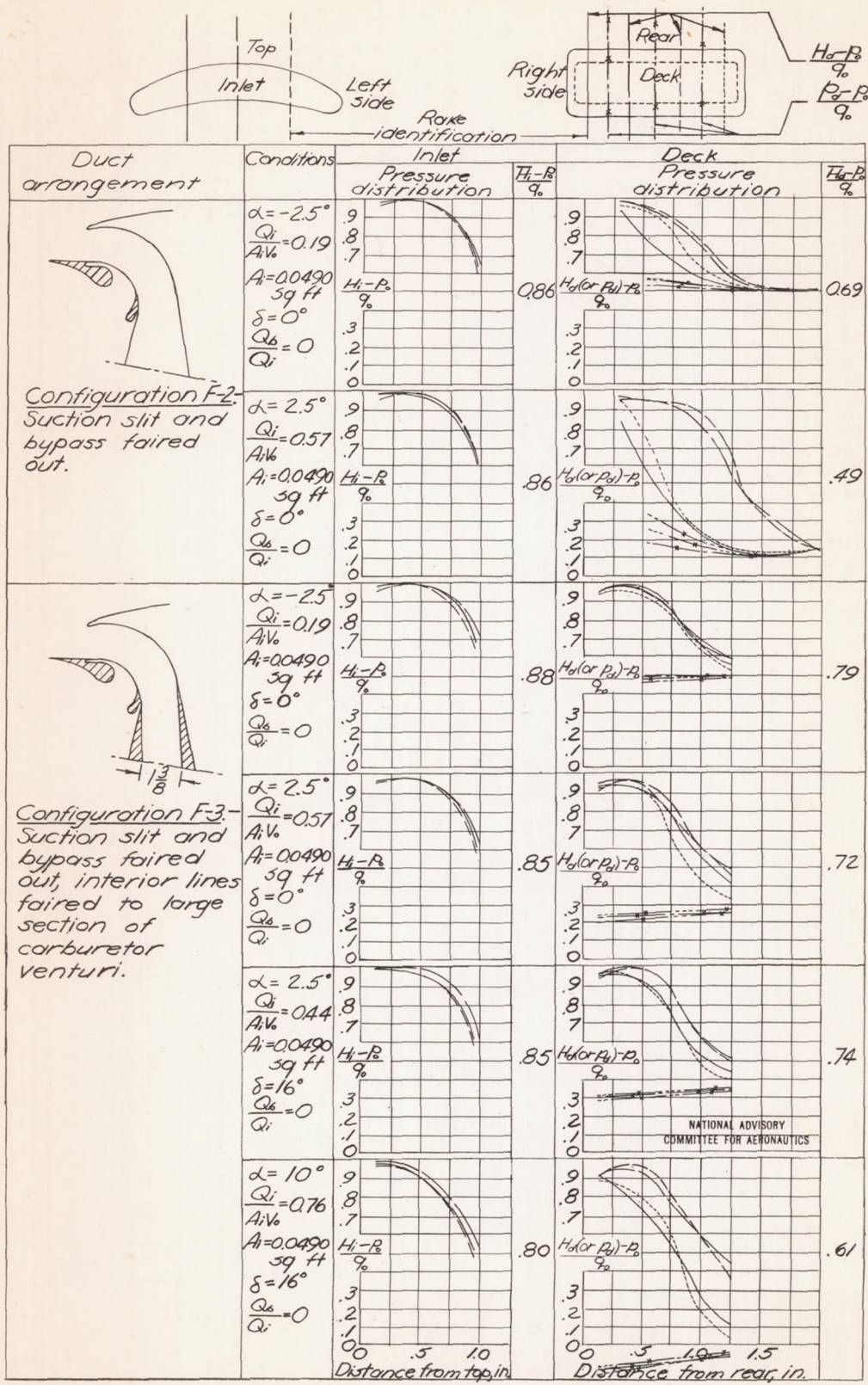


Figure 26.-Continued.

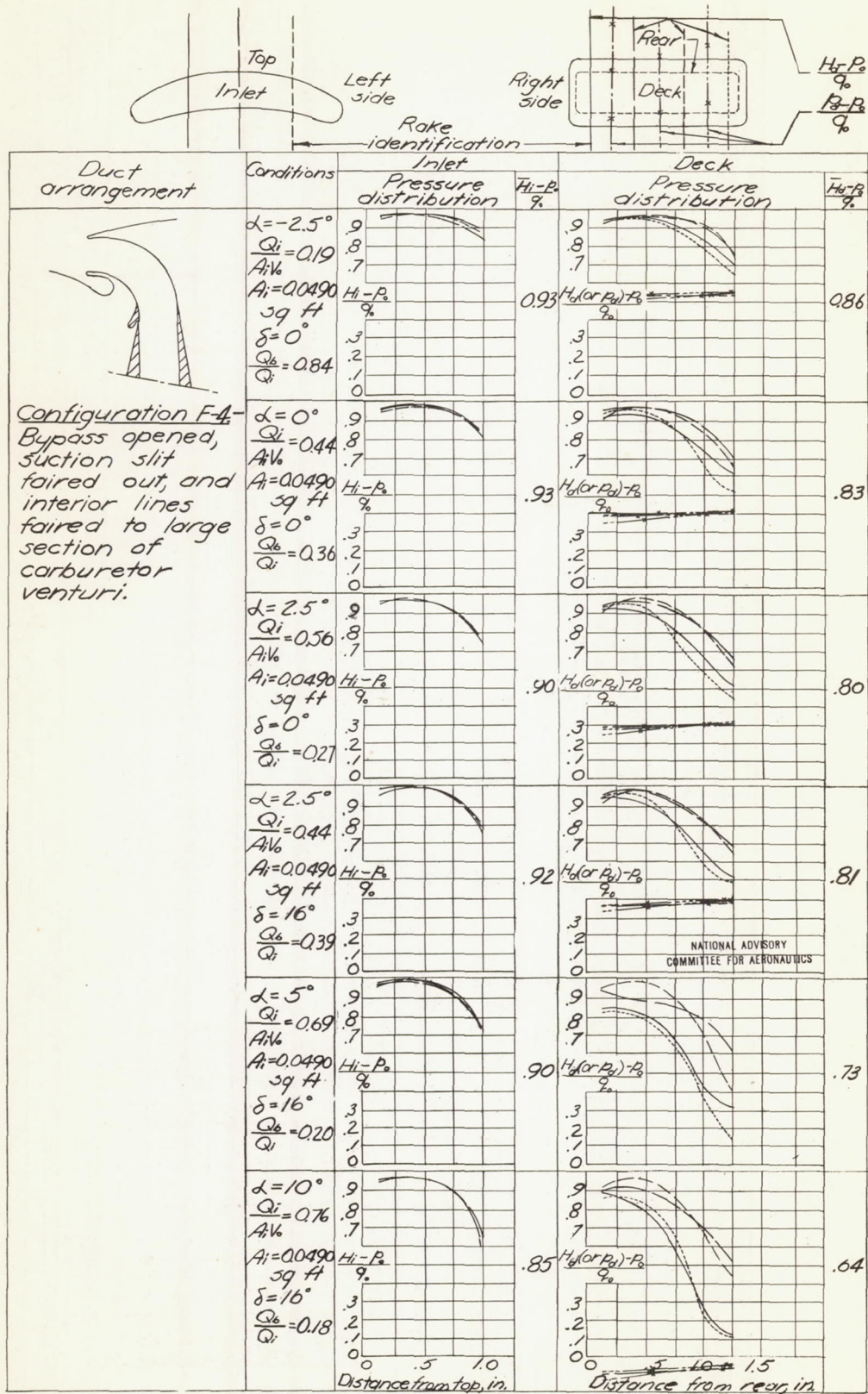


Figure 26 .- Concluded.

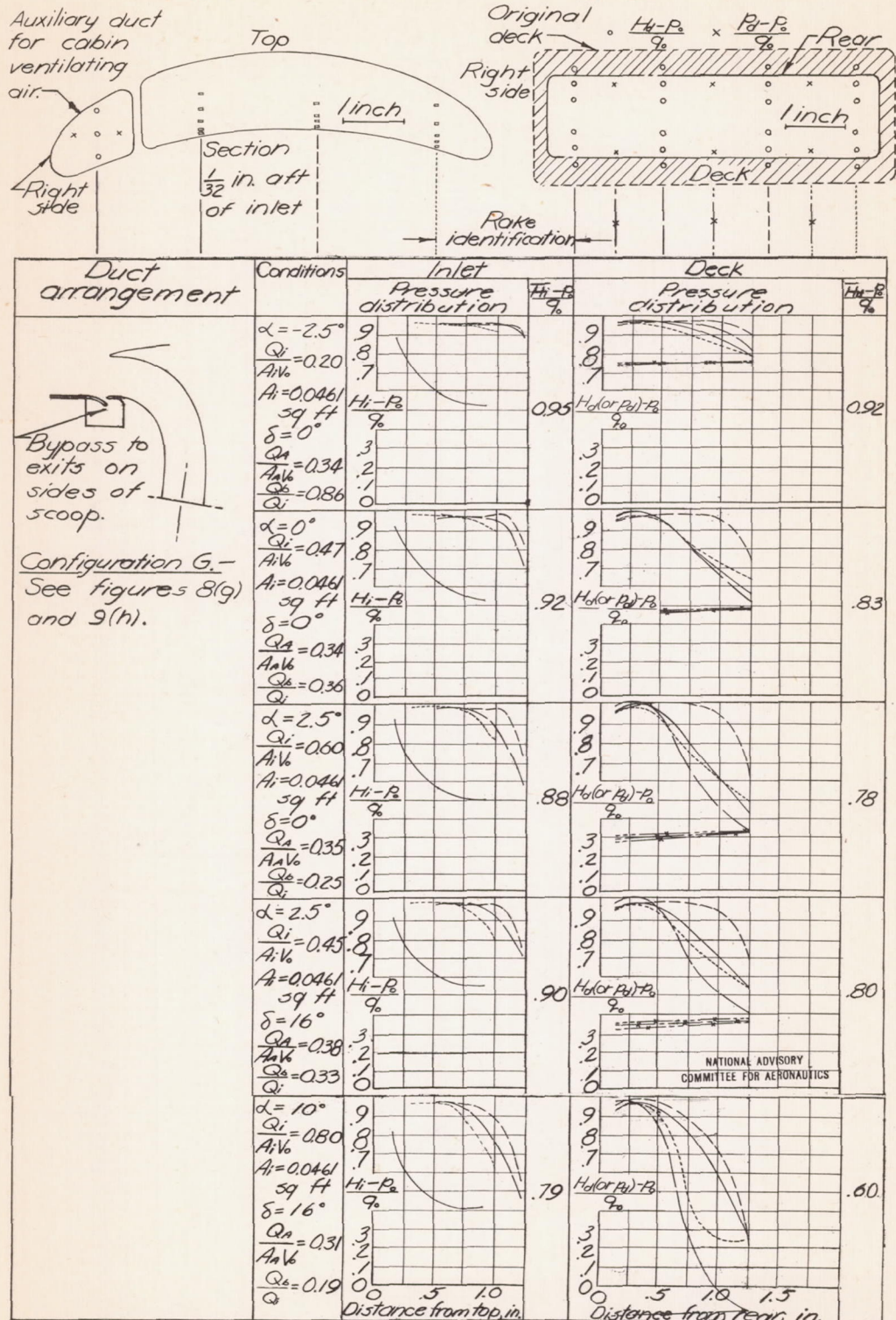


Figure 27.—Pressure distribution and average recoveries for series G carburetor ducts.

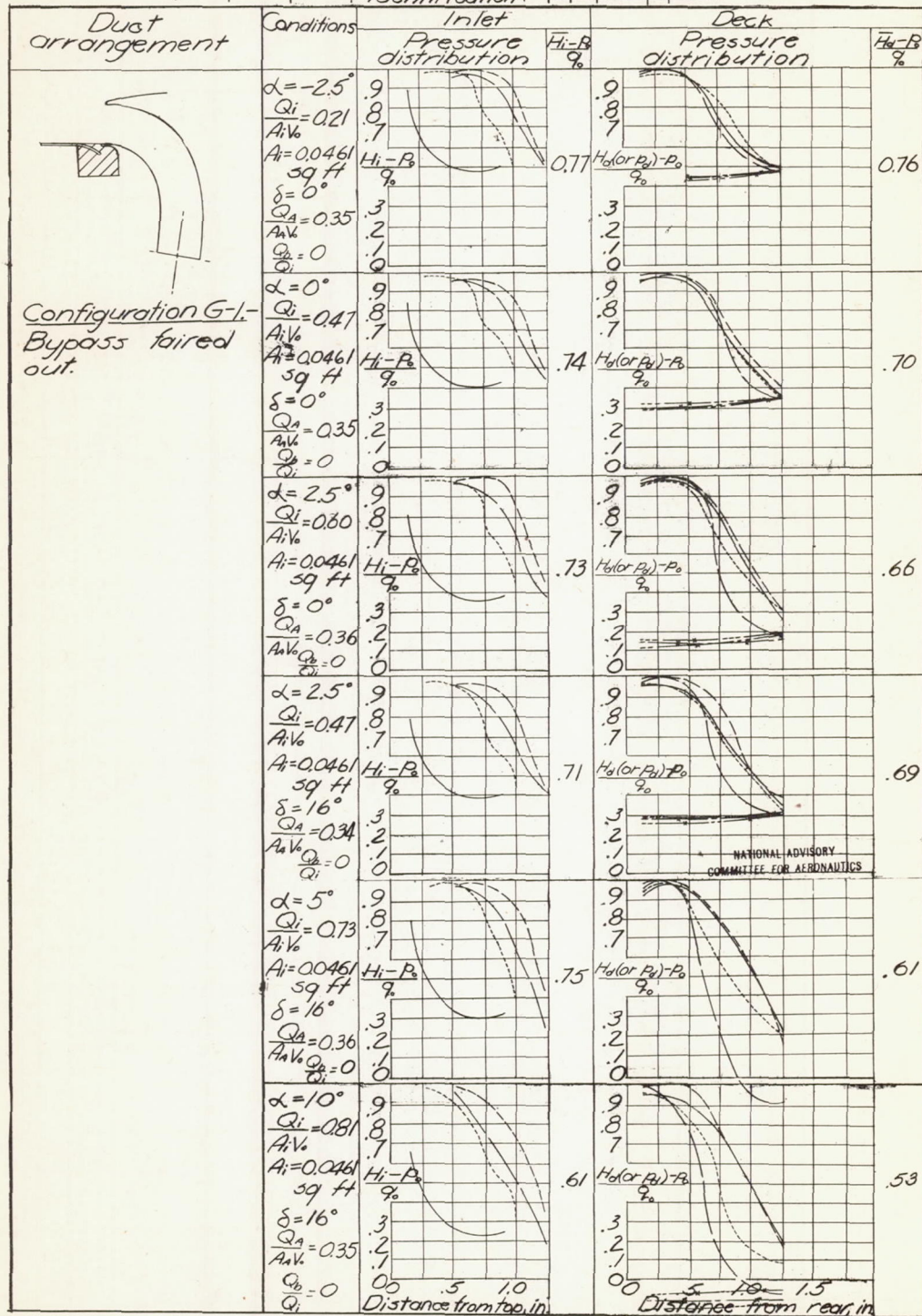
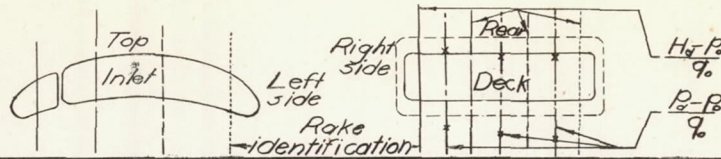


Figure 27. — Concluded.

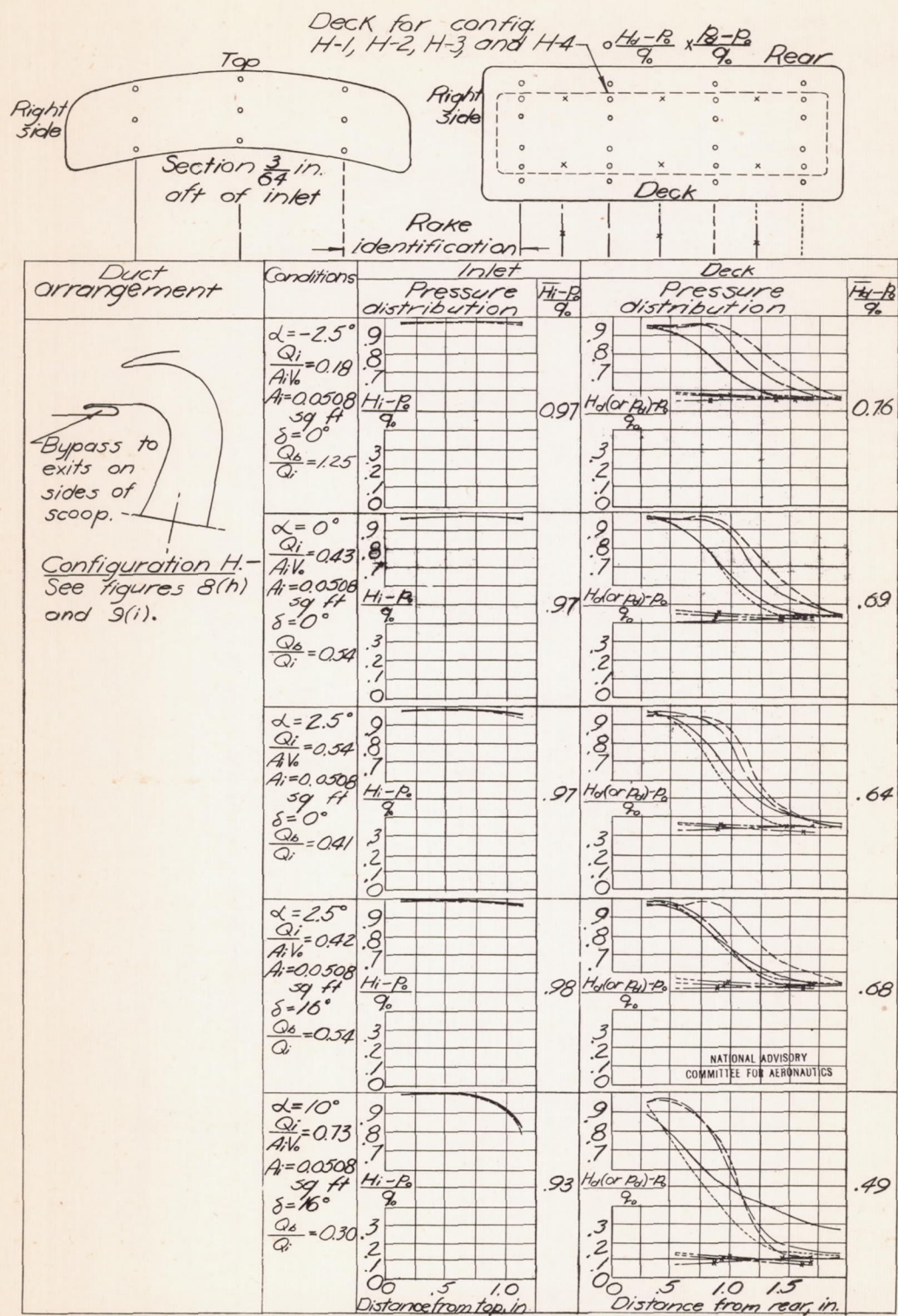


Figure 28.—Pressure distributions and average recoveries for series H carburetor ducts.

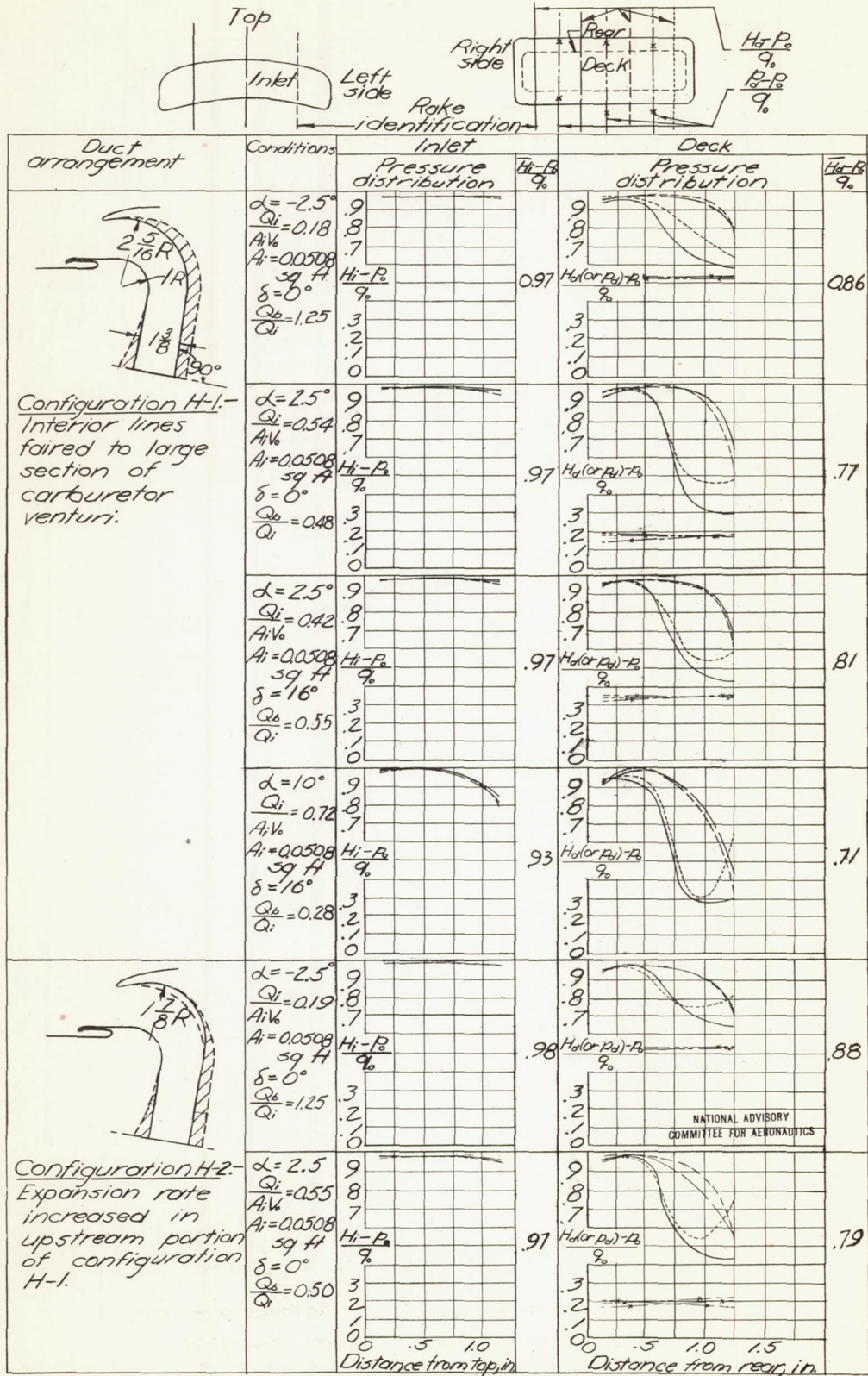


Figure 28 . - Continued.

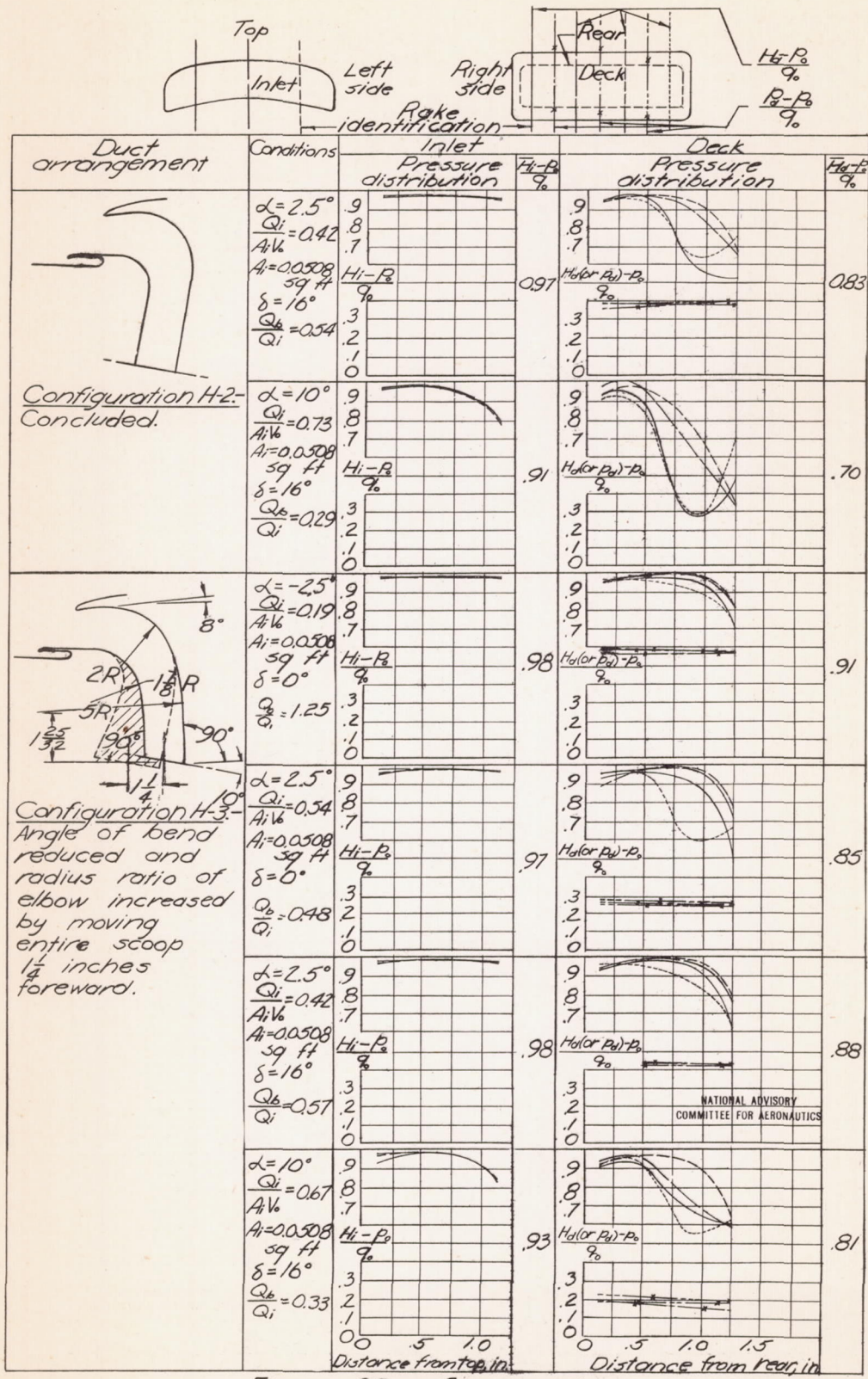


Figure 28. — Continued.

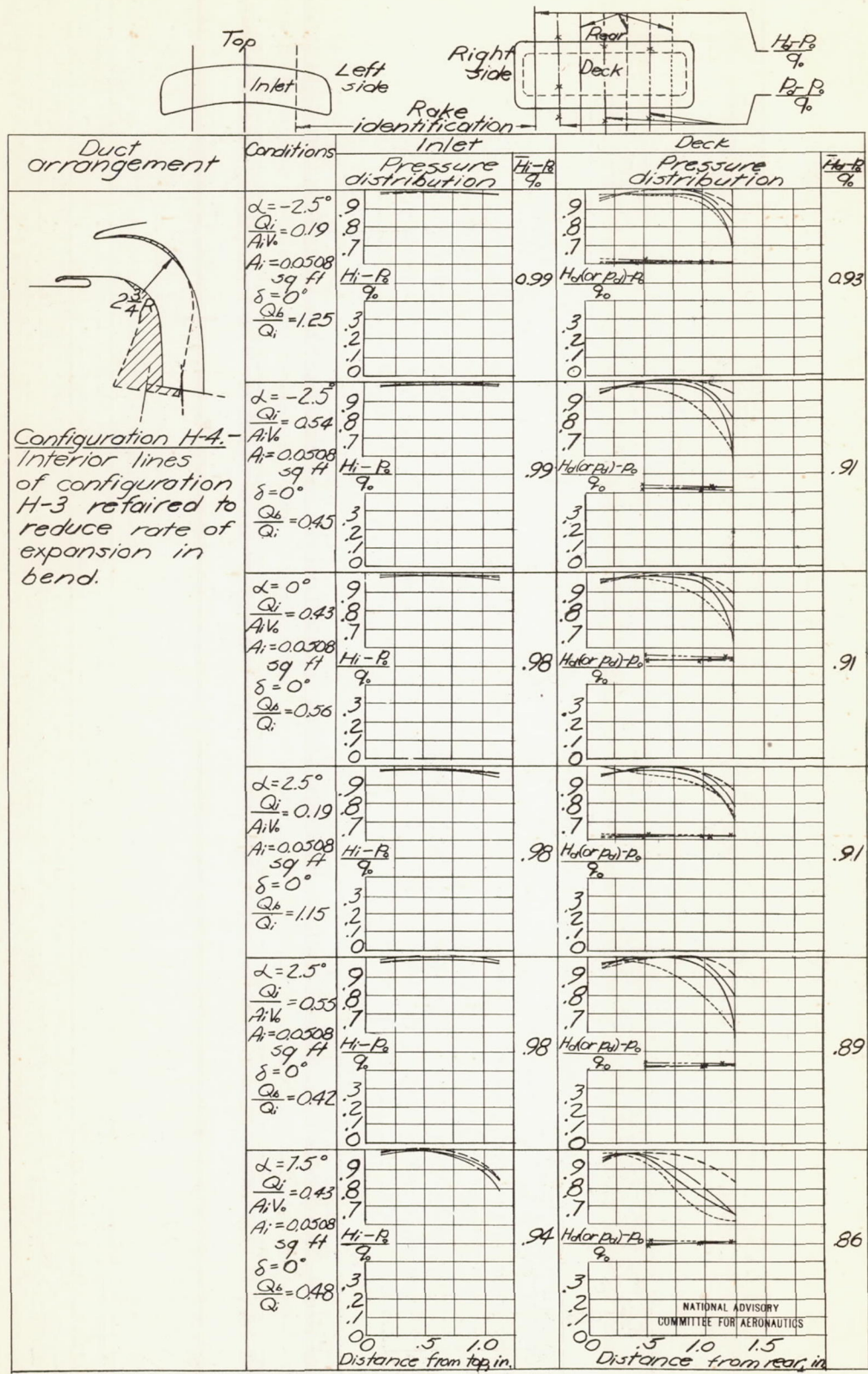


Figure 28. - Concluded.

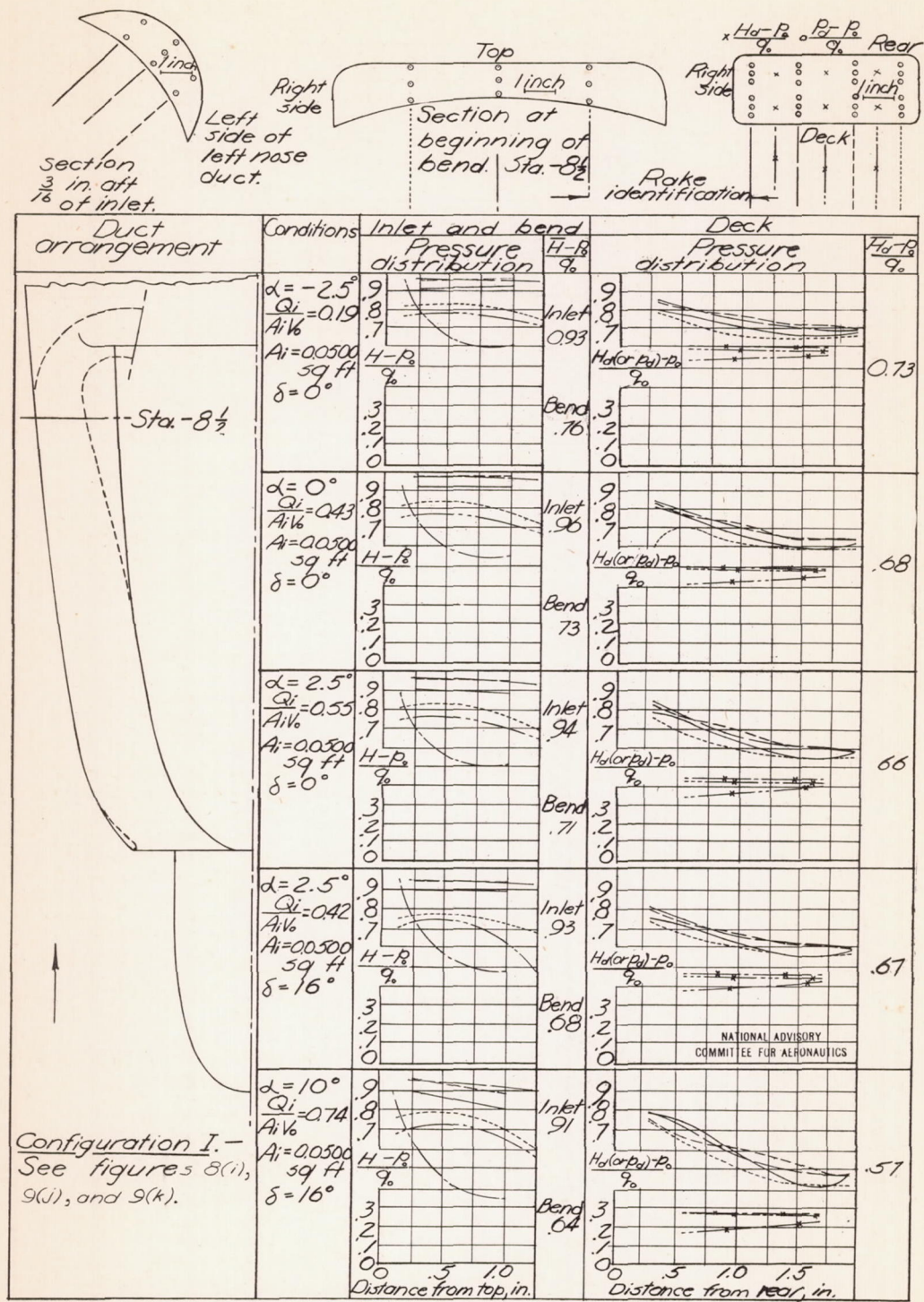


Figure 29. - Pressure distributions and average recoveries for series I carburetor ducts.

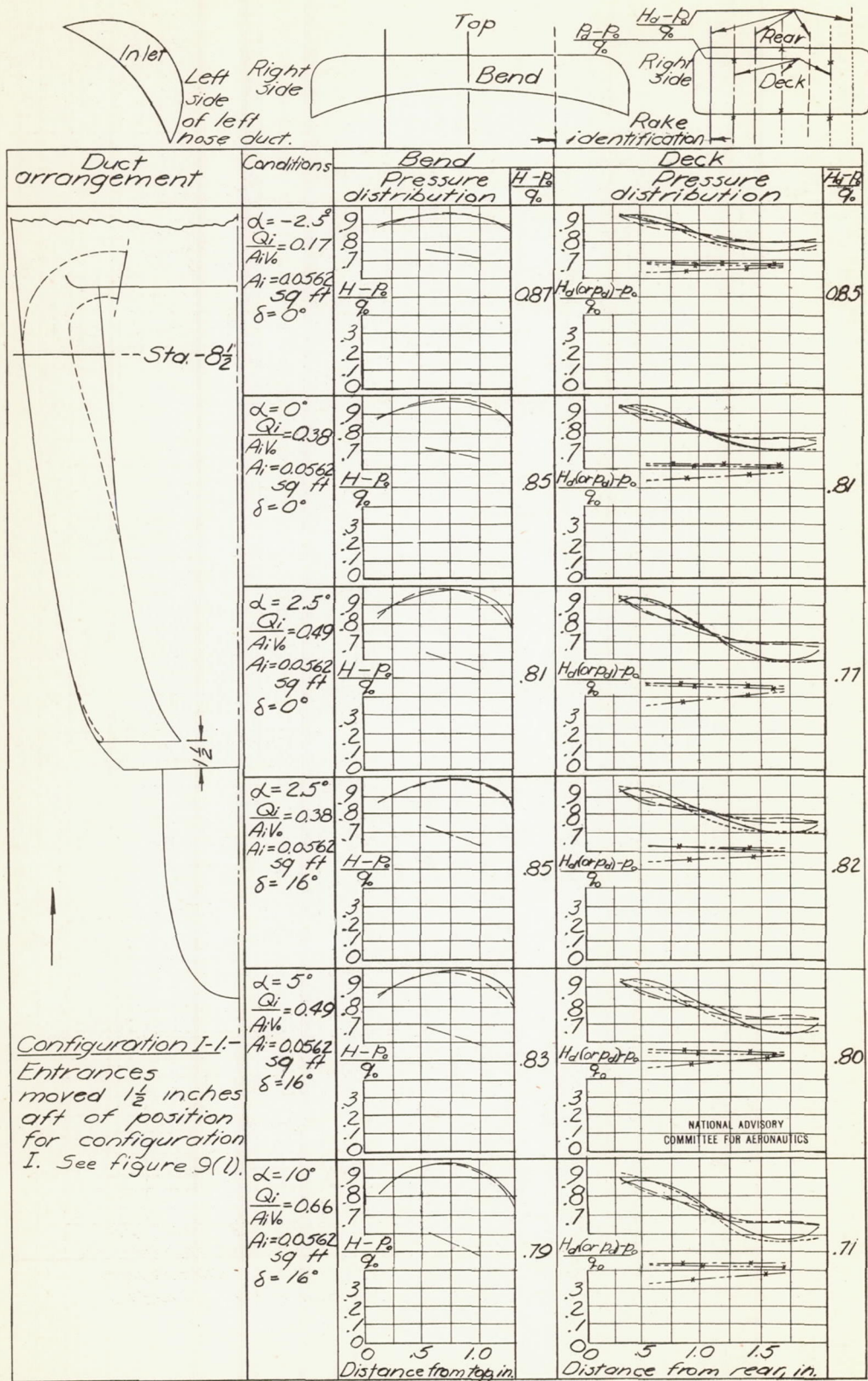
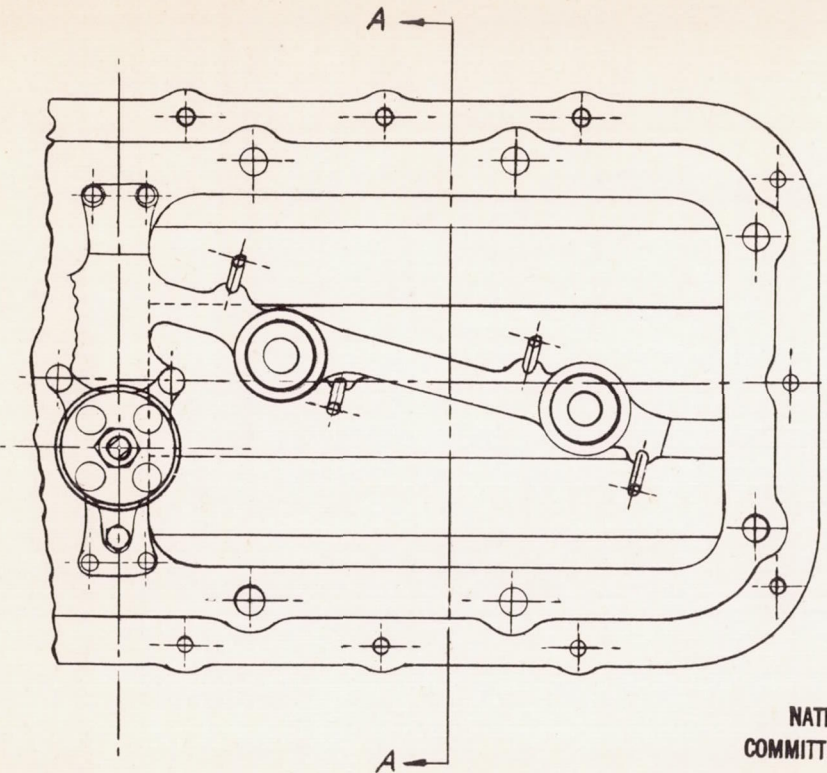
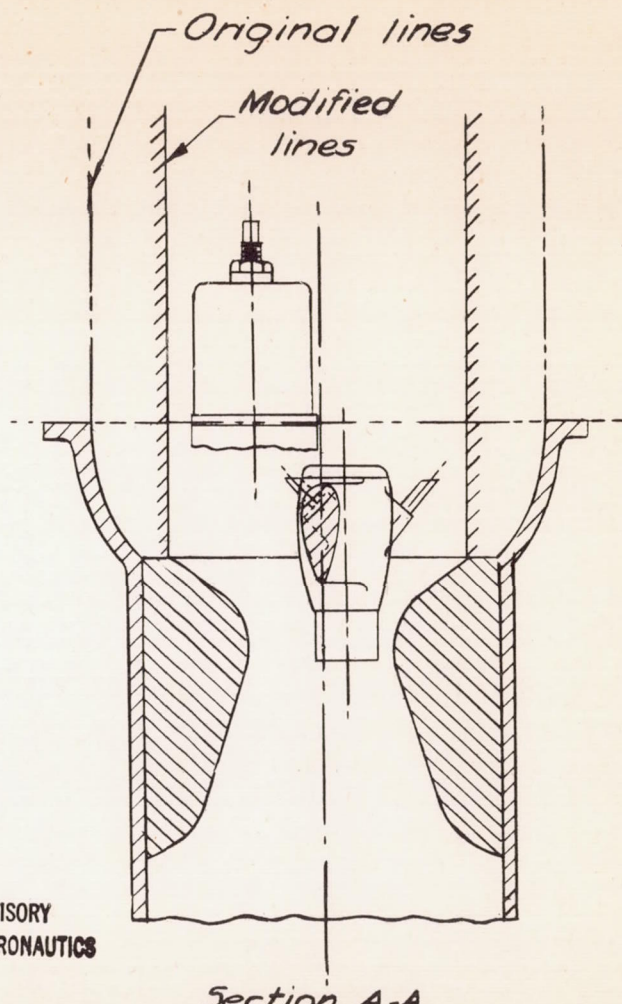


Figure 29.—Concluded.



Plan view - carburetor top deck.

NATIONAL ADVISORY
COMMITTEE FOR AERONAUTICS



Section A-A

Figure 30.- Sketch of carburetor showing original and modified interior duct lines.

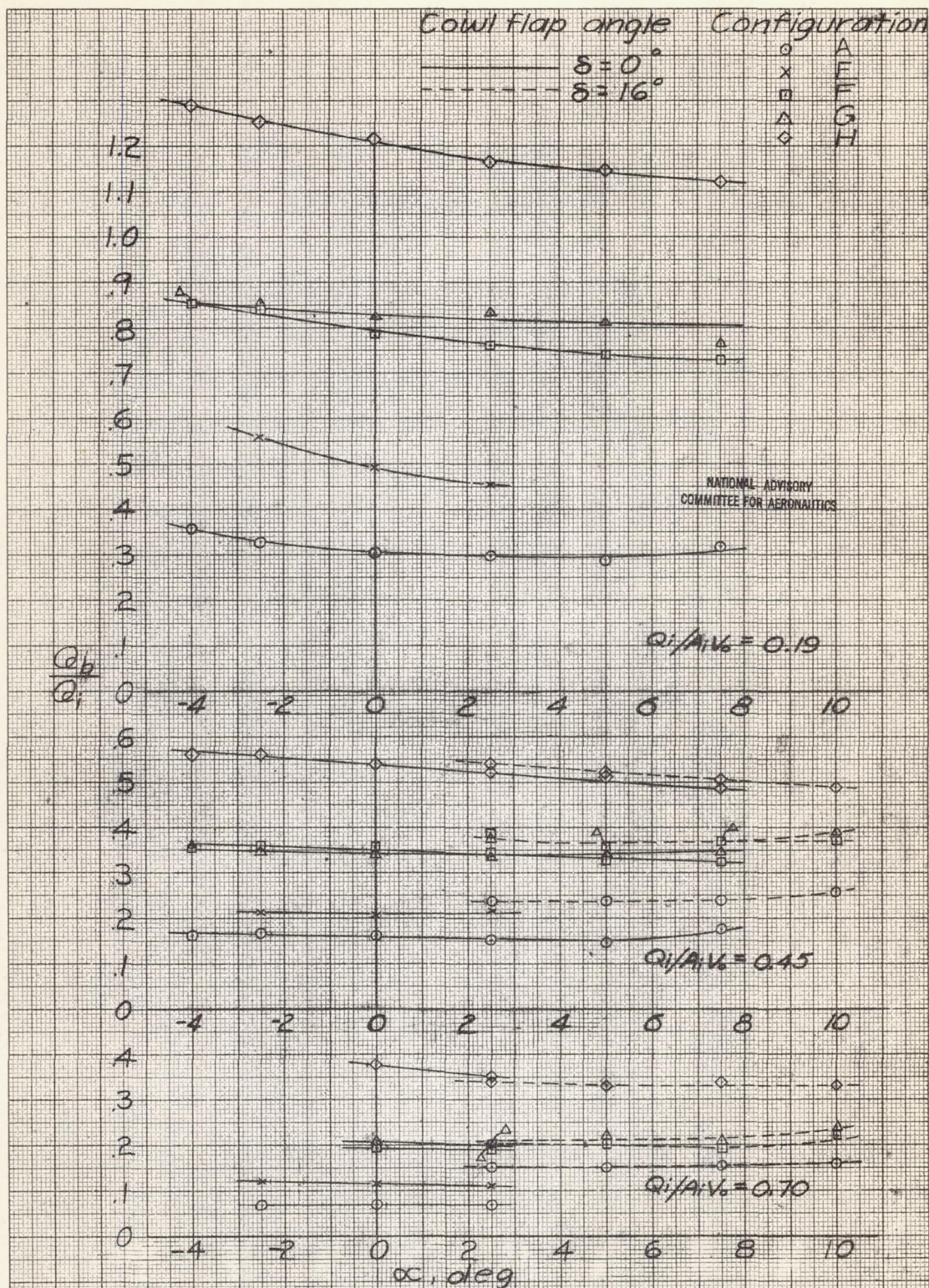


Figure 31 - Variation of bypass flow with angle of attack at several inlet-velocity ratios

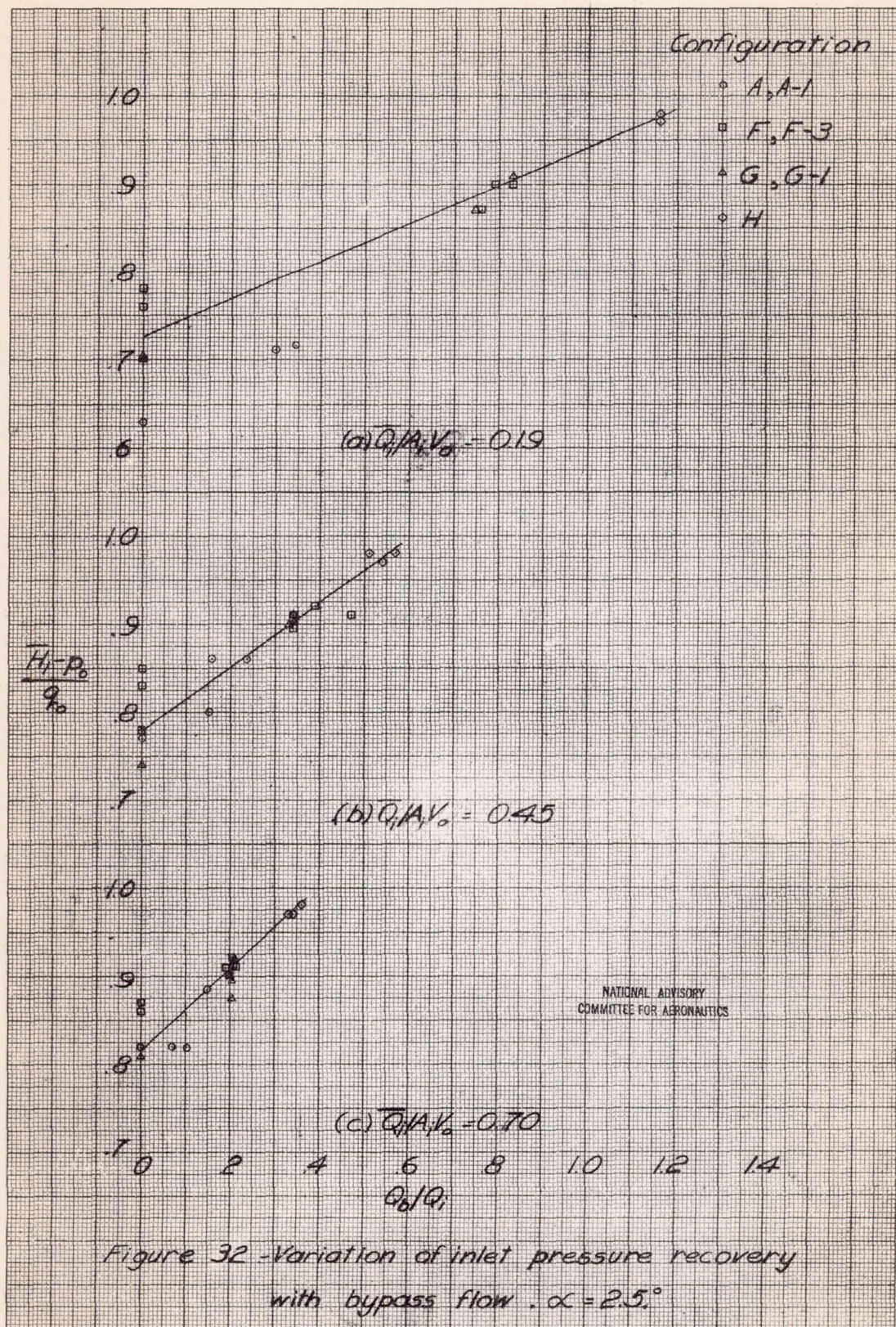


Figure 32 - Variation of inlet pressure recovery with bypass flow. $\alpha = 2.5^\circ$

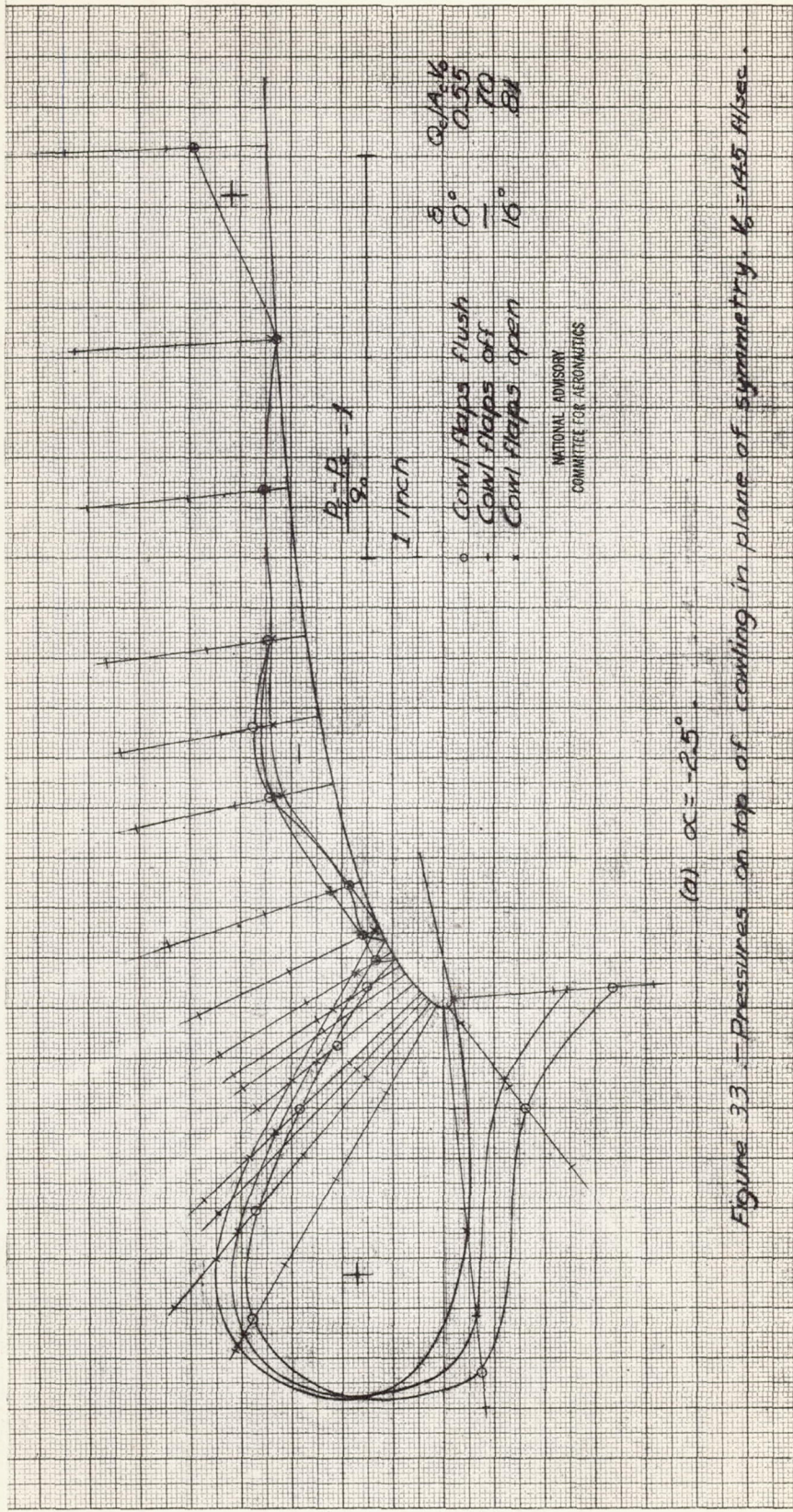
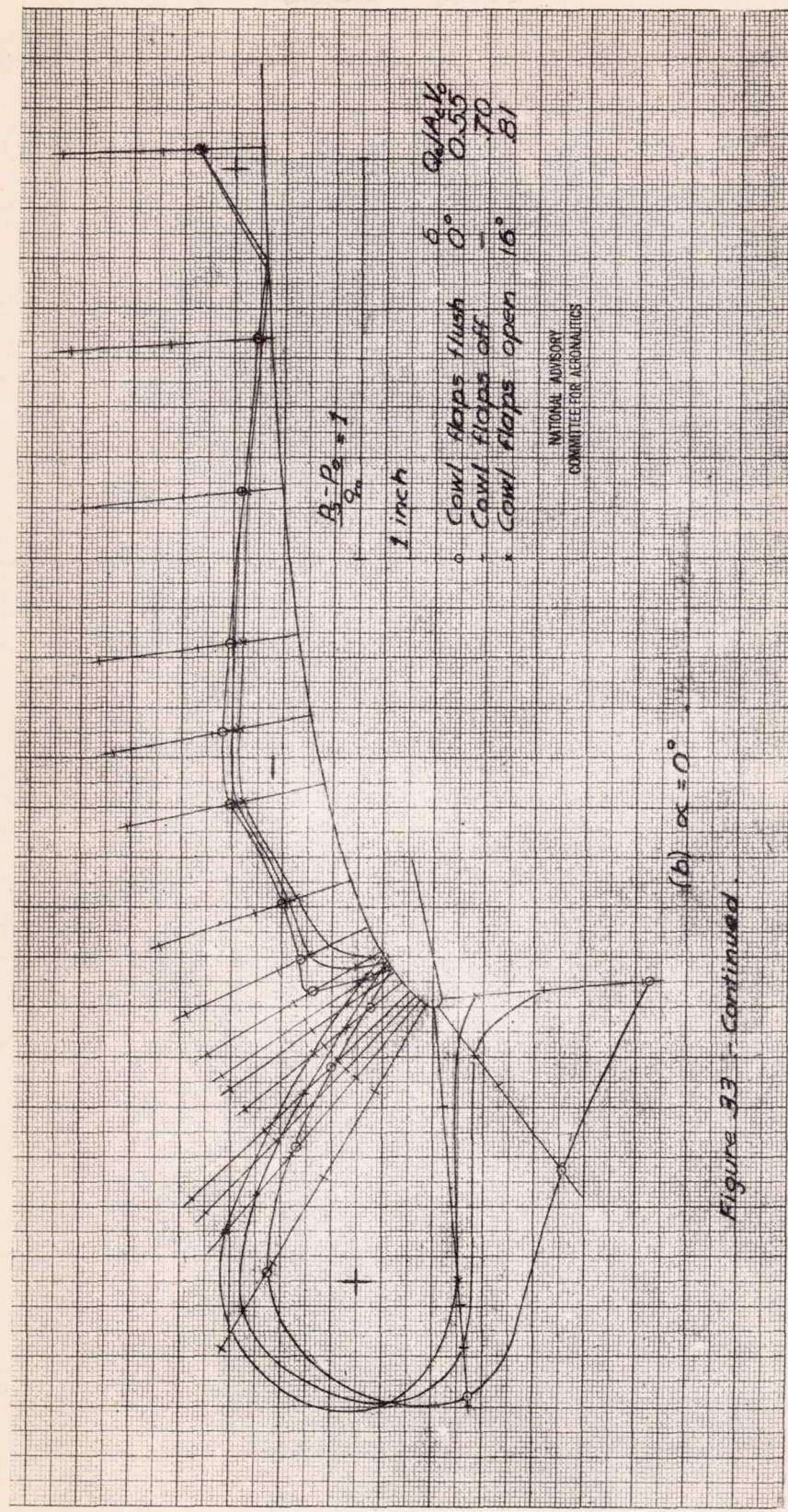


Figure 33.—Pressures on top of wing in plane of symmetry, $V = 142.5$ ft/sec.
(a) $\alpha = -2.5^\circ$.



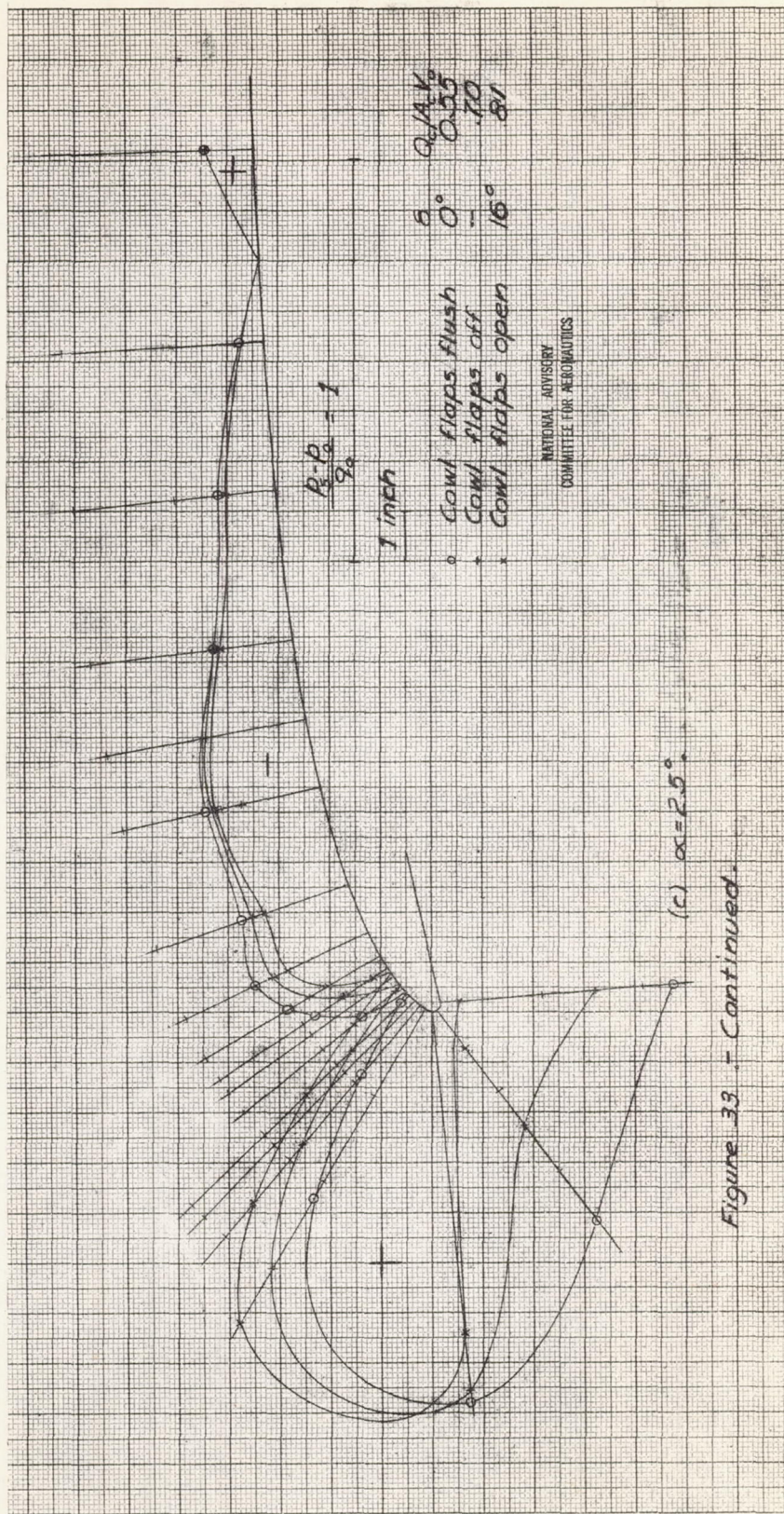


Figure 33 - Continued.

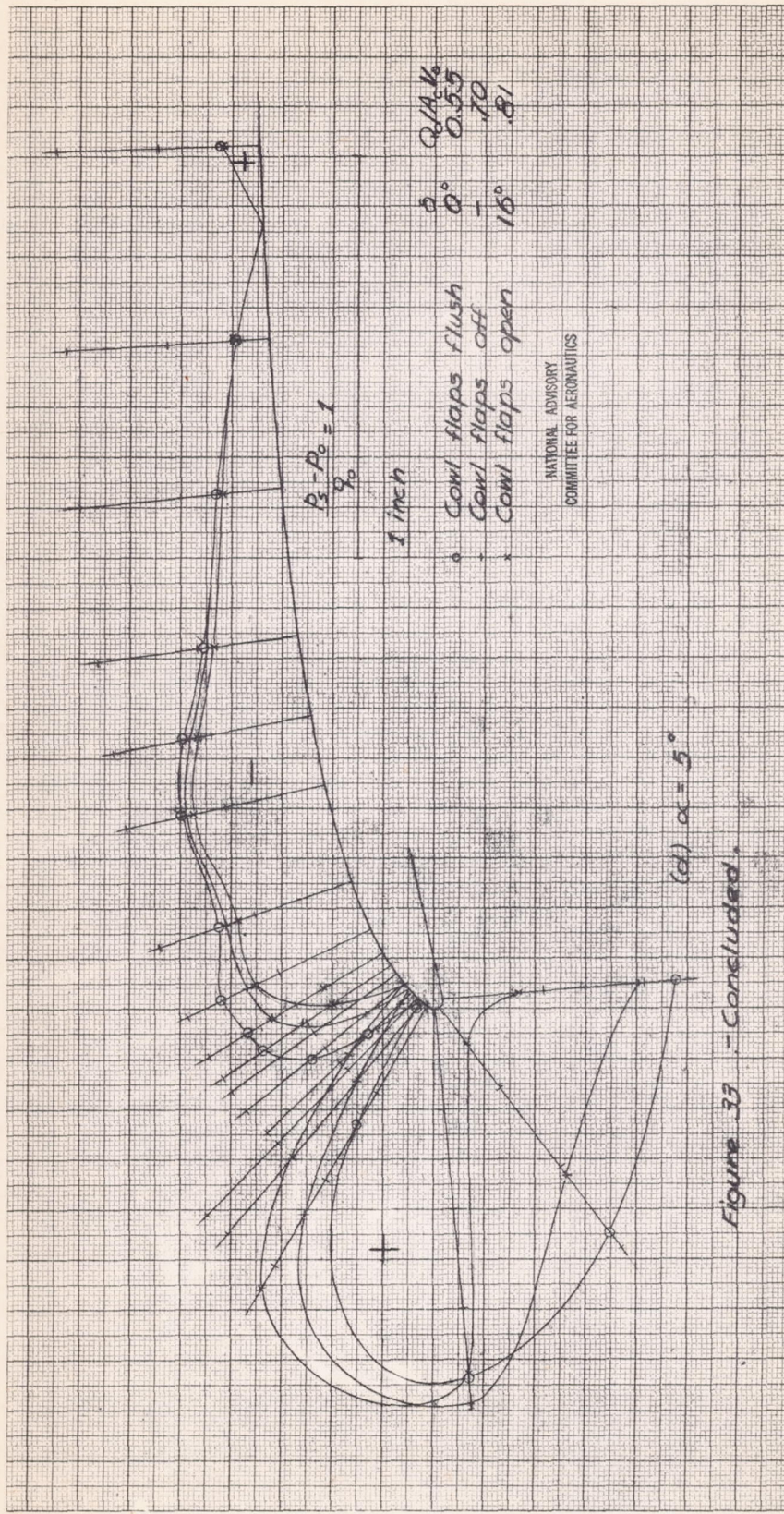
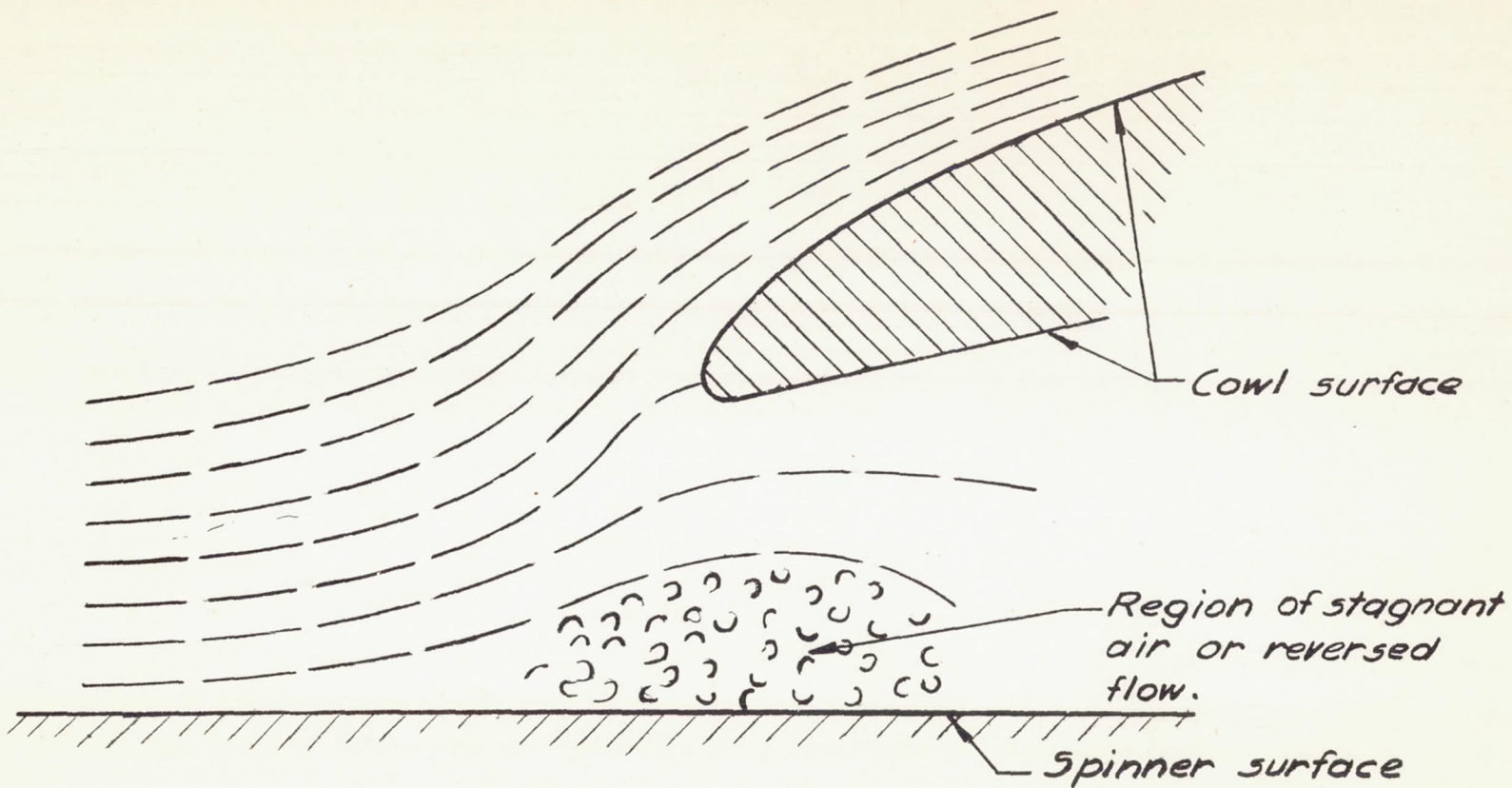


Figure 35 - concluded.



NATIONAL ADVISORY
COMMITTEE FOR AERONAUTICS

Figure 34.- Configuration of streamlines at top of cowl entry from tuft observations and pressure measurements on the cowl lip and at the top of the cowl orifice plate, $\alpha = 25^\circ$, $Q_i/A_i V_0 = 0.55$.

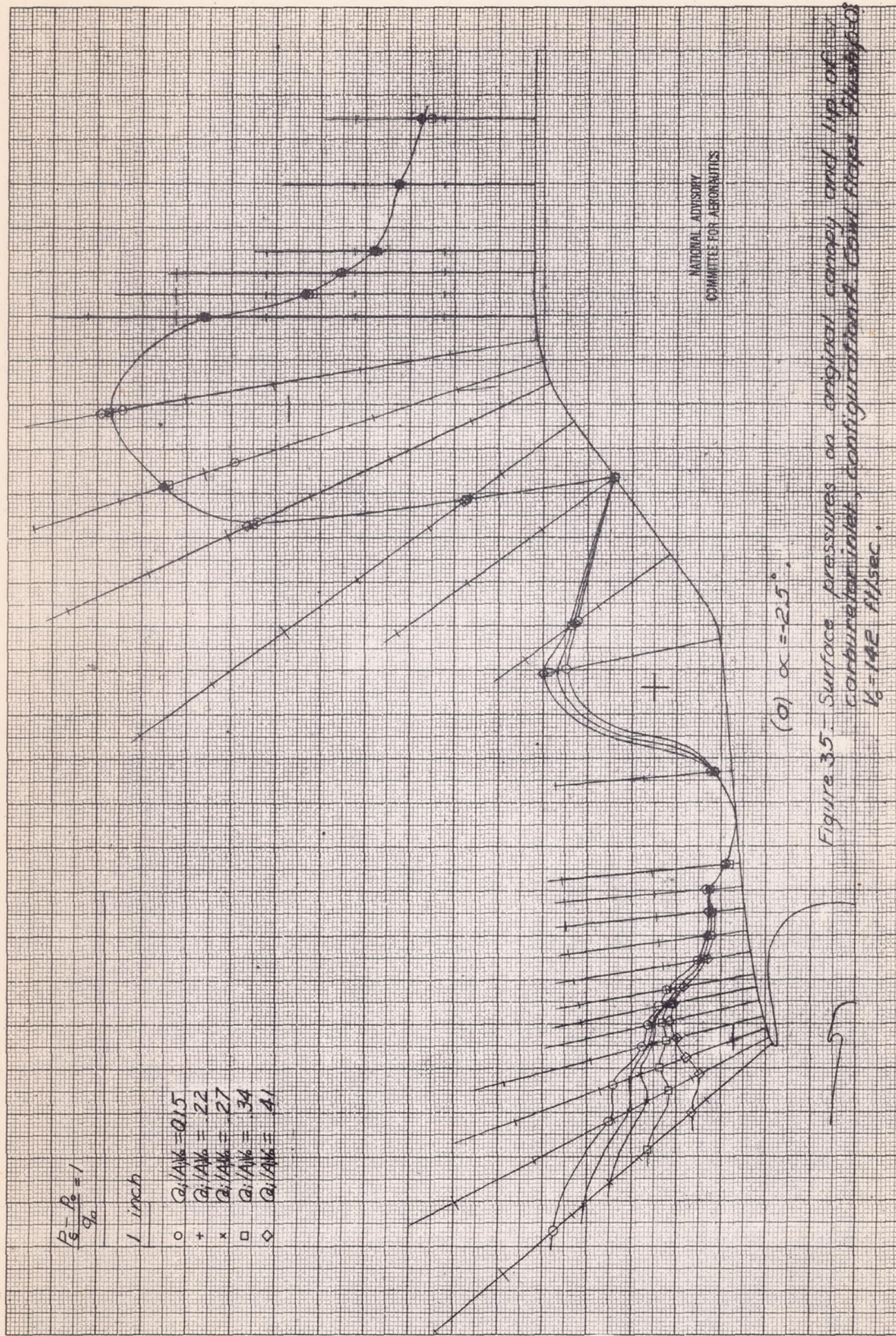
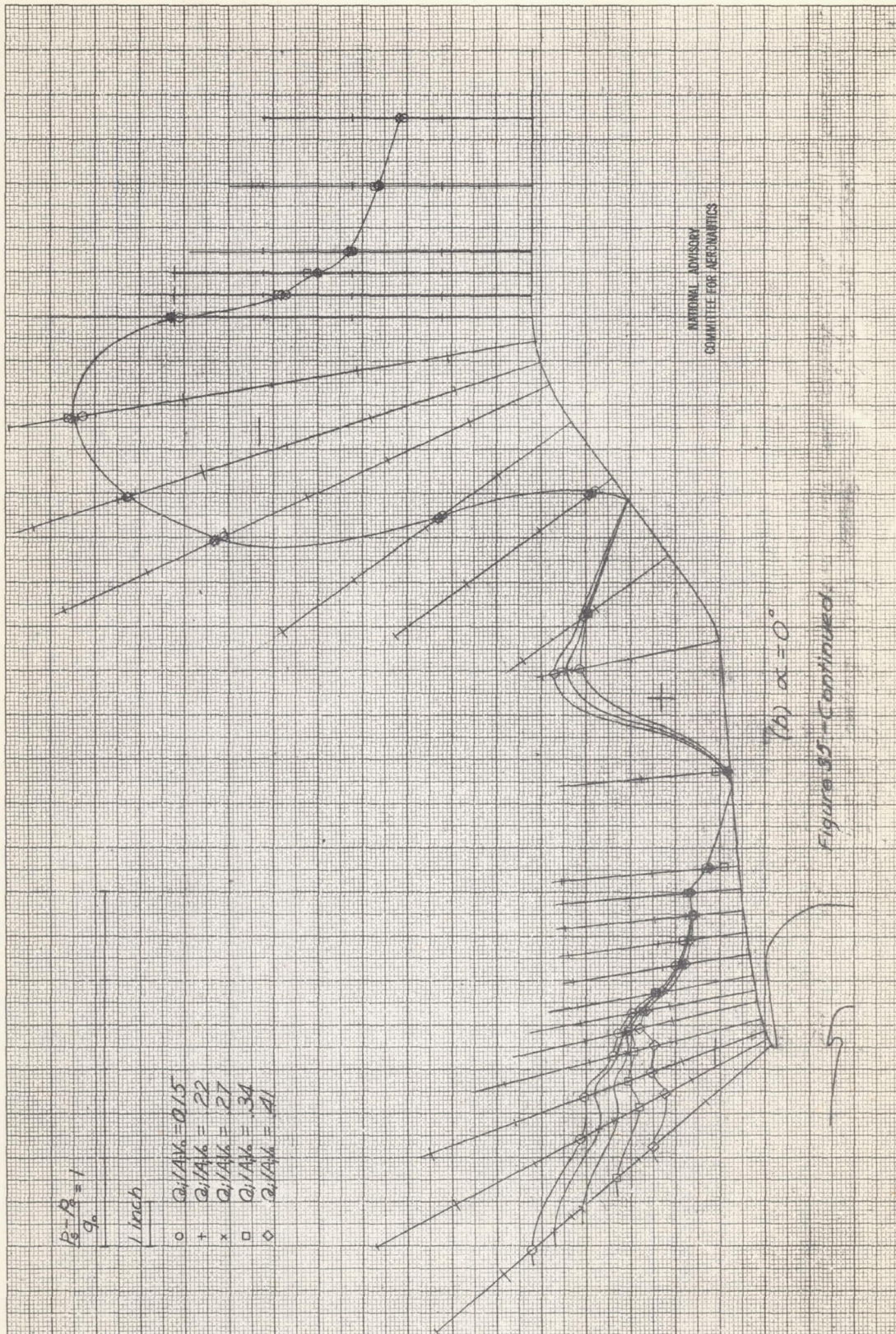
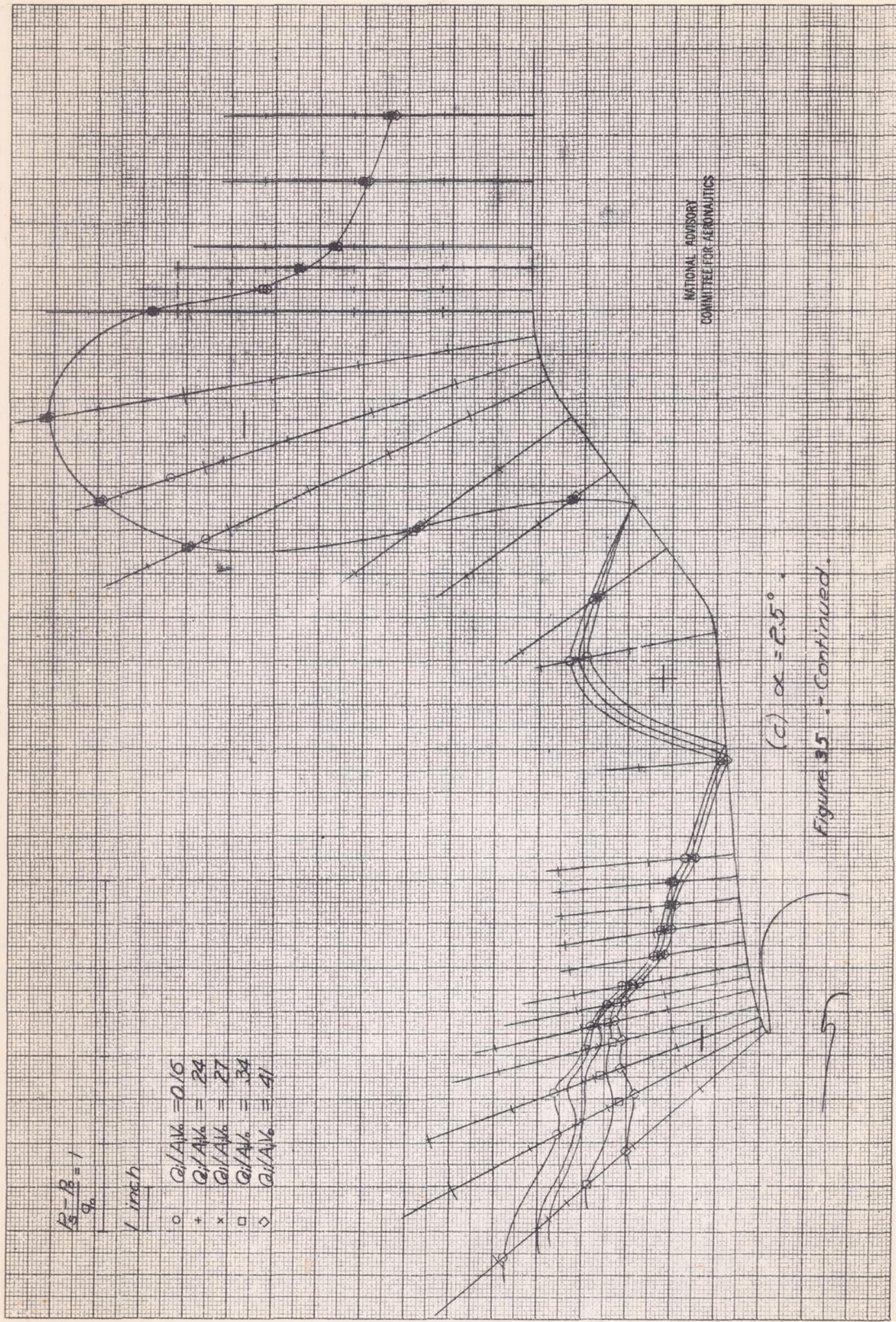
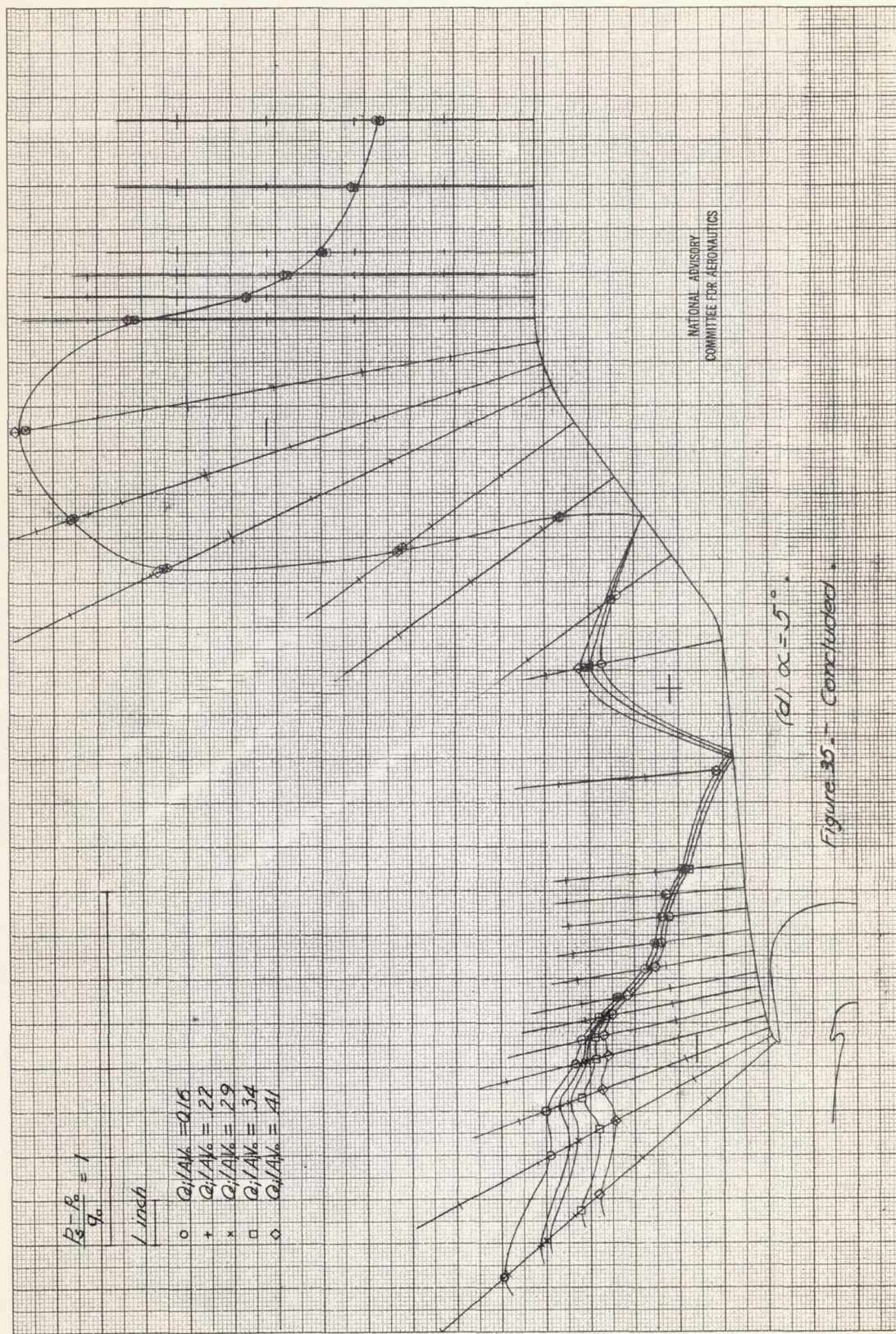
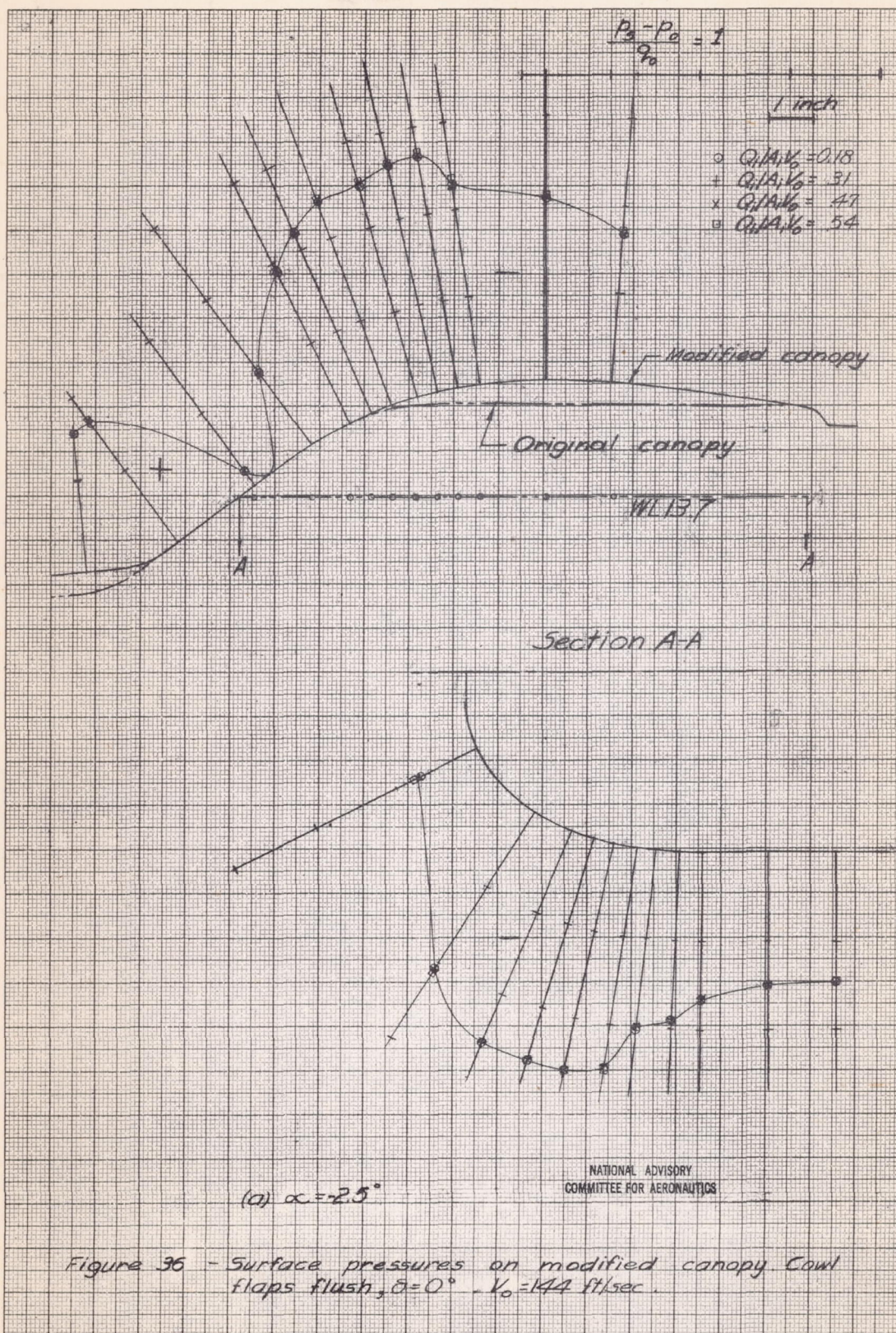


Figure 35—Surface pressures on original conical configuration at -25 degrees angle of attack.
 $t_0 = 102 \text{ msec}$.









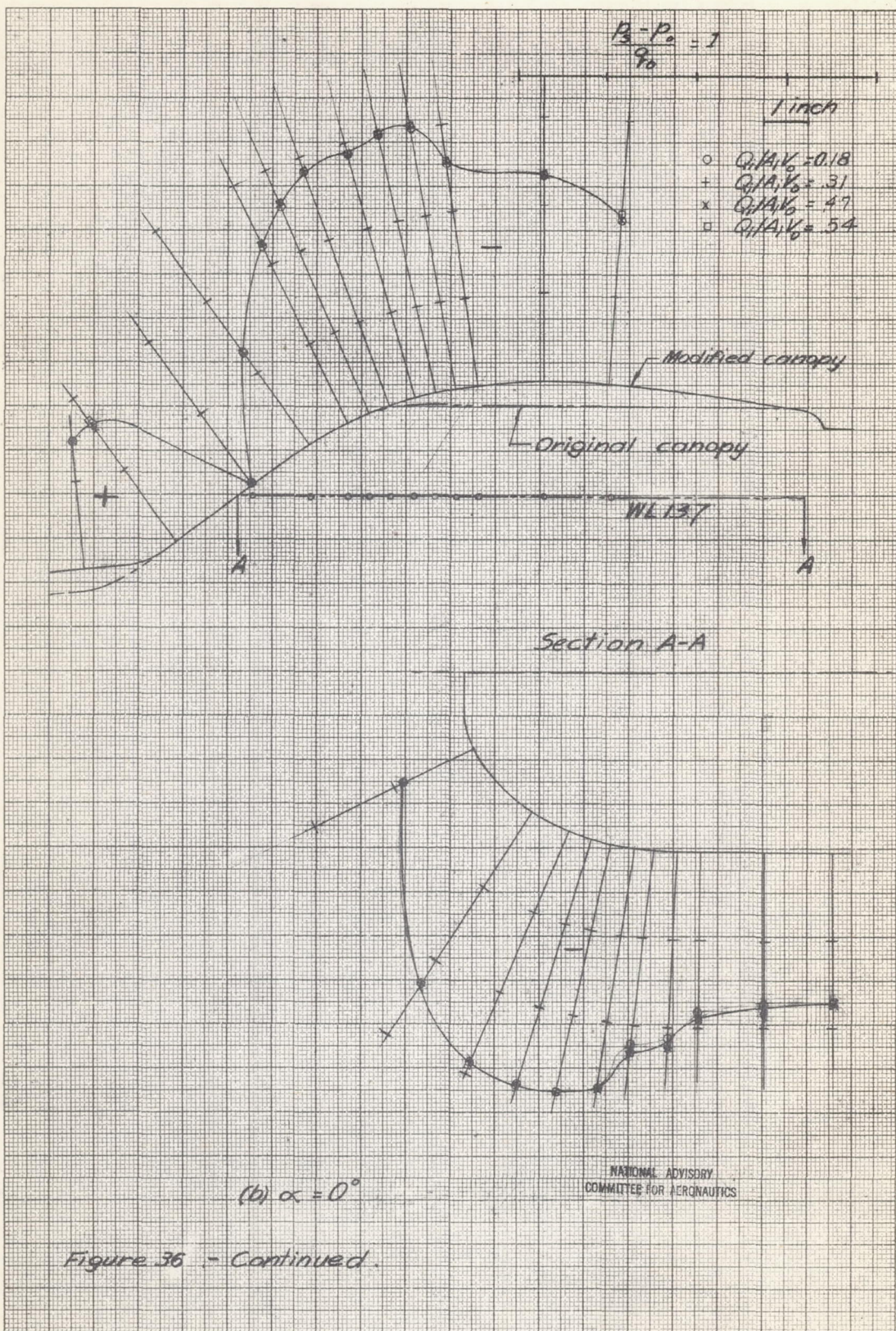
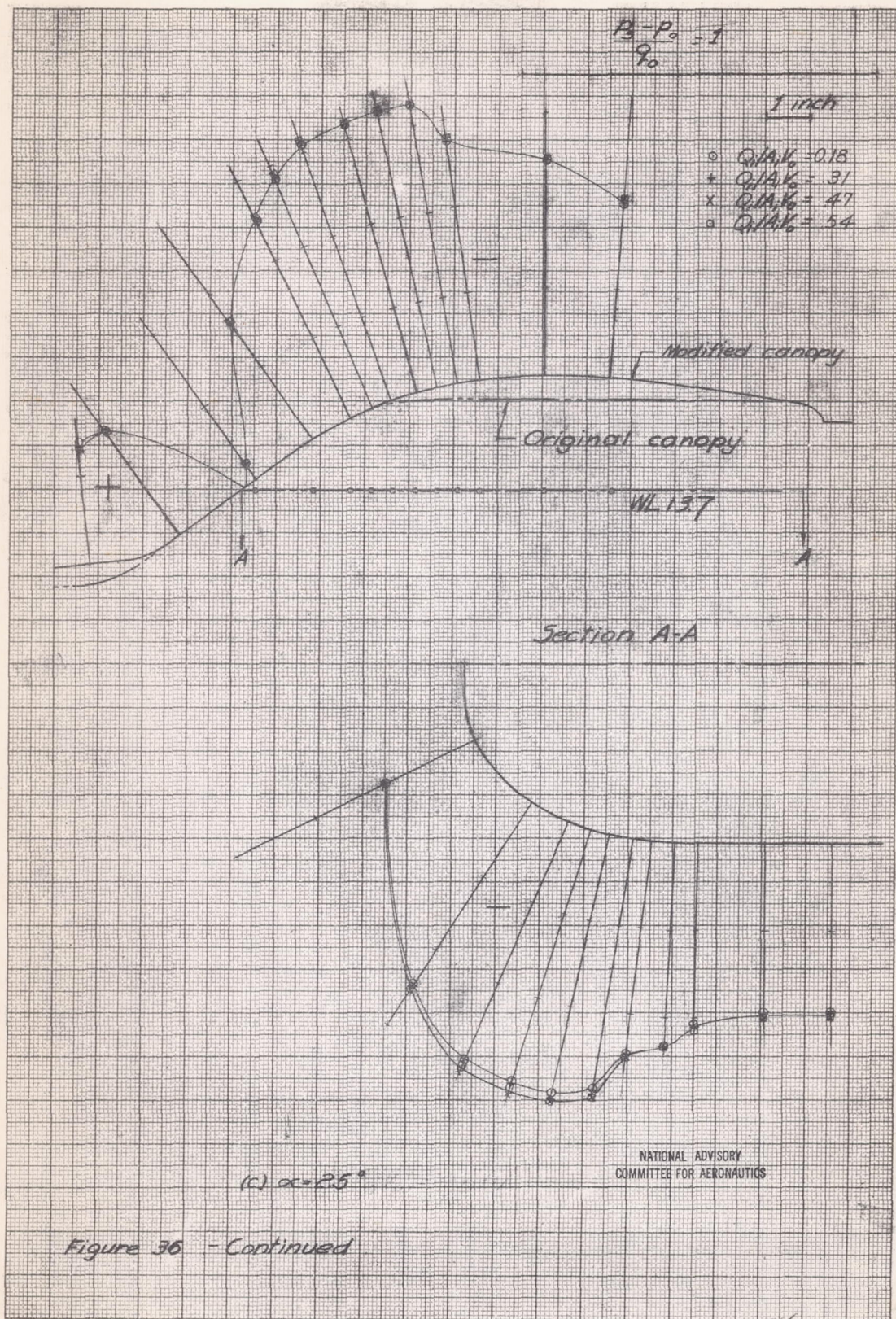


Figure 36 - Continued.



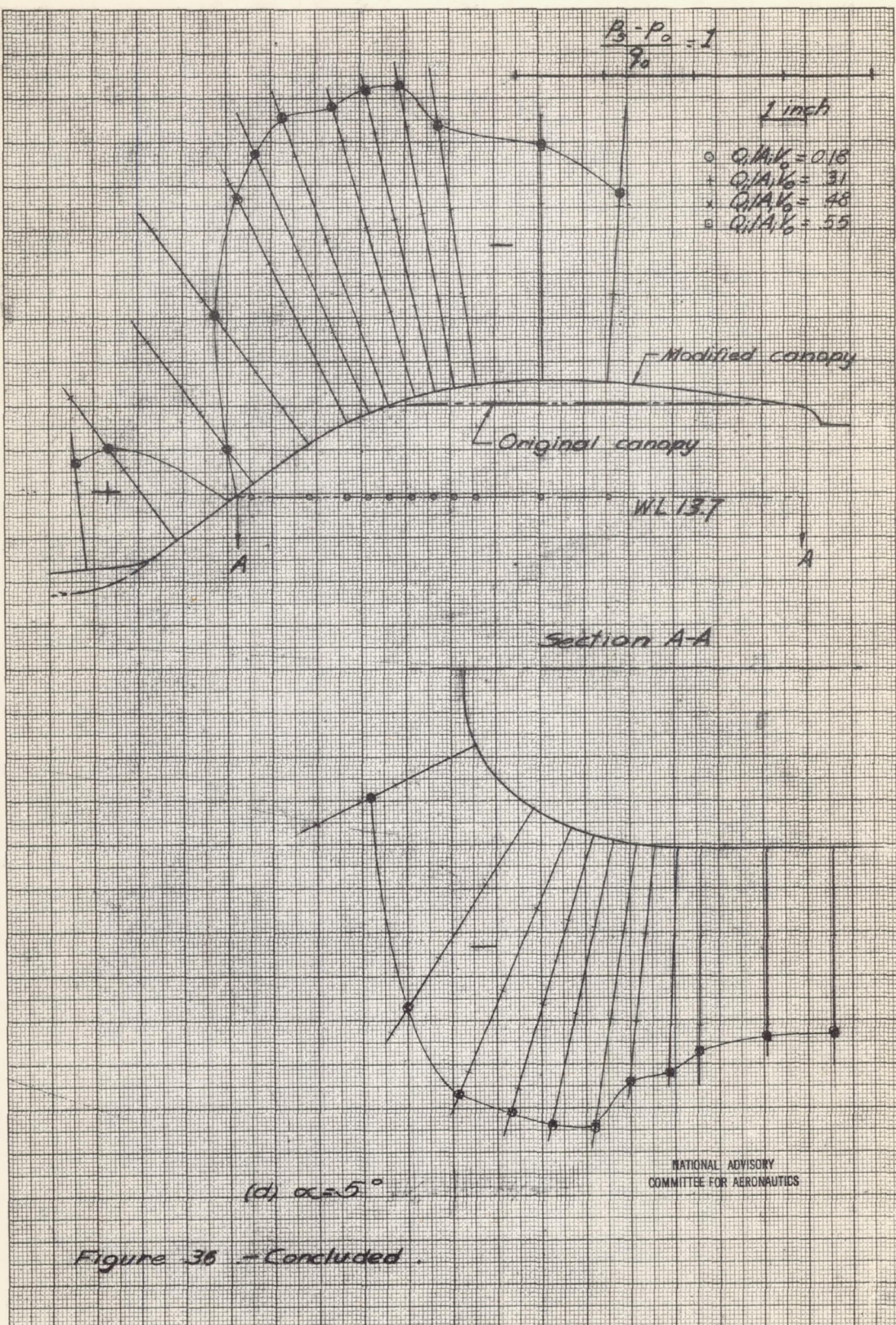


Figure 36 - Concluded.